

# TUNE-OUT AND MAGIC WAVELENGTHS, AND ELECTRIC QUADRUPOLE TRANSITION PROPERTIES OF THE SINGLY CHARGED ALKALINE-EARTH METAL IONS

Mandeep Kaur<sup>a</sup>, Sukhjit Singh<sup>a</sup>, B. K. Sahoo<sup>b</sup>, Bindya Arora<sup>a</sup>

<sup>a</sup>*Guru Nanak Dev University, Amritsar, Punjab-143005, India.*

<sup>b</sup>*Atomic, Molecular and Optical Physics Division, Physical Research Laboratory, Navrangpura, Ahmedabad-380009, India.*

## Abstract

In continuation to our earlier reported data on the electric dipole (E1) matrix elements and lifetimes of the metastable states of the alkaline earth ions in [Atomic Data and Nuc. Data Tables **137** (2021) 101381], we present here the tune-out and magic wavelengths of the  $Mg^+$ ,  $Ca^+$ ,  $Sr^+$  and  $Ba^+$  alkaline earth-metal ions by determining dynamic E1 polarizabilities. Furthermore, we have evaluated the electric quadrupole (E2) matrix elements of a large number of forbidden transitions using an all-order relativistic many-body method and compare them with the previously reported values for a few selective transitions. Compilation of both the E1 and E2 transition matrix elements, will now provide a more complete knowledge about the transition properties of the considered singly charged alkaline earth-metal ions. Similarly, the listed precise values of tune-out and magic wavelengths due to the dominant E1 polarizabilities can be helpful to conduct experiments using the above ions with reduced systematics. Therefore, all these data will be immensely useful for various applications for carrying out the high-precision experiments and laboratory simulations in atomic physics, and interpreting transition lines in the astrophysical observations.

## Contents

1. Introduction . . . . .	2
2. Theory and Methods for calculations . . . . .	5
2.1. Relativistic all-order method . . . . .	5
2.2. Evaluation of matrix elements . . . . .	6
2.3. Electric quadrupole transition properties . . . . .	6
2.4. Electric polarizabilities . . . . .	7
2.4.1. Dipole polarizability . . . . .	7
2.4.2. Quadrupole polarizability . . . . .	8
2.5. Procedure adopted for polarizability evaluation . . . . .	9
3. Data analysis and discussion . . . . .	10
3.1. Reduced E2 matrix elements . . . . .	10
3.2. E2 transition probabilities . . . . .	10
3.3. Static Dipole polarizability . . . . .	11
3.3.1. $Mg^+$ . . . . .	12
3.3.2. $Ca^+$ . . . . .	12

\*Guru Nanak Dev University, Amritsar, Punjab-143005

Email address: E-mail: bindya.phy@gndu.ac.in (Bindya Arora<sup>a</sup>)

3.3.3. Sr <sup>+</sup> .....	12
3.3.4. Ba <sup>+</sup> .....	13
3.4. Static quadrupole polarizability .....	13
3.4.1. Mg <sup>+</sup> .....	13
3.4.2. Ca <sup>+</sup> .....	14
3.4.3. Sr <sup>+</sup> .....	14
3.4.4. Ba <sup>+</sup> .....	14
3.5. Magic and tune-out wavelengths .....	15
3.5.1. Mg <sup>+</sup> .....	15
3.5.2. Ca <sup>+</sup> .....	16
3.5.3. Sr <sup>+</sup> .....	17
3.5.4. Ba <sup>+</sup> .....	18
3.6. Dynamic quadrupole polarizabilities .....	19
4. Conclusion .....	68
References .....	68

## 1. Introduction

Accurate knowledge of spectroscopic properties like transition probabilities, oscillator strengths, static and dynamic polarizabilities, etc. of atomic systems, particularly of the singly charged alkaline-earth metal ions, possess immense importance as these are the potential candidates for conducting high-precision fundamental experiments. Owing to the innovation in laser cooling and trapping techniques, these ions have created benchmark in the field of quantum state manipulation experiments [1, 2], atomic clocks [3], investigating nuclear charge radii [4, 5], studying parity [6] and Lorentz-invariance symmetry violations [7, 8] and so on. The systematic fractional uncertainties of  $10^{-18}$  are expected to be attained in the frequency standards based on the frequency measurements of the forbidden transitions of the cold singly charged Ca<sup>+</sup> [9, 10] and Sr<sup>+</sup> [11–13] ions. The accurate estimates of the systematics due to Stark effects, quadrupole shifts and black-body radiation (BBR) shifts are essential to reach the asserted uncertainty in these ions. Estimation of the Stark and BBR shifts require dipole polarizabilities, whereas estimation of quadrupole shifts require quadrupole moments and quadrupole polarizabilities. These quantities can be determined with the help of a large number of electric dipole and quadrupole transition matrix elements.

The static dipole polarizability values for  $3S_{1/2}$ ,  $3P_{3/2,1/2}$  and  $3D_{5/2,3/2}$  states of Mg<sup>+</sup> were calculated by Mitroy et al. [14] using a semi-empirical single electron analysis combined with the relativistic all-order single-double method (MBPT-SD). The theoretical calculations for the static dipole polarizabilities of Ca<sup>+</sup> for the  $4S_{1/2}$ ,  $4P_{3/2,1/2}$  and  $3D_{5/2,3/2}$  states were given by Tang et al. [15], Mitroy et al. [16] and Sahoo et al. [17] using relativistic structure model, diagonalizing semi-empirical Hamiltonian and relativistic coupled-cluster (RCC) methods respectively. The spectral analysis technique

measurement for the static dipole polarizability for the ground state of  $\text{Ca}^+$  is given by Chang et al. [18]. Similarly, for  $\text{Sr}^+$ , RCC calculations by Sahoo et al. [19], relativistic all-order calculations by Jiang et al. [20] and semi-empirical calculations by Mitroy et al. [21] are available for the  $5S$  and  $4D$  states. Also, Safronova and co-workers [22] have reported dipole polarizabilities for the  $(6-8)S$ ,  $(5-7)P$  and  $(4-6)D$  states for  $\text{Sr}^+$ . Experimental results by Barklem et al. and Nuankaew et al. [23, 24] are also available. Sahoo et al. [19] and Barrett et al. [25] have calculated polarizabilities for the  $6S$  and  $5D$  states of  $\text{Ba}^+$ . Moreover, the dipole polarizability of the  $6S$  state of  $\text{Ba}^+$  is also reported by Safronova et al. using relativistic all-order method [26] whereas, Stark ionization spectroscopy measurement by Snow et al. [27] and radio frequency resonance measurement by Gallagher et al. [28] for the  $6S$  state of  $\text{Ba}^+$  are also given. Static quadrupole polarizability for the ground state of  $\text{Mg}^+$  have been calculated by Mitroy et al. [16] using the semi-empirical Hamiltonian method and by Sahoo et al. [29] using the RCC method. Relativistic all-order calculations by Safronova et al. [30] and semi-empirical Hamiltonian calculations by Mitroy et al. [16] provided quadrupole static polarizabilities values for the  $4S_{1/2}$  state of  $\text{Ca}^+$ . Scalar components of the quadrupole polarizability for the  $5S$ ,  $5P$  and  $4D$  states of  $\text{Sr}^+$  were reported by Jiang et al [31]. The RCC calculations by Sahoo et al. [32], relativistic all-order method calculations by Iskrenova et al. [26] and experimental measurements by Snow et al. [27] are available for the  $6S_{1/2}$  ground state of  $\text{Ba}^+$ .

At the tune-out wavelengths ( $\lambda_T$ ), the dynamic dipole polarizability of atomic systems vanishes. Similarly, the differential dynamic polarizabilities nullify at the magic wavelengths ( $\lambda_{\text{magic}}$ ). Both these quantities provide state-insensitive trapping to reduce the large systematics in high-precision experiments. Theoretical relativistic structure model calculations by Tang et al. [15] and relativistic configuration interaction plus core-polarization (RCICP) calculations by Jiang et al. [33] as well as experimental measurements by Liu et al. [34] have given these values for  $\text{Ca}^+$ , whereas, Jiang et al. [31] have predicted  $\lambda_{\text{magic}}$  values for  $\text{Sr}^+$ . Moreover, the tune-out wavelengths  $\lambda_T$  are also presented for some of the states of considered alkaline earth metal ions for linearly polarized light in the Ref. [35]. Apprehension of these  $\lambda_T$  values are prerequisite for the sympathetic cooling of possible singly and multiply charged ions in two-species mixtures [36, 37].

In the earlier theoretical studies, Stark shifts of the clock transitions in the alkaline-earth metal ions were determined considering contributions only from the ionic dipole polarizabilities. But, the next generation of high-precision optical frequency standards today face the challenge of systematics due to the stray electric field gradients to which atoms or ions are susceptible. In an optical lattice ion clock, quadrupole shifts due to the stray electric field and gradients produced from the neighboring ions can significantly affect the determination of stark shifts. Even though the contributions from the quadrupole polarizabilities are orders of magnitudes smaller than that of the dipole polarizabilities, they do have non-negligible contributions to the total Stark shifts. There are two most important reasons for which contributions from quadrupole polarizability are often neglected in the estimations of the Stark shifts. First, these contributions were assumed to be negligible at the previously considered precision level of interest. Second, it is cumbersome to determine the tensor components of quadrupole polarizability of atomic states. But, it is possible to determine these quantities now by extending our recent derivations on evaluating higher-components of static quadrupole polarizabilities [38].

Owing to the revolution in the observational techniques, it has become possible to observe weak and forbidden quadrupole transitions from astronomical objects [39–41]. Thus, the forbidden transition properties are of great astrophysical interests. In interstellar medium, many alkaline earth metals are present in the abundance predominantly in the singly ionized form that is  $\text{Mg}^+$  [39],  $\text{Ca}^+$  [42, 43],  $\text{Sr}^+$  [44, 45] and  $\text{Ba}^+$  [42] and are considered as the significant con-

stituent of interstellar medium. Information about the structure and physical characteristics of these interstellar clouds can be inferred using the quadrupole transition probabilities of these ions [46, 47]. Forbidden emission lines of  $Mg^+$  from the metastable levels are important as they are abundant in the Solar flares [48]. Electric quadrupole transition probabilities are important in the plasma diagnostic studies, plasma temperature and dynamics [49]. Owing to the long coherence time of the ground and metastable states, the quadrupole transitions of the alkaline-earth metal ions are used for encoding the quantum bit in order to realize quantum logic techniques [50, 51]. Calculations of electric quadrupole transitions provide better insights of the roles of electron correlation effects in the atomic systems [52, 53]. Since atomic clock frequency measurements are aimed at achieving below  $10^{-19}$  precision level today, it is absolutely necessary to investigate effects like contributions from the applied electric field-gradients in the experiments that would appear at such unprecedented precision level. These quadrupole energy shifts can be evaluated using quadrupole polarizabilities. Long-range interatomic interactions, ion mobility, van der Waals constant between different systems, scattering properties of collisions between a neutral atom and its ions [54] can be evaluated using quadrupole polarizability. To realize all these properties, quadrupole matrix elements are needed. However, only a few quadrupole matrix elements for ground and metastable states of the  $Ca^+$ ,  $Sr^+$  and  $Ba^+$  ions are available.

A few groups have studied the quadrupole transition probabilities for  $Mg^+$ ,  $Ca^+$ ,  $Sr^+$  and  $Ba^+$  alkaline-earth metal ions using relativistic and non-relativistic methods. The weakest bound electron potential model theory (WBEMPT) calculations of Celik et al. [55], the RCC calculations by Majumder et al. [56] and non-relativistic multi-configuration Hartree-Fock calculations by Fischer et al. [57] have provided quadrupole transition probabilities of the  $Mg^+$ . The semi-empirical core-potential calculations for  $Ca^+$ ,  $Sr^+$  and  $Ba^+$  are provided by Filippin et al. [58] for the ground state to metastable state transition probabilities. Similarly, the RCC calculations by Guan et al. [59] for  $Ca^+$  and pseudo-relativistic Hartree-Fock method calculations by Gurell et al. [60] for  $Ba^+$  are given for the transition probabilities between ground state and metastable states.

In this work, we intend to present data tables for the accurate values of quadrupole matrix elements for a large number of transitions of the above ions, E2 radiative properties, tune-out wavelengths and magic wavelengths of the  $Mg^+$ ,  $Ca^+$ ,  $Sr^+$  and  $Ba^+$  ions. We have estimated the quadrupole matrix elements and other related radiative properties of the transitions involving the  $nS_{1/2} - n'D_{5/2,3/2}$ ,  $n'D - n''D$ ,  $n'D_{5/2,3/2} - mG_{9/2,7/2}$ ,  $qP - q'P$  and  $qP - m'F$  E2 transitions with  $\{n, n', n''\} = 3 - 6$ ,  $m = 5, 6$ ,  $\{q, q'\} = 3 - 5$  and  $m' = 4 - 5$  in  $Mg^+$ ;  $n = 4 - 7$ ,  $\{n', n''\} = 3 - 6$ ,  $m = 5, 6$ ,  $\{q, q'\} = 4 - 6$  and  $m' = 4 - 5$  in  $Ca^+$ ;  $n = 5 - 8$ ,  $\{n', n''\} = 4 - 7$ ,  $m = 5, 6$ ,  $\{q, q'\} = 5 - 8$  and  $m' = 4 - 5$  in  $Sr^+$ ; and  $n = 6 - 9$ ,  $\{n', n''\} = 5 - 8$ ,  $m = 5, 6$  and  $\{q, q'\} = 6 - 8$  in  $Ba^+$ . The static dipole polarizabilities for the  $nS_{1/2}$ ,  $n'P_{3/2,1/2}$  and  $mD_{5/2,3/2}$  states with  $n = 3 - 5$ ,  $n' = 3 - 5$  and  $m = 3 - 4$  in  $Mg^+$ ;  $n = 4 - 6$ ,  $n' = 4 - 6$  and  $m = 3 - 5$  in  $Ca^+$ ;  $n = 5 - 8$ ,  $n' = 5 - 7$  and  $m = 4 - 6$  in  $Sr^+$  and  $n = 6 - 8$ ,  $n' = 6 - 8$  and  $m = 5$  in  $Ba^+$ . The static quadrupole polarizabilities are given for the  $nS$ ,  $n'P$  and  $mD$  states with  $\{n, n', m\} = 3$  in  $Mg^+$ ;  $\{n, n'\} = 4$  and  $m = 3$  in  $Ca^+$ ;  $\{n, n'\} = 5$  and  $m = 4$  in  $Sr^+$  and  $n = 6$  and  $m = 5$  in  $Ba^+$ . The dynamic dipole polarizabilities for the transitions  $nS - nP$  and  $nS - nD$  in case of  $Mg^+$  ( $n=3$ ), whereas for the transitions  $nS - nP$  and  $nS - (n-1)D$  in case of  $Ca^+$  ( $n=4$ );  $Sr^+$  ( $n=5$ ) and  $Ba^+$  ( $n=6$ ) are presented using the dipole matrix elements given in our previous work [61]. Using these dipole dynamic polarizabilities, the magic wavelengths are obtained by locating the crossings between the dynamic polarizabilities of the  $nS_{1/2}$ ,  $nP_{1/2}$ ,  $nP_{3/2}$ ,  $nD_{3/2}$  and  $nD_{5/2}$  states of  $Mg^+$ ( $n=3$ );  $nS_{1/2}$ ,  $nP_{1/2}$ ,  $nP_{3/2}$ ,  $(n-1)D_{3/2}$  and  $(n-1)D_{5/2}$  states of  $Ca^+$ ( $n=4$ ),  $Sr^+$ ( $n=5$ ) and  $Ba^+$ ( $n=6$ ) plotted against the wavelengths in the range

300-1300 nm. The dipole dynamic polarizabilities are also plotted to evaluate tune-out wavelengths for the  $nS$ ,  $n'P$  and  $mD$  states having  $\{n, n', m\} = 3$  in  $Mg^+$ ;  $\{n, n'\} = 4$  and  $m = 3$  in  $Ca^+$ ;  $\{n, n'\} = 5$  and  $m = 4$  in  $Sr^+$  and  $\{n, n'\} = 6$  and  $m = 5$  in the case of  $Ba^+$ . The dynamic quadrupole polarizabilities are also presented for the  $Ca^+$ ,  $Sr^+$  and  $Ba^+$  ions, which involve transitions between the ground state and metastable states.

## 2. Theory and Methods for calculations

In this section, we mention the procedures adopted for calculating atomic wave functions, which are then used to evaluate the electric dipole (E1) and quadrupole (E2) matrix elements for different transitions. Thereafter, general formulae for the calculation of transition probabilities, oscillator strengths and static as well as dynamic dipole and quadrupole polarizabilities are given. All the quantities are listed in atomic units (a.u.) unless otherwise mentioned.

### 2.1. Relativistic all-order method

The atomic wave functions, which are prerequisite for the evaluation of all the above mentioned spectroscopic properties, are evaluated by employing the relativistic all-order method [62–65]. We have considered only the singles and doubles excitations through this approach (SD method), in which the wave function of an atomic state having a closed-shell configuration and a valence orbital is given by

$$|\Psi_v\rangle_{SD} = \left[ 1 + \sum_{ma} \rho_{ma} a_m^\dagger a_a + \frac{1}{2} \sum_{mnab} \rho_{mnab} a_m^\dagger a_n^\dagger a_b a_a + \sum_{m \neq v} \rho_{mv} a_m^\dagger a_v + \sum_{mna} \rho_{mnva} a_m^\dagger a_n^\dagger a_a a_v \right] |\Phi_v\rangle, \quad (1)$$

where  $|\Phi_v\rangle$  is the reference state function and defined as  $|\Phi_v\rangle = a_v^\dagger |0_c\rangle$  with the Dirac-Hartree-Fock (DHF) wave function of the closed-core of the respective ion  $|0_c\rangle$ ,  $a_i^\dagger$  and  $a_i$  are the creation and annihilation second quantization operators, respectively, with subscripts  $m, n, \dots$  and  $a, b, \dots$  refer to the virtual and occupied orbitals, respectively, of the reference state, and the index  $v$  represents for the valence orbital. In the above expression,  $\rho_{ma}$  and  $\rho_{mv}$  are amplitudes of the single excitations involving core and valence electrons, respectively. Similarly,  $\rho_{mnab}$  and  $\rho_{mnva}$  are the amplitudes of the double excitations involving core and core with valence electrons. These excitation coefficients are obtained by solving the Schrödinger equation for the Dirac-Coulomb Hamiltonian in the iterative procedure till self-consistent solutions are achieved.

In order to verify contributions from the next level of excitations in the all-order method, we have added important triple excitations in the perturbative approach (SDpT method) by defining additional term as defined below

$$|\Psi_v\rangle_{SDpT} \approx |\Psi_v\rangle_{SD} + \left[ \frac{1}{18} \sum_{mnabc} \rho_{mnabc} a_m^\dagger a_n^\dagger a_r^\dagger a_c a_b a_a + \frac{1}{6} \sum_{mnrab} \rho_{mnrvab} a_m^\dagger a_n^\dagger a_r^\dagger a_b a_a a_v \right] |\Phi_v\rangle, \quad (2)$$

where  $\rho_{mnabc}$  and  $\rho_{mnrvab}$  denote the amplitudes of the perturbative triple excitations involving the core and core with valence electrons, respectively.

We have used 70 B-splines of order  $k = 11$  for each angular momentum in order to obtain the single particle orbitals in the DHF method. We have defined the radial functions on a non-linear grid, which are constrained to large spherical cavity having radius  $R = 220$  a.u.. A sufficiently large number of virtuals are accommodated by this choice of cavity radius and quality of the orbitals are ensured due to consideration of a sufficiently large number of B-splines.

## 2.2. Evaluation of matrix elements

After obtaining the wave functions either from the SD or SDpT approximations, we evaluate transition matrix element of an one-body operator  $O$  between the states  $|\Psi_v\rangle$  and  $|\Psi_w\rangle$  as

$$O_{vw} = \frac{\langle\Psi_v|O|\Psi_w\rangle}{\sqrt{\langle\Psi_v|\Psi_v\rangle\langle\Psi_w|\Psi_w\rangle}}, \quad (3)$$

where  $O$  corresponds to either of the E1 or E2 operators. After substituting expressions from Eqs. (1) and (2) for the SD and SDpT expressions, one can classify these contributions into core and valence correlation contributions. Thus, it gives rise to two terms have dominant contributions to the transition matrix elements and those are [66]

$$O_{vw}^{(a)} = \sum_{ma}(o_{am}\tilde{\rho}_{vmwa} + o_{ma}\tilde{\rho}_{wmva}^*), \quad (4)$$

and

$$O_{vw}^{(c)} = \sum_m(o_{vm}\rho_{mw} + o_{mw}\rho_{mv}^*), \quad (5)$$

where  $\tilde{\rho}_{vmwa} = \rho_{vmwa} - \rho_{mvaw}$  and  $*$  represents the complex conjugate term. In our approach,  $o_{vw}$  gives rise the lowest order DHF values to the estimated matrix elements.

To estimate contributions from the neglected higher-level excitations, we have also carried out semi-empirical scaling of the wave functions in the SD and SDpT methods. For this purpose, we only modify the dominant contributions to single valence excitations by defining as [67]

$$\rho'_{mv} = \rho_{mv} \frac{\delta E_v^{\text{expt}}}{\delta E_v^{\text{theory}}}, \quad (6)$$

where  $\rho'_{mv}$  are the modified single excitation coefficients that are used to recalculate the matrix elements and the modified values are referred to as the “scaled” matrix elements. When the scaled wave functions from the SD and SDpT methods are used for the evaluation of matrix elements, the corresponding results are termed as  $O_{sc}^{\text{SD}}$  and  $O_{sc}^{\text{SDpT}}$ , respectively. The recommended values for the matrix elements are given by comparing the ratio  $R = O_{vw}^{(c)}/O_{vw}^{(a)}$ . If  $R > 1$ , then the  $SD_{sc}$  values are regarded as the final ( $O^{\text{Final}}$ ) values, otherwise the SD results are used as the  $O^{\text{Final}}$  values. This procedure can be found in more detail elsewhere (e.g. see Refs. [62, 66]).

## 2.3. Electric quadrupole transition properties

The E2 transition probability ( $A_{vk}^{E2}$ ) in inverse second ( $\text{s}^{-1}$ ) from an upper energy level described by state wave function  $|\Psi_v\rangle$  with angular momentum  $J_v$  to a lower energy level with wave function  $|\Psi_k\rangle$  and angular momentum  $J_k$ , in terms of the fundamental constants, is given by [68]

$$A_{vk}^{E2} = \frac{1}{120} \alpha c \pi \sigma \times \left(\frac{\alpha \sigma}{R_\infty}\right)^4 \times \frac{S^{E2}}{g_v}, \quad (7)$$

where  $\alpha = \frac{e^2}{4\pi\epsilon_0\hbar c}$  is the fine structure constant,  $R_\infty = \frac{\alpha^2 m_e c}{2\hbar}$  is the Rydberg constant,  $c$  is the speed of light and  $\sigma = E_v - E_k$  is the energy difference between the upper ( $E_v$ ) and lower ( $E_k$ ) levels of the transition and  $S^{E2} = |\langle J_v || \mathbf{Q} || J_k \rangle|^2$  is the line strength with E2 operator  $\mathbf{Q} \equiv \sum_j \mathbf{q}_j = -\frac{e}{2} \sum_j (3z_j^2 - r_j^2)$ . We have used the values of the fundamental constants as  $\alpha = 7.297352 \times 10^{-3}$ ,  $c = 29979245800 \text{ cm s}^{-1}$  and  $R_\infty = 1.0973731 \times 10^5 \text{ cm}^{-1}$  from Ref. [69] for the

evaluations of the E2 transition probabilities. By substituting the values of fundamental constants and wavelength ( $\lambda$ ) of the transition in Å,  $A_{vk}^{E2}$  is determined using the following formula given in [70] as

$$A_{vk}^{E2} = \frac{1.1199 \times 10^{18}}{g_v \lambda^5} \times S^{E2}, \quad (8)$$

where  $g_v$  is the degeneracy factor of corresponding state.

Using the above transition probability equation, the absorption oscillator strengths  $f_{kv}^{E2}$  for the E2 transition operator are calculated as [68, 70]

$$\begin{aligned} f_{kv}^{E2} &= \left( \frac{R_\infty}{2c\alpha^3\pi} \right) \frac{g_v}{g_k} \times \frac{A_{vk}^{E2}}{\sigma^2} \\ &= 1.4992 \times 10^{-16} \times \frac{g_v}{g_k} A_{vk}^O \lambda^2, \end{aligned} \quad (9)$$

which follows that

$$\begin{aligned} f_{kv}^{E2} &= \frac{1}{240\alpha} \left( \frac{\alpha\sigma}{R_\infty} \right)^3 \times \frac{S^{E2}}{g_k} \\ &= \frac{167.90}{g_k \lambda^3} \times S^{E2}. \end{aligned} \quad (10)$$

#### 2.4. Electric polarizabilities

The application of oscillating electric field of trapping laser beam induces the Stark shift in the energy levels of an atomic or ionic system. This Stark shift of an energy level  $E_n$  can be quantified as [71–73]

$$\Delta E_n = -\frac{1}{4}\alpha_n^d(\omega)\mathcal{E}^2 - \frac{1}{16}\alpha_n^q(\omega)\nabla\mathcal{E}^2 + \dots, \quad (11)$$

where  $\alpha_n^d(\omega)$  is the dynamic dipole polarizability,  $\alpha_n^q(\omega)$  is the dynamic quadrupole polarizability,  $\mathcal{E}$  is the applied electric field strength and  $\nabla\mathcal{E}$  is a tensor describing the gradient of the electric field at the position of the atomic system. For an uniform electric field, the second term on the right side of Eq. (11) diminishes as the gradient for uniform field is zero. However, for the inhomogeneous electric field, the second term contributes to the differential shift in energy.

##### 2.4.1. Dipole polarizability

For an atomic system in state  $|\Psi_n\rangle \equiv |\gamma_n J_n M_{J_n}\rangle$  with angular momentum  $J_n$  and its azimuthal quantum number  $M_{J_n}$ , the Stark shift due to the electric field of the applied AC electric field at frequency  $\omega$  is given by the first term of Eq. (11). On applying the sum-over-states approach of perturbative theory, the  $\alpha_n^d(\omega)$  can be determined as

$$\alpha_n^d(\omega) = -\sum_{m \neq n} (p^*)_{nm}(p)_{mn} \times \left[ \frac{1}{\delta E_{nm} + \omega} + \frac{1}{\delta E_{nm} - \omega} \right]. \quad (12)$$

With  $(p)_{mn} = \langle \Psi_m | D | \Psi_n \rangle$  as the E1 matrix element having  $\mathbf{D} = \sum_j \mathbf{d}_j = -e \sum_j \mathbf{r}_j$  being the electric dipole (E1) operator and  $\delta E_{nm} = E_m^0 - E_n^0$  considered as the difference in the unperturbed energies of the corresponding states involved in the transition in accordance with the dipole selection rules. For linearly polarized light, we can express  $\alpha_n^d(\omega)$  by rewriting it as [74]

$$\alpha_n^d(\omega) = \alpha_n^{d(0)}(\omega) + \frac{3M_{J_n}^2 - J_n(J_n + 1)}{J_n(2J_n - 1)} \alpha_n^{d(2)}(\omega), \quad (13)$$

where  $\alpha_n^{d(0)}(\omega)$  and  $\alpha_n^{d(2)}(\omega)$  represent the scalar and tensor of rank 2 part of dipole dynamic polarizability and can be written as

$$\alpha_n^{d(0)}(\omega) = \sum_{m \neq n} W_n^{(0)} \left[ \frac{|\langle \gamma_n J_n || \mathbf{D} || \gamma_m J_m \rangle|^2}{E_n - E_m + \omega} + \frac{|\langle \gamma_n J_n || \mathbf{D} || \gamma_m J_m \rangle|^2}{E_n - E_m - \omega} \right] \quad (14)$$

and

$$\alpha_n^{d(2)}(\omega) = \sum_{m \neq n} W_{n,m}^{(2)} \left[ \frac{|\langle \gamma_n J_n || \mathbf{D} || \gamma_m J_m \rangle|^2}{E_n - E_m + \omega} + \frac{|\langle \gamma_n J_n || \mathbf{D} || \gamma_m J_m \rangle|^2}{E_n - E_m - \omega} \right] \quad (15)$$

with the coefficients  $W_n^{(0)} = -\frac{1}{3(2J_n+1)}$  and  $W_{n,m}^{(2)} = 2\sqrt{\frac{5J_n(2J_n-1)}{6(J_n+1)(2J_n+3)(2J_n+1)}} \times (-1)^{J_n+J_m+1} \begin{Bmatrix} J_n & 2 & J_n \\ 1 & J_m & 1 \end{Bmatrix}$ . The selection rules of the six-j symbol ensures that only the scalar term contributes towards the total dipole polarizability to the states with angular momentum  $J = 1/2$ , whereas both the scalar and tensor components contribute to the states with angular momenta  $J = 3/2$  and  $J = 5/2$ . According to the Eq. (13), the total polarizability of the  $J = 3/2$  state is given by  $\alpha_n^d(\omega) = \alpha_n^{d(0)}(\omega) - \alpha_n^{d(2)}(\omega)$  for  $M_J = \pm 1/2$  and it corresponds to  $\alpha_n^d(\omega) = \alpha_n^{d(0)}(\omega) + \alpha_n^{d(2)}(\omega)$  for  $M_J = \pm 3/2$ . Similarly for the states with  $J = 5/2$ , the total polarizabilities are given by  $\alpha_n^d(\omega) = \alpha_n^{d(0)}(\omega) - 0.8\alpha_n^{d(2)}(\omega)$  for  $M_J = \pm 1/2$ ,  $\alpha_n^d(\omega) = \alpha_n^{d(0)}(\omega) - 0.2\alpha_n^{d(2)}(\omega)$  for  $M_J = \pm 3/2$  and  $\alpha_n^d(\omega) = \alpha_n^{d(0)}(\omega) + \alpha_n^{d(2)}(\omega)$  for  $M_J = \pm 5/2$ . It can be noted that the static dipole polarizability values correspond to  $\omega = 0$ .

For finding the tune-out wavelengths, we first plot the dynamic polarizability of considered states and then identify the value of  $\omega$  where the polarizability value turns out to be zero. This value of  $\omega$  corresponds to the  $\lambda_T$ . Similarly,  $\lambda_{\text{magic}}$  corresponds to the null differential dynamic polarizability of a transition at a given value of  $\omega$ . The differential AC Stark shift of the transition involving the ground and an excited state is due to the dominant dipole polarizability contribution is given by

$$\delta(\Delta E)_{ge}^d(\omega) = -\frac{1}{4} [\alpha_g^d(\omega) - \alpha_e^d(\omega)] \mathcal{E}^2,$$

where the subscripts  $g$  and  $e$  stand for the ground and excited states. In our work, we identify the magic wavelengths by plotting the dynamic dipole polarizabilities against  $\omega$  values and finding out their crossings for the ground and the excited states. The two polarizability curves usually cross in between of any two resonant transitions of the the states and the  $\omega$  values at those crossings are referred to as the magic wavelengths.

#### 2.4.2. Quadrupole polarizability

The quadrupole Stark shift in the energy level of an atomic system in state  $|\Psi_n\rangle \equiv |\gamma_n J_n M_{J_n}\rangle$  due to the electric field gradient at frequency  $\omega$  is given by second term of Eq. (11). In the sum-over-states approach, these polarizabilities are given by

$$\alpha_n^q(\omega) = - \sum_{m \neq n} (q^*)_{nm}(q)_{mn} \times \left[ \frac{1}{\delta E_{nm} + \omega} + \frac{1}{\delta E_{nm} - \omega} \right]. \quad (16)$$

Here  $(q)_{mn} = \langle \Psi_m | Q | \Psi_n \rangle$  is the E2 matrix element and  $\delta E_{nm} = E_n^0 - E_m^0$  being the unperturbed energies of the corresponding states as mentioned above. For linearly polarized light, we can conveniently evaluate  $\alpha_n^q(\omega)$  by rewriting it in terms of different tensor components as [38]

$$\alpha_n^q(\omega) = \alpha_n^{q(0)}(\omega) + \frac{3M_{J_n}^2 - J_n(J_n+1)}{J_n(2J_n-1)} \alpha_n^{q(2)}(\omega) + \frac{3(5M_{J_n}^2 - J_n^2 - 2J_n)(5M_{J_n}^2 + 1 - J_n^2) - 10M_{J_n}^2(4M_{J_n}^2 - 1)}{J_n(J_n-1)(2J_n-1)(2J_n-3)} \alpha_n^{q(4)}(\omega), \quad (17)$$

where  $\alpha_n^{q(0)}(\omega)$ ,  $\alpha_n^{q(2)}(\omega)$  and  $\alpha_n^{q(4)}(\omega)$  are defined as the scalar, tensor component of rank 2 and tensor component of rank 4 of  $\alpha_n^q(\omega)$ , respectively, of the quadrupole polarizability. The corresponding expressions for different components can be given in terms of  $\langle \gamma_n J_n || \mathbf{Q} || \gamma_m J_m \rangle$  reduced E2 matrix elements by

$$\alpha_n^{q(0)}(\omega) = \sum_{m \neq n} W_n^{q(0)} |\langle \gamma_n J_n || \mathbf{Q} || \gamma_m J_m \rangle|^2 \left[ \frac{1}{\delta E_{nm} + \omega} + \frac{1}{\delta E_{nm} - \omega} \right], \quad (18)$$

$$\alpha_n^{q(2)}(\omega) = \sum_{m \neq n} W_{n,m}^{q(2)} |\langle \gamma_n J_n || \mathbf{Q} || \gamma_m J_m \rangle|^2 \left[ \frac{1}{\delta E_{nm} + \omega} + \frac{1}{\delta E_{nm} - \omega} \right] \quad (19)$$

and

$$\alpha_n^{q(4)}(\omega) = \sum_{m \neq n} W_{n,m}^{q(4)} |\langle \gamma_n J_n || \mathbf{Q} || \gamma_m J_m \rangle|^2 \left[ \frac{1}{\delta E_{nm} + \omega} + \frac{1}{\delta E_{nm} - \omega} \right]. \quad (20)$$

In the above expressions, the coefficients are given by

$$W_n^{q(0)} = -\frac{1}{5(2J_n + 1)}, \quad (21)$$

$$W_{n,m}^{q(2)} = -\sqrt{\frac{10J_n(2J_n - 1)}{7(J_n + 1)(2J_n + 1)(2J_n + 3)}} (-1)^{J_n + J_m + 1} \left\{ \begin{array}{ccc} J_n & 2 & J_n \\ 2 & J_m & 2 \end{array} \right\} \quad (22)$$

and

$$W_{n,m}^{q(4)} = \sqrt{\frac{J_n(J_n - 1)(2J_n - 1)(2J_n - 3)}{70(2J_n + 1)(J_n + 1)(J_n + 2)}} \frac{9(-1)^{J_n + J_m + 1}}{\sqrt{(2J_n + 5)(2J_n + 3)}} \left\{ \begin{array}{ccc} J_n & 4 & J_n \\ 2 & J_m & 2 \end{array} \right\}. \quad (23)$$

The above expressions can be used to evaluate both the static ( $\omega = 0$ ) and dynamic ( $\omega \neq 0$ ) quadrupole polarizabilities. Only the scalar component will contribute to the states with angular momentum  $J = 1/2$ , while both the scalar and tensor components with rank 2 will contribute to the states with  $J = 3/2$  and the tensor quadrupole polarizability corresponding to the rank 4 appears for states with  $J = 5/2$ . It can be followed from this is that it is more laborious and challenging to obtain accurate values of the quadrupole polarizabilities of the  $D$  states as they will need many more matrix elements involving a large number of intermediate states. According to the Eq. (17), the total polarizabilities for the states with  $J = 3/2$  is evaluated as  $\alpha_n^q(\omega) = \alpha_n^{q(0)}(\omega) - \alpha_n^{q(2)}(\omega)$  for  $M_J = 1/2$  and as  $\alpha_n^q(\omega) = \alpha_n^{q(0)}(\omega) + \alpha_n^{q(2)}(\omega)$  for  $M_J = 3/2$ . The total polarizability for the states with  $J = 5/2$  can be calculated as  $\alpha_n^q(\omega) = \alpha_n^{q(0)}(\omega) - 0.8\alpha_n^{q(2)}(\omega) + 4\alpha_n^{q(4)}(\omega)$  for  $M_J = \pm 1/2$ , as  $\alpha_n^q(\omega) = \alpha_n^{q(0)}(\omega) - 0.2\alpha_n^{q(2)}(\omega) - 6\alpha_n^{q(4)}(\omega)$  for  $M_J = \pm 3/2$  and as  $\alpha_n^q(\omega) = \alpha_n^{q(0)}(\omega) + \alpha_n^{q(2)}(\omega) + 2\alpha_n^{q(4)}(\omega)$  for  $M_J = \pm 5/2$ .

## 2.5. Procedure adopted for polarizability evaluation

Each component of dipole as well as quadrupole polarizabilities in the considered alkaline earth metal ions can be conveniently estimated by calculating contributions separately due to the core, core-valence and valence correlations [75, 76]. These can be written as

$$\alpha_n^o(\omega) = \alpha_{n,c}^o(\omega) + \alpha_{n,cv}^o(\omega) + \alpha_{n,v}^o(\omega), \quad (24)$$

where  $o$  denotes either  $d$  or  $q$  for the E1 or E2 polarizability respectively. The  $\alpha_{n,c}^o(\omega)$ ,  $\alpha_{n,cv}^o(\omega)$  and  $\alpha_{n,v}^o(\omega)$  present the core, core-valence and valence correlation effects respectively. The most important contributions to different components

of polarizability arises through  $\alpha_{n,v}^o(\omega)$ , since it takes into account the dominant correlation effects from the calculations of atomic wave functions. For calculating the  $\alpha_{n,v}^o(\omega)$  contribution, we first calculate the wave functions of atomic states and matrix elements of as many as low-lying states of the considered alkaline earth metal ions using relativistic all-order method as already explained earlier in this section. The dominant contribution to  $\alpha_{n,v}^o(\omega)$  is evaluated by combining these matrix elements with the experimental energies listed in the National Institute of Science and Technology database (NIST) [77]. This is called as the “Main” contribution to  $\alpha_{n,v}^o(\omega)$ , whereas the smaller contributions from the high-lying excited states are evaluated using the DHF method and are termed as the “Tail” contribution to  $\alpha_{n,v}^o(\omega)$ . The smaller contributions arising from the valence-core correlation contribution  $\alpha_{n,cv}^o(\omega)$  is evaluated using DHF method and from the core correlation contribution  $\alpha_{n,c}^o(\omega)$  have been evaluated using the random phase approximation (RPA).

### 3. Data analysis and discussion

#### 3.1. Reduced E2 matrix elements

The reduced E2 matrix elements calculated using the DHF, SD, SDsc, SDpT and SDpTsc methods for a number of  $S-D$ ,  $D-G$ ,  $P-P$  and  $P-F$  transitions of the  $Mg^+$ ,  $Ca^+$ ,  $Sr^+$  and  $Ba^+$  alkaline-earth metal ions are listed in Tables A, B, C and D, respectively. We also list our recommended values along with the uncertainties for the considered transitions in the same tables. For the range  $0.5 < R < 1.5$ , the uncertainties are determined as the maximum difference between the final value of matrix element and the other three all-order values. However for  $1.5 < R < 3$ , the uncertainties are calculated as  $\max(SDsc - SD, SDsc - SDpT, SDsc - SDpTsc)$ . Also, if  $R > 3$ , the uncertainties are given as  $\max(SDsc - SDpT, SDsc - SDpTsc)$ . We have calculated these E2 matrix elements for about 114 transitions in  $Mg^+$ , 114 transitions in  $Ca^+$ , 130 transitions in  $Sr^+$  and 96 transitions in  $Ba^+$ .

#### 3.2. E2 transition probabilities

By using our recommended values of the E2 matrix elements and experimental values for the wavelengths, we have calculated the line strengths  $S_{vk}$ , transition probabilities  $A_{vk}$  and oscillator strengths  $f_{kv}$  for all the considered E2 transitions of  $Mg^+$ ,  $Ca^+$ ,  $Sr^+$  and  $Ba^+$  which are presented in Tables E, F, G and H respectively. The experimental values for the wavelengths were derived from the excitation energies listed in the NIST database [77]. This includes  $nS_{1/2}-n'D_{5/2,3/2}$ ,  $n'D-n''D$ ,  $n'D_{5/2,3/2}-mG_{9/2,7/2}$ ,  $qP-q'P$  and  $qP_{3/2,1/2}-m'_{7/2,5/2}F$  E2 transitions with  $\{n,n',n''\} = 3-6$ ,  $m = 5,6$ ,  $\{q,q'\} = 3-5$  and  $m' = 4-5$  in  $Mg^+$ ;  $n = 4-7$ ,  $\{n',n''\} = 3-6$ ,  $m = 5,6$ ,  $\{q,q'\} = 4-6$  and  $m' = 4-5$  in  $Ca^+$ ;  $n = 5-8$ ,  $\{n',n''\} = 4-7$ ,  $m = 5,6$ ,  $\{q,q'\} = 5-8$  and  $m' = 4-5$  in  $Sr^+$ ; and  $n = 6-9$ ,  $\{n',n''\} = 5-8$ ,  $m = 5,6$  and  $\{q,q'\} = 6-8$  in  $Ba^+$ . We have made comparison of the our evaluated data with the previously available literature below.

In Table I, a comparison of our calculated data for  $Mg^+$  is presented with previously available literature. Comparison with the NIST database indicates very good agreement for all the available transitions except for the  $3D_{5/2} - 3S_{1/2}$  and  $4D_{5/2} - 3S_{1/2}$  transitions. However, our evaluated results for these transitions are in excellent agreement with the WBEMPT calculations by Celik et al. [55], RCC calculations by Majumder et al. [56] and MCHF calculations by Fischer et al. [57], which expresses the reliability in our calculations for these transitions despite of differences with NIST database. Celik et al. [55], Majumder et al. [56] and Fischer et al. [57] have also provided calculations of transition probabilities of many other transitions. It is reflected in the table that, in general our evaluated data is in very good

agreement with the available literature except for a few discrepancies discussed next. For the  $3P_{3/2} - 3P_{1/2}$  transition a good agreement of our value is seen with [55] and [56], whereas a small discrepancy can be noticed with the MCHF results in Ref. [57]. For the  $4P - 3P$  transitions our results match extremely well with the results in Ref. [57] as compared to slight difference with those presented in Refs. [55, 56], whereas, for the  $5P_{3/2} - 5P_{1/2}$  transition our value is much closer to the values in Ref. [55]. It can be noticed that our relativistic all-order calculations for the  $5P - 4F$  and  $3D_{3/2} - 3D_{5/2}$  transitions present major discrepancy with the RCC calculations of Majumder et al. [56]. The reason could be we have used here B-spline basis functions, whereas Majumder et al. [56] have used Gaussian type orbitals (GTOs) to describe the orbitals. Unless, suitable optimized parameters are used to describe  $4F$  orbitals GTOs do not generate enough bound orbitals. Since we have imposed boundary conditions with a large cavity radius and our bound orbitals obtained using the numerical approach, we assume our results for the  $4F$  orbitals are more reliable. The comparison of the transition probability value for the  $5D_{3/2} - 3D_{5/2}$  transition depicts that our value matches neither with the values presented in Ref. [55] nor with Ref. [56]. For this transition, the values of Ref. [55] and Ref. [56] also show mutual conflict with each other. Such disagreements could be partly because of the aforementioned reason. In addition, electron correlation effects arising through non-linear terms and triple excitations that are neglected in our all-order theory contribute significantly to the states with higher angular momentum [78]. Inclusion of these contributions in the calculations may remove most of these discrepancies.

In Table J, we have presented the comparison of the transition probabilities  $A_{vk}$  and oscillator strengths  $f_{kv}$  for the  $nD - (n + 1)S$  and  $nD_{5/2} - nD_{3/2}$  transitions of  $\text{Ca}^+(n = 3)$ ,  $\text{Sr}^+(n = 4)$  and  $\text{Ba}^+(n = 5)$  with available literature. In our previous paper [61], we had presented a few E2 matrix elements by employing the SD method approximation. Here, in present paper we have used the recommended values of the matrix elements based on the criteria mentioned in Sec 2.2. In this table, we have also presented the comparison of our data with the values available in the NIST database. In literature, values for the E2 transition probabilities are available only for the  $3D - 4S$  transitions in  $\text{Ca}^+$  [58, 59, 79];  $4D - 5S$  transitions in  $\text{Sr}^+$  [58]; the  $5D - 6S$  transitions in  $\text{Ba}^+$  [58, 60] and the  $3D_{5/2} - 3D_{3/2}$  [58],  $4D_{5/2} - 4D_{3/2}$  [58] and  $5D_{5/2} - 5D_{3/2}$  [58, 60] transitions in  $\text{Ca}^+$ ,  $\text{Sr}^+$  and  $\text{Ba}^+$  respectively. We notice that discrepancy is found for the results in  $\text{Ca}^+$  whereas, our results for  $\text{Sr}^+$  exhibit excellent agreement with values from NIST database [77]. More importantly our calculated quadrupole transition probability for the  $3D_{5/2} - 4S_{1/2}$  transition in  $\text{Ca}^+$  is in excellent agreement with the recent experimental result reported by Shao et al. [79]. This strongly advocates for the accuracy of our results. Also, our estimated values for  $\text{Ca}^+$  exhibit good agreement with the recent semi-empirical core potential calculations by Filippin et al. [58] and RCC calculations by Guan et al. [59]. Similarly, the transition probabilities of  $\text{Sr}^+$  and  $\text{Ba}^+$  are in good agreement with the results provided by Filippin et al. [58]. For  $\text{Ba}^+$ , our values show good agreement with the pseudo-relativistic Hartree-Fock method calculations by Gurell et al. [60].

### 3.3. Static Dipole polarizability

Using our previously reported E1 matrix elements in Ref. [61] and the experimental energies taken from the NIST database, we evaluate the static dipole polarizabilities of the ground and excited states of  $\text{Mg}^+$ ,  $\text{Ca}^+$ ,  $\text{Sr}^+$  and  $\text{Ba}^+$  ions. Then, we compare these values with the previously available experimental and theoretical results in Tables K, L, M and N. The scalar polarizabilities of the considered ground and excited states along with the tensor polarizabilities for the states with  $J > 1/2$  are presented separately. The contributions from the ‘Main’ and ‘Tail’ parts of the valence

correlations along with the contributions from the core-valence and core correlations are also given in the same tables. We discuss these results for the individual ion below.

### 3.3.1. $Mg^+$

Table K presents the tabulation of the static polarizability values for the  $(3-5)S_{1/2}$ ,  $(3-5)P_{3/2,1/2}$  and  $(3-4)D_{5/2,3/2}$  states of  $Mg^+$ . Along with this, the comparison of our results for the  $3S_{1/2}$ ,  $3P_{3/2,1/2}$  and  $3D_{5/2,3/2}$  states with the values provided by Mitroy et al. [14] is made in the same table. The static polarizability values by Mitroy et al. [14] are computed using a semi-empirical single electron analysis combined with the MBPT-SD method. It can clearly be noticed that our ground state polarizability values are in excellent agreement with their values. A similar trend of remarkable agreement can be seen for the scalar as well as tensor polarizability values of the  $3P$  states as well as of the  $3D$  states between our and their values. Hence, the accuracy of our results for excited states can also be ascertained from this. The literature values for the static polarizabilities for other excited states are not available and these calculations have been carried out for the first time in this work.

### 3.3.2. $Ca^+$

As can be seen that Table L enlists the values of the static polarizabilities for the states  $(4-6)S_{1/2}$ ,  $(4-6)P_{3/2,1/2}$  and  $(3-5)D_{5/2,3/2}$  states of  $Ca^+$ . Our estimated values of the polarizabilities for the  $4S$ ,  $4P$  and  $3D$  states are in excellent agreement with the MBPT-SD calculations by Safranova et al. [30]. Our calculated value of  $76.0 \pm 0.6$  a.u. for the  $4S_{1/2}$  state is in close agreement with the other theoretical calculations that is using the relativistic structure model by Tang et al. [15] and diagonalizing semi-empirical Hamiltonian calculations by Mitroy et al. [16], which are 75.28 a.u. and 75.49 a.u. respectively. Along with the ground state results, our calculated polarizability values for the  $3D_{3/2}$  and  $3D_{5/2}$  states are also compared with Mitroy et al. [16] and Tang et al. [15], which represent very good agreements. The comparison of our calculated polarizability values for the  $4S_{1/2}$ ,  $3D_{3/2}$  and  $3D_{5/2}$  states show reasonable agreement within error bars with *ab initio* RCC calculations by Sahoo et al. [17]. Also, our estimated  $4S_{1/2}$  state polarizability value is very close to the experimental result, obtained with spectral analysis technique by Chang et al. [18], within the uncertainty limits. However, large discrepancy can be noticed between our values of the scalar polarizabilities for the  $4P$  states with Tang et al. and Mitroy et al. [15, 16]. To our knowledge, no data is available in the literature for comparison of the the static polarizability of other excited states that are calculated in the present work.

### 3.3.3. $Sr^+$

In this subsection, we compare our static polarizability results for the  $Sr^+$  ion tabulated in Table M for the  $(5-8)S_{1/2}$ ,  $(5-7)P_{3/2,1/2}$  and  $(4-6)D_{5/2,3/2}$  states. Our estimated value for the  $5S_{1/2}$  state is in very good agreement with the relativistic RCC calculations given by Sahoo et al. [19], relativistic all-order values by Jiang et al. and Safranova [20, 22] and semi-empirical calculations by Mitroy et al. [21]. Along with the theoretical results, the ground state polarizability is also in agreement within error bars with the measurements by Barklem et al. and Nunkaew et al. [23, 24]. However, a considerable discrepancy of our polarizabilities for the  $4D$  states can be noticed with the values reported by Barklem et al. [23]. The origin of this discrepancy is mainly from the fact that core contribution is omitted in their calculations. Relativistic all-order calculations by Safranova et al. [22] are available for the  $(6-8)S$ ,  $(5-7)P$  and  $(4-6)D$  states and our values for these states exhibit good accord with them. Mitroy et al. [21] have also given polarizabilities for the

$6S$ ,  $(5 - 6)P$  and  $4D$  states which show slight disagreement with our values. However, our values are produced by using the relativistic all-order method and expected to be more accurate. Our polarizability values for the  $4D$  states are in agreement within uncertainty limits with the results reported in Refs. [19, 20, 31].

### 3.3.4. $Ba^+$

Table N tabulates the static polarizability results for the  $(6 - 8)S_{1/2}$ ,  $(6 - 8)P_{3/2,1/2}$  and  $5D_{5/2,3/2}$  states of  $Ba^+$ . For the ground state, our polarizability value of  $124 \pm 2$  a.u. is an excellent agreement with the high-precision measurement presented by Snow et al [27] based on the resonant excitation Stark ionization spectroscopy and with the radio frequency resonance measurement by Gallagher et al [28]. Also, our ground state polarizability value for ground state is in very good agreement with the value reported by Safronova et al. [26]. Along with this, our values for the  $6S_{1/2}$ ,  $5D_{3/2}$  and  $5D_{5/2}$  states are also compared with the RCC calculations by Sahoo et al. [19] and Barrett et al [25]. For ground state, the agreement is reasonable between our and their reported values. Similarly, for the  $5D_{5/2}$  state, our values match well with Sahoo et al. and Barrett et al. [19, 25] within uncertainty limits. However, our polarizability value for the  $5D_{3/2}$  state lies just outside the uncertainty limits of the value by Sahoo et al. [19]. Also, the non availability of the literature for the static polarizability values of other excited states restricts us from making comparison of our values for those states.

## 3.4. Static quadrupole polarizability

In this section we present the static quadrupole polarizabilities of  $Mg^+$ ,  $Ca^+$ ,  $Sr^+$  and  $Ba^+$  ions in Tables O, P, Q and R, respectively. We give the scalar polarizabilities of the ground and excited states as well as the tensor rank 2 component of polarizabilities for the states with  $J > 1/2$  of the above ions. In this case, there are also contributions to the states with  $J = 5/2$  [38]. Also, contributions from ‘Main’ and ‘Tail’ of the valence correlations, and core-valence and core correlations are enlisted in the same tables for all the considered ions. We have used our recommended set of E2 matrix elements and the experimental energies available in the NIST database to determine the ‘Main’ contributions. As can be seen from the above tables, the valence-core and ‘Tail’ contributions towards the total polarizabilities are very small in all investigated states of the ions. This is why we have evaluated them by using the DHF method. Since the core correlation contributions are little large, we have estimated them using RPA to account for the core-polarization correlation effects to all-order. We discuss the quadrupole polarizability values below for each ion.

### 3.4.1. $Mg^+$

Table O enlists the quadrupole static polarizability values for the  $3S_{1/2}$ ,  $3P_{3/2,1/2}$  and  $3D_{5/2,3/2}$  states of  $Mg^+$ . Its core correlation contribution is estimated to be  $0.52 \pm 0.03$  a.u. using RPA. As can be seen from the table that there are not much studies of these quantities are available in the literature for  $Mg^+$  to make rigorous comparison of our calculations. The only values available in the literature are for the polarizability of the  $3S_{1/2}$  state. Our value  $156.0 \pm 0.4$  a.u. for this ground state agrees perfectly with the values 156.1 a.u. reported by Mitroy et al. [16] using the diagonalization of semi-empirical Hamiltonian in a large-dimension single-electron basis. Also, an excellent agreement can be noticed between our value and the value  $156.02 \pm 1.27$  a.u. reported by Sahoo et al. [29] using the RCC method.

### 3.4.2. $\text{Ca}^+$

We present the static quadrupole polarizabilities of the  $4S_{1/2}$ ,  $4P_{3/2,1/2}$  and  $3D_{5/2,3/2}$  states of  $\text{Ca}^+$  in Table P. The RPA value for the core correlation came out to be  $6.9 \pm 0.3$  a.u.. The E2 polarizability values for the  $4S_{1/2}$  and  $4P_{1/2}$  states come only from the scalar component, whereas both the scalar as well as tensor rank 2 components are present in the E2 polarizabilities of the  $4P_{3/2}$  and  $3D_{5/2,3/2}$  states. However, the E2 polarizability of the  $3D_{5/2}$  state can also have contribution from the tensor rank 4 component. It can clearly be noticed that our value for the ground state quadrupole polarizability,  $874 \pm 9$  a.u., is in excellent agreement with the relativistic all-order value  $871 \pm 4$  a.u. reported by Safronova et al. [30] as well as with value  $875.1$  a.u. reported by Mitroy and Zhang [16]. No other data is available in the literature to compare our values for the  $4P_{3/2,1/2}$  and  $3D_{5/2,3/2}$  states. The values of the quadrupole polarizabilities reported for the  $4S$  and  $3D$  states in our previous work [38] were carried out using the SD and SDpT methods, whereas in present work we have used the recommended matrix elements based on criteria mentioned in Sec. 2.2 to improve their accuracies.

### 3.4.3. $\text{Sr}^+$

Table Q summarizes the static quadrupole polarizabilities of the  $5S_{1/2}$ ,  $5P_{3/2,1/2}$  and  $4D_{5/2,3/2}$  states of  $\text{Sr}^+$ . The core correlation contribution is estimated using RPA as  $17.1 \pm 0.9$  a.u.. Our quadrupole polarizability value  $1375 \pm 16$  a.u. of the ground state differs by 0.9 percent from the value of  $1346$  a.u. reported by Mitroy and Zhang [21]. Whereas, the comparison of our calculation with the value calculated by Jiang et al. [31] obtained using the relativistic semi-empirical approach and Safronova [22] calculated using the relativistic all-order method show very good agreements. Jiang et al. [31] have also reported the scalar components of the quadrupole polarizability for the  $5P_{3/2,1/2}$  and  $4D_{5/2,3/2}$  states. A very good agreement between our results for  $5P_{3/2,1/2}$  with [31] is noticed. However, the difference of approximately 1.8 percent can be found between our and their values for the  $4D_{3/2}$  state whereas the polarizability value for  $4D_{5/2}$  state matches within error bars with them. Our ground state polarizability value shows significant difference with the experimental value reported by Nunkaew et al. [24], who have used indirect spin-orbit K splittings techniques to obtain their result. Such discrepancy was also seen from another theoretical work by Jiang et al [31].

### 3.4.4. $\text{Ba}^+$

The static scalar quadrupole polarizability values for the  $6S_{1/2}$  and  $5D_{5/2,3/2}$  states of  $\text{Ba}^+$  are tabulated in Table R. The tensor contributions to the E2 polarizabilities of the  $5D_{5/2,3/2}$  states are also illustrated in the same table. The RPA value for the core contributions is obtained as  $46 \pm 2$  a.u. for  $\text{Ba}^+$ . Many calculations of the ground state quadrupole polarizability of this ion are reported by different groups by using a variants of many-body methods. Our ground-state scalar quadrupole polarizability value of came out to be  $4192 \pm 47$  a.u., which is in perfect agreement with the value of  $4182 \pm 34$  a.u. within uncertainty limits reported by Iskrenova et al. [26]. However, a slight difference can be noticed between our value and the value reported by Safronova [80]. The corresponding experimental result is reported as  $4420 \pm 250$  a.u. by Snow et al. [27] and it is very clear that our value lies within the uncertainty of this measurement. The value of our scalar quadrupole polarizability for the  $5D_{3/2}$  state lies very well within the uncertainty limits of the value provided by Sahoo et al. [32], whereas the value for the  $5D_{5/2}$  and  $6S_{1/2}$  states are found to be close to the uncertainty limits. Hence, the accuracy of our results is emphasized as to be reliable.

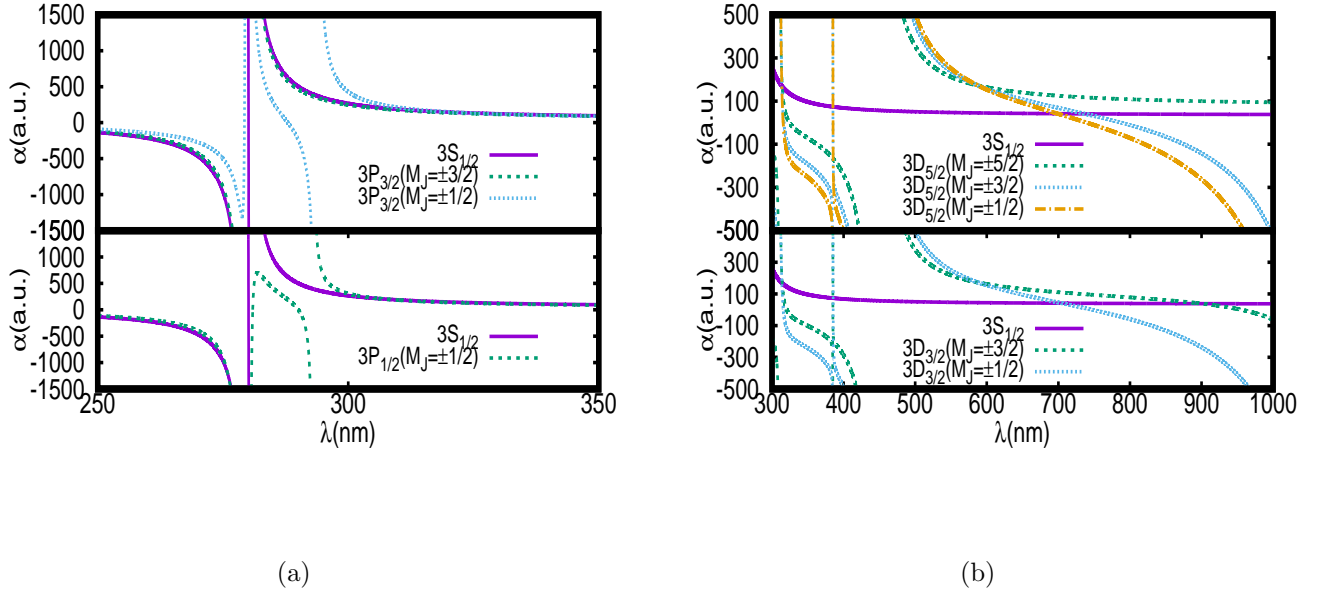


**Fig. 1:** Plots depicting dynamic E1 polarizabilities of (a) the ground  $3S_{1/2}$  and excited  $3P_{3/2,1/2}$  states, and (b) the ground  $3S_{1/2}$  and excited  $3D_{5/2,3/2}$  states in  $Mg^+$  for the linearly polarized light. The crossings of polarizability curves between two resonances correspond to the magic wavelengths.

### 3.5. Magic and tune-out wavelengths

We now discuss here magic and tune-out wavelengths inferred for the  $Mg^+$ ,  $Ca^+$ ,  $Sr^+$  and  $Ba^+$  ions. For this purpose, we have evaluated the dynamic E1 polarizabilities of the atomic states of interest for a wide range of wavelengths. Since these dynamic polarizabilities are evaluated by adopting the same procedure as the static E1 polarizabilities that were discussed in the previous sub-section, we anticipate that the dynamic E1 polarizabilities are of similar accuracies with the static values. As mentioned earlier, we have assumed that the external electric field is linearly polarized for the determination of these E1 polarizabilities, and at the  $\lambda_T$  values the dynamic E1 polarizabilities of a given atomic state vanish while the differential dynamic E1 polarizabilities of an atomic transition nullify at the  $\lambda_{\text{magic}}$  values. We present both the  $\lambda_T$  and  $\lambda_{\text{magic}}$  values for each of the considered ion below.

#### 3.5.1. $Mg^+$

In Table S, we list the magic wavelengths for the  $3S_{1/2}-3P_{3/2,1/2}$  and  $3S_{1/2}-3D_{5/2,3/2}$  transitions of  $Mg^+$  at different  $M_J$  sublevels. These values are inferred from the plots of dynamic polarizabilities as shown in Figs. 1(a) and 1(b). As can be seen from the table and figures that the magic wavelength at  $276.1 \pm 0.7$  nm has large negative polarizability which is  $-1266$  a.u.. It means that it can support blue detuned trap to conduct an experiment at this wavelength to reduce systematics due to the Stark effect. Similarly, the magic wavelengths at the  $307 \pm 2$  nm for the  $3S_{1/2}-3P_{1/2}$  transition and at the  $324 \pm 3$  nm for the  $3S_{1/2}-3P_{3/2}$  transition support the red detuned trap. Also six  $\lambda_{\text{magic}}$  values are observed for the  $3S_{1/2}-3D_{3/2}$  transition between different resonances. Out of them two at  $385.011 \pm 0.003$  nm and  $385.376 \pm 0.003$  nm are found to be very close to the  $3D_{3/2}-5P_{1/2}$  resonance. For the magic wavelengths at  $705 \pm 1$  nm and  $901 \pm 3$  nm, the polarizabilities are very small which make these wavelengths of less practical importance. Again, for

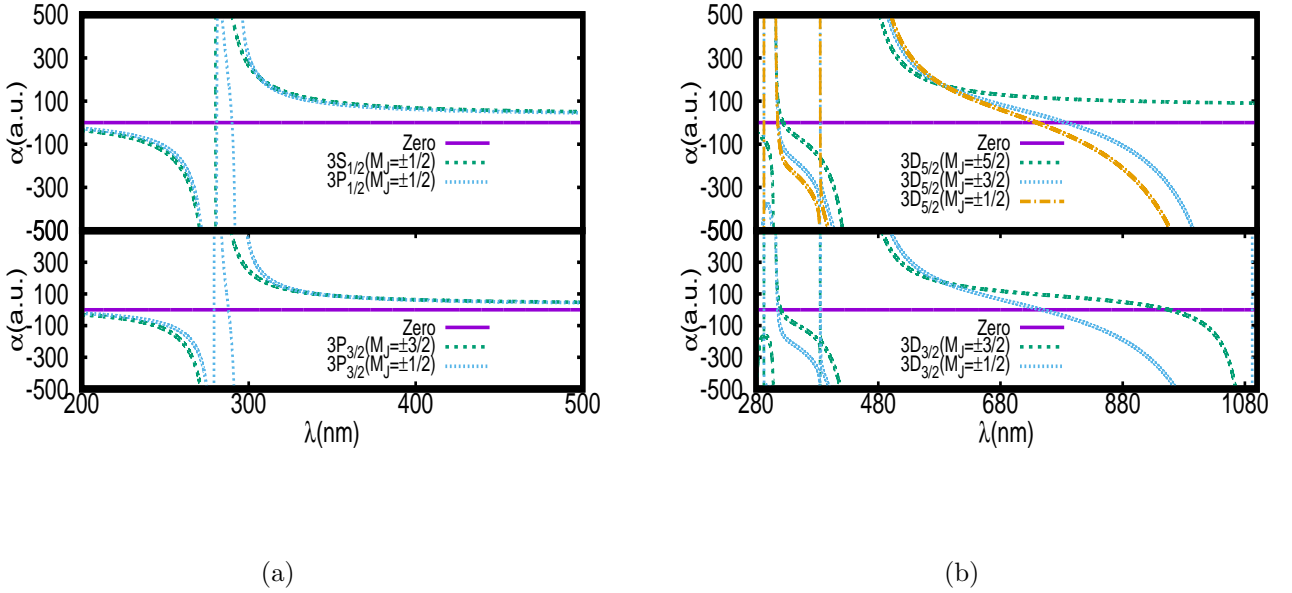


**Fig. 2:** Plots for the dynamic E1 polarizabilities of (a) the ground  $3S_{1/2}$  and  $3P_{3/2,1/2}$  states, and (b) the  $3D_{5/2,3/2}$  states in  $\text{Mg}^+$  for the linearly polarized light. The crossings of the dynamic dipole polarizability curves with zero depict the tune-out wavelengths.

the  $3S_{1/2} - 3D_{5/2}$  transition, seven magic wavelengths are found. Out of these, three magic wavelengths lie very close to the  $3D_{5/2} - 5F_{5/2}$  transition and two other at  $385.121 \pm 0.003$  nm and  $385.170 \pm 0.003$  nm are in the close vicinity of resonant transition  $3D_{5/2} - 5P_{3/2}$ . It can be noticed that most of the magic wavelengths of  $\text{Mg}^+$  support very shallow red detuned traps.

In Table W, we have illustrated the tune-out wavelengths for the  $nS_{1/2}$ ,  $nP_{3/2,1/2}$  and  $nD_{5/2,3/2}$  states of  $\text{Mg}^+$  with  $n = 3$ . These values are inferred from Figs. 2(a) and 2(b). We have presented the cancellation of all contributions to the polarizabilities of the  $3S_{1/2}$  and  $3P_{3/2,1/2}$  states at  $\lambda_T$  in Fig. 2(a). The  $\lambda_T$  values at  $280.110 \pm 0.009$  nm and at  $280.95 \pm 0.04$  nm of the  $3S_{1/2}$  and  $3P_{1/2}$  states, respectively, lie close to the  $3P_{1/2} - 3S_{1/2}$  resonance. For the  $3P_{1/2}$  state, the  $\lambda_T$  value at  $290.05 \pm 0.06$  nm can be found between the  $3P_{1/2} - 3S_{1/2}$  and  $3P_{1/2} - 4S_{1/2}$  resonances. All these tune-out wavelengths including those for the  $3P_{3/2}$  state lie in ultraviolet region so are of less practical use. Further, Fig. 2(b) exhibits the tune-out wavelengths for the  $3D_{5/2,3/2}$  states. For the  $3D_{3/2}$  state, the  $\lambda_T$  values at  $385.04 \pm 0.01$  nm and  $385.42 \pm 0.01$  nm are very near to the  $3D_{3/2} - 5P_{1/2}$  resonance whereas the one at  $747 \pm 2$  nm lie well within the visible region. Hence, the latter one appears to gain the experimental importance. The  $\lambda_T$  at  $955 \pm 2$  nm falls in the infrared region. Similarly for the  $3D_{5/2}$  state, the tune-out wavelengths at  $385.17 \pm 0.01$  nm and  $385.21 \pm 0.01$  nm are in the close vicinity of the  $3D_{5/2} - 5P_{3/2}$  transition at  $384.93$  nm, whereas  $\lambda_{TS}$  at  $739 \pm 2$  nm lies in the visible region.

### 3.5.2. $\text{Ca}^+$

Table T enlists our evaluated magic wavelengths for the  $4S_{1/2} - 4P_{3/2,1/2}$  and  $4S_{1/2} - 3D_{5/2,3/2}$  transitions of  $\text{Ca}^+$ , which are graphically presented in Figs. 3(a) and 3(b), respectively. Our results are compared with the available theoretical relativistic structure model calculations of Tang et.al. [15], RCICP calculations by Jiang et al. [33] and experimental results of Liu et al. [34]. A total of three magic wavelengths are located for the  $4S_{1/2} - 4P_{1/2}$  transition at

$368.08 \pm 0.04$  nm,  $395.18 \pm 0.02$  nm and  $693 \pm 2$  nm between the  $4P_{1/2} - 4D_{3/2}$ ,  $4P_{1/2} - 5S$ ,  $4P_{1/2} - 4S$  and  $4P_{1/2} - 3D_{3/2}$  resonant transitions. As can be clearly noticed that the our results are in excellent agreement with the results given by Tang et al. [15] and Jiang et al. [33] for magic wavelengths at  $368.08 \pm 0.04$  nm and  $395.18 \pm 0.02$  nm. However,  $693 \pm 2$  nm shows a slight difference with Tang et al. [15] whereas, this value is in perfect agreement and well within the uncertainty bars with the result provided by Jiang et al. [33]. Similarly, many  $\lambda_{\text{magic}}$  values are noticed for the  $4S_{1/2} - 4P_{3/2}$  transition. Among these the magic wavelengths at  $369.75 \pm 0.05$  nm,  $395.77 \pm 0.02$  nm,  $396.23 \pm 0.01$  nm are in very good accord with the results from Ref. [15] as well as Ref. [33]. The  $\lambda_{\text{magic}}$  at  $674 \pm 4$  nm and  $690 \pm 3$  nm are also in perfect accord with the calculations by Jiang et al. [33] within error bars but our values are slightly red detuned as compared to the values quoted in Ref. [15]. Our results indicate that  $\lambda_{\text{magic}}$ s at  $395.77 \pm 0.02$  nm and  $396.23 \pm 0.01$  nm are within the fine-structure splittings of the  $4P$  states, which are supported by the experimental measurements by Liu et al. [34] with magic wavelengths at  $395.7992 \pm 0.0007$  and  $395.7990 \pm 0.0007$  nm respectively. However, Ref. [15] have missed the magic wavelengths at  $850.117 \pm 0.006$  nm and  $850.92 \pm 0.02$  nm between the resonance  $4P_{3/2} - 3D_{3/2}$  and  $4P_{3/2} - 3D_{5/2}$  whereas these values from our calculations match very well with the values of Ref. [33]. It is clear that both for the  $4S_{1/2} - 3D_{3/2}$  and  $4S_{1/2} - 3D_{5/2}$  transitions, there is a single crossing of polarizability curves at  $395.79 \pm 0.01$  nm for all the magnetic sublevels. But, the values of polarizabilities are extremely small due to which this magic wavelength is not a good choice for experiments. The other  $\lambda_{\text{magic}}$ s at  $1288 \pm 3$  nm,  $1065 \pm 3$  nm and  $1312 \pm 2$  nm are blue detuned compared to the results presented in Ref. [15] but are in good agreement within uncertainty limits with the values in Ref. [33]. The large positive value of polarizability which is 2935 a.u., can be noticed for the  $\lambda_{\text{magic}}$  at  $395.18 \pm 0.02$  nm for the  $4S_{1/2} - 4P_{1/2}$  transition making them a good choice for red detuned traps.

Table W summarizes the tune-out wavelengths for  $nS_{1/2}$ ,  $nP_{3/2,1/2}$  and  $(n-1)D_{5/2,3/2}$  states of  $\text{Ca}^+$  with  $n = 4$ . The graphical representation of these tune-out wavelengths can be seen from Figs. 4(a) and 4(b). The tune-out wavelengths for the  $4S_{1/2}$  and  $4P_{3/2,1/2}$  can be seen in Fig. 4(a). The polarizability for the  $4S_{1/2}$  state vanishes at  $395.80 \pm 0.02$  nm which is in the visible region and lies very adjacent to the  $4P_{1/2} - 4S_{1/2}$  resonance. The  $\lambda_{\text{TS}}$  at  $364.13 \pm 0.07$  nm and  $431.60 \pm 0.85$  nm for the  $4P_{1/2}$  state along with  $\lambda_{\text{TS}}$  at  $365.46 \pm 0.07$  nm and  $453 \pm 1$  nm for the  $4P_{3/2}$  state occur away from the resonant transitions. However,  $850.120 \pm 0.009$  nm and  $850.900 \pm 0.009$  nm are very close to the  $4P_{3/2} - 3D_{3/2}$  resonance and are in infrared region. In a similar way, Fig. 4(b) exhibits that the tune-out wavelength at  $850.36 \pm 0.02$  nm for the  $3D_{3/2}$  state is adjacent to the  $4P_{3/2} - 3D_{3/2}$  resonance and is in infrared region. Whereas other  $\lambda_{\text{TS}}$  at  $433 \pm 7$  nm and  $647 \pm 7$  nm for the  $3D_{3/2}$  state and at  $423 \pm 9$  nm and  $468 \pm 8$  nm for the  $3D_{5/2}$  state fall well within the visible range of electromagnetic spectra.

### 3.5.3. $\text{Sr}^+$

The calculated  $\lambda_{\text{magic}}$ s for the  $5S - 5P_{1/2}$  and  $5S - 4D_{5/2,3/2}$  transitions of  $\text{Sr}^+$  are presented in Table U by locating at the crossings of the polarizability curves for the considered states as shown in Figs. 5(a) and 5(b). The polarizability values at the respective magic wavelengths along with different resonant lines are also listed in the same table. The only magic wavelength available for the  $5S - 5P_{1/2}$  transition at  $767 \pm 2$  nm is in good agreement with the value reported by Jiang et al. [31], who have used relativistic semi-empirical-core-potential approach using Laguerre and Slater spinors to determine it. However, a series of magic wavelengths for the  $5S - 5P_{3/2}$  transition are located between various resonances. The  $\lambda_{\text{magic}} = 438.5 \pm 0.2$  nm matches excellently with the value given by [31]. The values of polarizabilities for all the

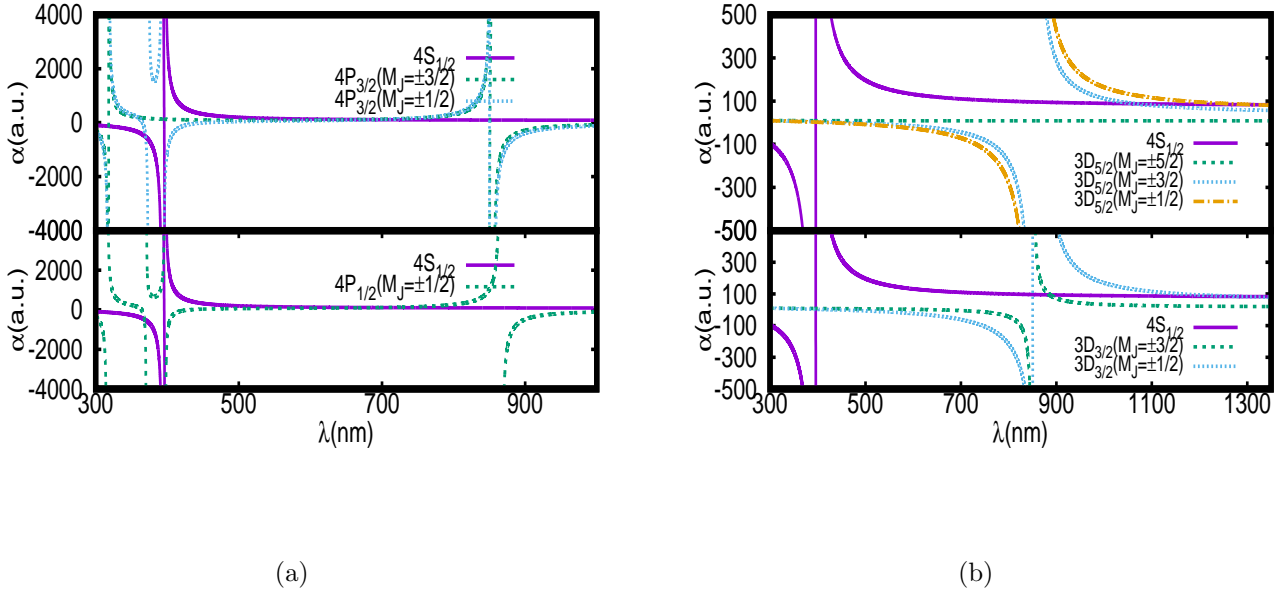


**Fig. 3:** Plots depicting dynamic E1 polarizabilities of (a) the ground  $4S_{1/2}$  and excited  $4P_{3/2,1/2}$  states, and (b) the ground  $4S_{1/2}$  and excited  $3D_{5/2,3/2}$  states in  $\text{Ca}^+$  for the linearly polarized light. The crossings of polarizability curves between two resonances correspond to the magic wavelengths.

$\lambda_{\text{magic}}$  are very small except for the magic wavelength at  $419.31 \pm 0.04$  nm, which has a very large negative value of polarizability  $-1526$  a.u.. Hence, it is very useful for trapping  $\text{Sr}^+$  ion using blue detuned traps. Some other  $\lambda_{\text{magic}}$ s at  $713 \pm 2$  nm and  $722 \pm 2$  nm arise due to gradual increase in the  $5S_{1/2}$  state polarizability and the gradual decrease in the  $5P_{3/2}$  state polarizability when the wavelength approaches the  $5S - 5P_j$  resonant wavelength. Similarly, two  $\lambda_{\text{magic}}$ s at  $1004.47 \pm 0.05$  nm and  $\lambda_{\text{magic}}=1009.8 \pm 0.1$  nm lie in the infrared region and they are recommended for the red detuned traps. All of these  $\lambda_{\text{magic}}$  values, at  $713 \pm 2$  nm,  $722 \pm 2$  nm,  $1004.47 \pm 0.05$  nm and  $1009.8 \pm 0.1$  nm, are in close agreement with the values reported in Ref. [31]. For the  $\lambda_{\text{magic}}$ s at  $416.99 \pm 0.06$  nm and  $417.01 \pm 0.06$  nm for the  $5S - 4D$  transitions, the associated polarizability values are extremely small, so are of limited experimental use.  $\lambda_{\text{magic}}$  at  $1085$  nm, which is in good accord with the values calculated in Ref. [31], is in vicinity of the  $4D_{3/2} - 5P_{3/2}$  resonant transition.

We have also provided the tune-out wavelengths for the  $nS_{1/2}$ ,  $nP_{3/2,1/2}$  and  $(n-1)D_{5/2,3/2}$  states of  $\text{Sr}^+$  with  $n = 5$  by plotting dynamic polarizabilities in the Figs. 6(a) and 6(b). These values are also tabulated in Table W. The graphical representation of the tune-out wavelengths for the  $5S_{1/2}$  and  $5P_{3/2,1/2}$  states is given in Fig. 6(a). It can be inferred from the figure that for the  $5P_{3/2,1/2}$  states two  $\lambda_{\text{TS}}$ s at  $1004.43 \pm 0.05$  nm and  $1009.37 \pm 0.12$  nm lie in infrared region whereas other tune-out wavelengths lie in the visible region. Similarly, it can be noticed from Fig. 6(b) that all the  $\lambda_{\text{TS}}$ s for the  $4D_{3/2}$  and  $4D_{5/2}$  states are in visible region except  $1005.67 \pm 0.16$  nm which is in the infrared region.

### 3.5.4. $\text{Ba}^+$

The magic wavelengths for the  $\text{Ba}^+$  presented in Figs. 7(a) and 7(b) are summarized in Table V. Four  $\lambda_{\text{magic}}$  are found for the  $6S_{1/2} - 6P_{1/2}$  transition in  $\text{Ba}^+$  at  $323 \pm 2$  nm,  $451.72 \pm 0.04$  nm,  $468.9 \pm 0.3$  nm and  $599 \pm 1$  nm with  $\lambda_{\text{magic}}$  at  $451.72 \pm 0.04$  nm yielding a very large negative value of polarizability  $-4557$  a.u. which makes it a useful wavelength for

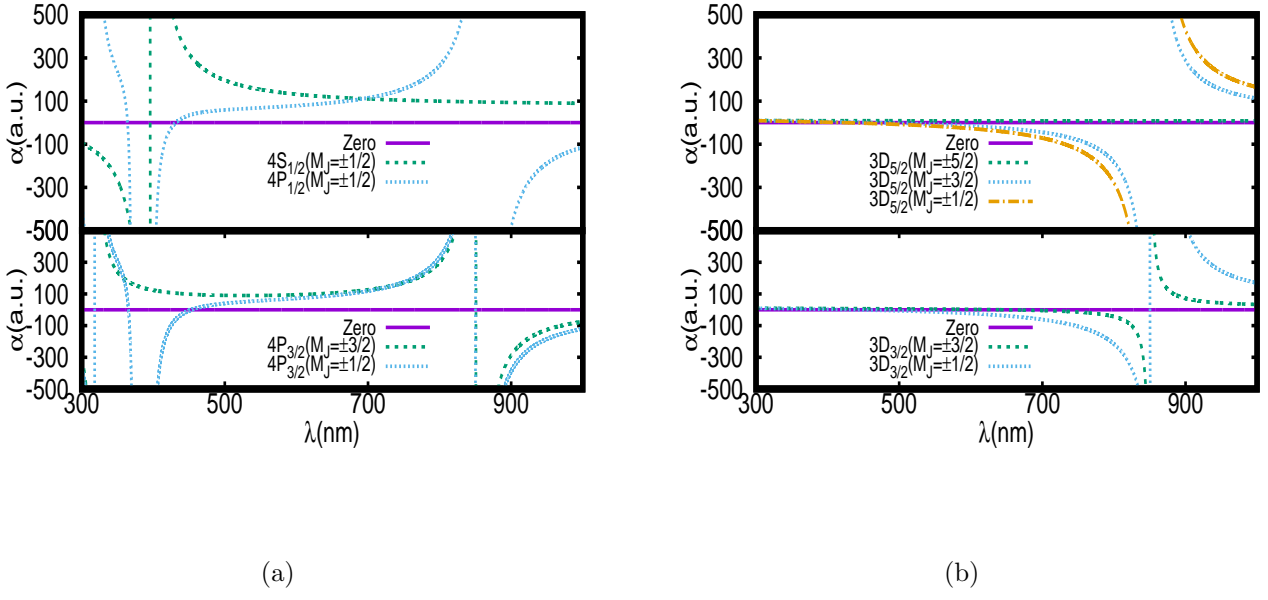


**Fig. 4:** Plots for the dynamic E1 polarizabilities of (a) the ground  $4S_{1/2}$  and  $4P_{3/2,1/2}$  states, and (b) the  $3D_{5/2,3/2}$  states in  $\text{Ca}^+$  for the linearly polarized light. The crossings of the dynamic dipole polarizability curves with zero depict the tune-out wavelengths.

trapping  $\text{Ba}^+$ . Also, the  $\lambda_{\text{magic}}$   $468.9 \pm 0.3$  carries significant value of polarizability. We also identify at least five  $\lambda_{\text{magic}}$  for the  $6S_{1/2} - 6P_{3/2}$  transition between various resonant transitions. Out of these, magic wavelengths around 416 nm,  $552 \pm 2$  nm and  $561 \pm 1$  nm hold reasonably large values of polarizability. Similarly, several  $\lambda_{\text{magic}}$ s are also located for the  $6S - 5D_{3/2}$  and  $6S - 5D_{5/2}$  transitions in the wavelength range  $300 - 800$  nm. Among these, the wavelengths around 480 nm are of negligible use due to very small values of associated polarizability. Some other  $\lambda_{\text{magic}}$ s at  $585.99 \pm 0.05$  nm,  $592.5 \pm 0.2$  nm,  $766 \pm 4$  nm,  $665 \pm 2$  nm and  $713 \pm 3$  nm are also presented with comparatively good values of polarizabilities.

Along with this, the tune-out wavelengths are shown graphically in Figs. 8(a) and 8(b) for the  $nS_{1/2}$ ,  $nP_{3/2,1/2}$  and  $(n-1)D_{5/2,3/2}$  states of  $\text{Ba}^+$  with  $n = 6$  and they are also tabulated in Table W. It can be inferred from Fig. 8(a) that the only  $\lambda_T$  at  $480.63 \pm 0.24$  nm for  $6S_{1/2}$  occurs between the  $6P_{1/2} - 6S_{1/2}$  and  $6P_{1/2} - 7S_{1/2}$  resonances and is in the visible region. Along with it, we find three  $\lambda_T$ s for the  $6P_{1/2}$  state at  $444.06 \pm 0.17$  nm,  $526.29 \pm 0.80$  nm in visible region and  $1071 \pm 6$  nm in infrared region. For the  $6P_{3/2}$  state,  $\lambda_T$ s at  $585.88 \pm 0.04$  nm and  $589.50 \pm 0.07$  nm lie very close to the  $6P_{3/2} - 5D_{3/2}$  resonance. Two  $\lambda_T$ s lie in the vicinity of the  $6P_{3/2} - 6D_{3/2}$  resonance at  $416.65 \pm 0.01$  nm and  $416.00 \pm 0.01$  nm. In the visible region, there are two tune-out wavelengths at  $731 \pm 5$  nm and  $785 \pm 5$  nm for this state. In a similar way, Fig. 8(b) presents the  $\lambda_T$ s for the  $5D_{3/2}$  and  $5D_{5/2}$  states. A total of 5 tune-out wavelengths were found for these two states in the considered wavelength range, and all of them are in the visible region.

### 3.6. Dynamic quadrupole polarizabilities

Here, we discuss the dynamic quadrupole polarizabilities of the ground  $nS_{1/2}$  and metastable  $(n-1)D_{5/2,3/2}$  states of  $\text{Ca}^+$ ,  $\text{Sr}^+$  and  $\text{Ba}^+$  ions for the principal quantum number  $n$  of the respective ion using Eqs. (16)-(23). It should be noted that for the  $nS_{1/2}$  states only the scalar part contributes, whereas for the  $(n-1)D_{3/2}$  and the  $(n-1)D_{5/2}$  states, both the scalar and tensor components contribute to the total values of quadrupole polarizabilities.

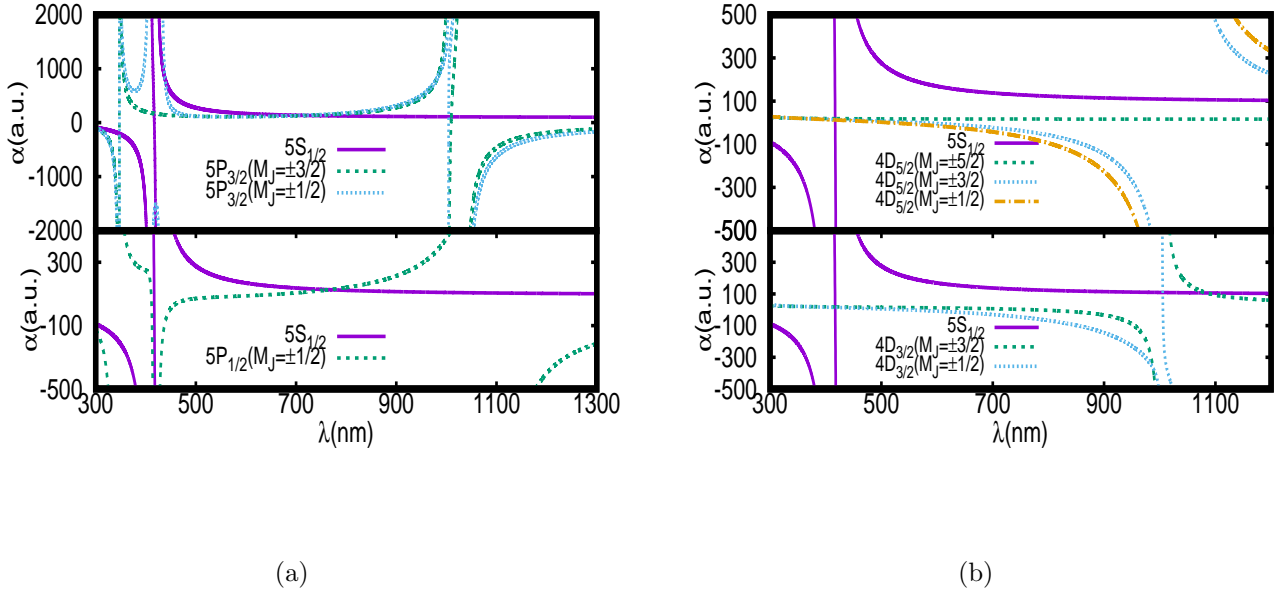


**Fig. 5:** Plots depicting dynamic E1 polarizabilities of (a) the ground  $5S_{1/2}$  and excited  $5P_{3/2,1/2}$  states, and (b) the ground  $5S_{1/2}$  and excited  $4D_{5/2,3/2}$  states in  $Sr^+$  for the linearly polarized light. The crossings of polarizability curves between two resonances correspond to the magic wavelengths.

The dynamic quadrupole polarizabilities of  $Ca^+$ ,  $Sr^+$  and  $Ba^+$  for the  $nS_{1/2}$  and  $(n-1)D_{3/2}$  states are shown in Fig. 9(a) for the wavelength range from 300 nm to 1300 nm. In the case of the  $(n-1)D_{3/2}$  states,  $\alpha_n^q$  is zero. The quadrupole polarizability for these states need to be determined separately for the cases with  $M_J = \pm 1/2$  and  $M_J = \pm 3/2$  owing to the presence of the tensor contributions to the total quadrupole polarizabilities of the  $D_{3/2}$  states. As shown in Fig. 9(a), in the considered wavelength range, the  $4S_{1/2}$  state quadrupole polarizability for  $Ca^+$  has two E2 resonances in the  $3D_{3/2} - 4S_{1/2}$  and  $3D_{5/2} - 4S_{1/2}$  transitions at 732.389 and 729.147 nm, respectively. Thus, the quadrupole polarizability for the  $4S_{1/2}$  state diverges at these two wavelength values. The  $3D_{3/2} - 4S_{1/2}$  resonant transition also contributes to the quadrupole polarizability of the  $3D_{3/2}(M_J = \pm 1/2)$  level. As a result, quadrupole polarizabilities for the  $4S_{1/2}$  and  $3D_{3/2}(M_J = \pm 1/2)$  levels are large but they have opposite signs in the vicinity of this resonance. However, for the  $3D_{3/2}(M_J = \pm 3/2)$  level, when  $\alpha_n^q = \alpha_{n0}^q + \alpha_{n2}^q$ , the  $3D_{3/2} - n'S_{1/2}$  transitions, with  $n'$  referring to higher excited quantum number, do not contribute to the total quadrupole polarizability of the  $3D_{3/2}$  state owing to the exact cancellation of the scalar  $\alpha_{n0}^q$  and tensor  $\alpha_{n2}^q$  contributions from the  $3D_{3/2} - n'S_{1/2}$  transitions as can be understood using Eq. (17). In this case, the  $W_{n,k}^{q(2)}$  factor of Eq. (22) is exactly equal to  $-W_n^{q(0)}$  of Eq. (21) leading to exact cancellation of the contributions from the  $3D_{3/2} - n'S_{1/2}$  transitions, and contributions to the total polarizability comes only from the  $3D_{3/2} - n'D_{5/2,3/2}$  and  $3D_{3/2} - n'G_{9/2,7/2}$  transitions, which do not cancel out and are small. As a result, there is no resonance for the  $M_J = \pm 3/2$  case at the wavelength corresponding to the  $3D_{3/2} - 4S_{1/2}$  transition leading to a straight quadrupole polarizability curve for this state (shown in blue dotted curve in Fig. 9(a)). A similar trend in the quadrupole polarizability for  $Sr^+$  ion is expected with two E2 resonances appearing in ground state polarizability between the 300-1300 nm range, the  $4D_{3/2} - 5S_{1/2}$  transition at 686.8171 nm and the  $4D_{5/2} - 5S_{1/2}$  transition at 673.8392 nm. The quadrupole polarizability for the  $4D_{3/2}(M_J = \pm 1/2)$  level is small in this range except

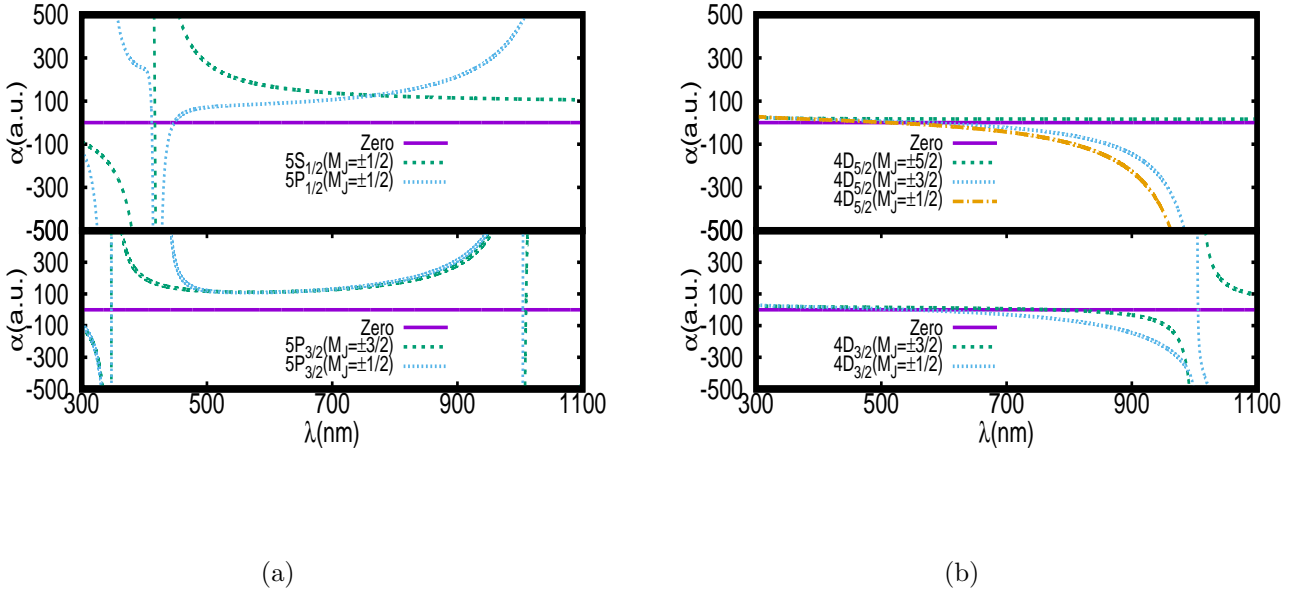


**Fig. 6:** Plots for the dynamic E1 polarizabilities of (a) the ground  $5S_{1/2}$  and  $5P_{3/2,1/2}$  states, and (b) the  $4D_{5/2,3/2}$  states in  $Sr^+$  for the linearly polarized light. The crossings of the dynamic dipole polarizability curves with zero depict the tune-out wavelengths.

in the close vicinity of the  $4D_{3/2} - 5S_{1/2}$  transition. For  $Sr^+$  ion as well, the  $4D_{3/2} - 5S_{1/2}$  transition does not contribute to the quadrupole polarizability of the  $4D_{3/2}(M_J = \pm 3/2)$  level. The case for the quadrupole polarizability of  $Ba^+$  is different. We did not find any E2 resonant transitions for the  $6S_{1/2}$  and  $5D_{3/2}$  states in the considered wavelength range. The corresponding quadrupole polarizability is generally not as high as it is for the other two ions in the considered wavelength range.

In Fig. 9(b), the dynamic quadrupole polarizabilities of the  $nS_{1/2}$  and  $(n-1)D_{5/2}$  states, with principal quantum number  $n$ , of the considered ions are presented. In this case, the rank four component of the tensor quadrupole polarizabilities are also involved. The polarizability curves for different values of  $M_J$  ( $1/2$ ,  $3/2$  and  $5/2$ ) are separately shown in the above figure. It can be noticed that the polarizability curves for  $J = 5/2$  exhibit same trend as that for  $J = 3/2$ . The quadrupole polarizability curve for  $M_J = \pm 5/2$  almost overlaps with the polarizability curve for  $M_J = \pm 3/2$  in the  $Ca^+$ ,  $Sr^+$  and  $Ba^+$  ions. There is no E2 resonance line found for the  $Ba^+$  ion in the considered wavelength range and it does not attain a very large value anywhere in this range.

Table A: Reduced E2 matrix elements (in a.u.) of  $Mg^+$  from the DHF, SD and SDpT methods, whereas the label “sc” indicates the scaled values. The second last and the last columns list the recommended  $O^{\text{Final}}$  values of the matrix elements and their absolute uncertainties, respectively.

Transition	$O^{\text{DHF}}$	$O^{\text{SD}}$	$O_{\text{sc}}^{\text{SD}}$	$O^{\text{SDpT}}$	$O_{\text{sc}}^{\text{SDpT}}$	$O^{\text{Final}}$	$\delta$
$3P_{3/2} - 3P_{1/2}$	12.721	12.309	12.312	12.309	12.311	12.312	0.003
$3D_{5/2} - 3S_{1/2}$	12.516	12.092	12.094	12.093	12.094	12.094	0.001
$3D_{5/2} - 4S_{1/2}$	37.631	36.804	36.800	36.808	36.799	36.800	0.008
$3D_{3/2} - 3S_{1/2}$	10.219	9.873	9.875	9.874	9.876	9.875	0.001

$3D_{3/2} - 4S_{1/2}$	30.727	30.051	30.047	30.055	30.046	30.047	0.008
$3D_{3/2} - 3D_{5/2}$	17.732	17.297	17.294	17.299	17.293	17.294	0.005
$4P_{1/2} - 3P_{3/2}$	9.243	9.004	9.004	9.005	9.007	9.004	0.003
$4P_{3/2} - 3P_{1/2}$	9.179	8.940	8.944	8.941	8.943	8.944	0.003
$4P_{3/2} - 3P_{3/2}$	9.220	8.981	8.983	8.982	8.985	8.983	0.002
$4P_{3/2} - 4P_{1/2}$	61.083	59.845	59.851	59.846	59.852	59.851	0.005
$5S_{1/2} - 3D_{5/2}$	13.748	13.602	13.594	13.603	13.593	13.594	0.009
$5S_{1/2} - 3D_{3/2}$	11.226	11.107	11.098	11.108	11.099	11.09	0.01
$4D_{5/2} - 3S_{1/2}$	2.395	2.336	2.335	2.336	2.334	2.335	0.001
$4D_{5/2} - 4S_{1/2}$	48.544	47.456	47.469	47.463	47.468	47.469	0.006
$4D_{5/2} - 3D_{5/2}$	26.595	26.142	26.141	26.146	26.139	26.141	0.005
$4D_{5/2} - 3D_{3/2}$	13.298	13.072	13.070	13.074	13.069	13.070	0.004
$4D_{5/2} - 5S_{1/2}$	142.709	140.441	140.430	140.448	140.429	140.43	0.02
$4D_{3/2} - 3S_{1/2}$	1.956	1.907	1.906	1.908	1.907	1.906	0.002
$4D_{3/2} - 4S_{1/2}$	39.634	38.746	38.760	38.752	38.759	38.760	0.008
$4D_{3/2} - 3D_{5/2}$	13.296	13.070	13.071	13.072	13.070	13.071	0.001
$4D_{3/2} - 3D_{3/2}$	20.313	19.967	19.965	19.970	19.964	19.965	0.005
$4D_{3/2} - 5S_{1/2}$	116.526	114.674	114.657	114.680	114.656	114.65	0.02
$4D_{3/2} - 4D_{5/2}$	71.557	70.374	70.363	70.378	70.361	70.36	0.02
$4F_{5/2} - 3P_{1/2}$	15.335	14.731	14.736	14.730	14.735	14.736	0.006
$4F_{5/2} - 3P_{3/2}$	8.223	7.901	7.902	7.900	7.903	7.902	0.002
$4F_{5/2} - 4P_{1/2}$	81.751	80.550	80.561	80.554	80.562	80.561	0.007
$4F_{5/2} - 4P_{3/2}$	43.744	43.104	43.107	43.106	43.109	43.107	0.002
$4F_{7/2} - 3P_{3/2}$	20.142	19.353	19.356	19.352	19.354	19.356	0.004
$4F_{7/2} - 4P_{3/2}$	107.151	105.584	105.591	105.589	105.594	105.591	0.003
$5P_{1/2} - 3P_{3/2}$	2.888	2.826	2.828	2.827	2.830	2.828	0.002
$5P_{1/2} - 4P_{3/2}$	36.489	35.839	35.835	35.840	35.836	35.835	0.005
$5P_{1/2} - 4F_{5/2}$	85.569	86.242	86.243	86.252	86.244	86.243	0.009
$5P_{3/2} - 3P_{1/2}$	2.881	2.818	2.819	2.817	2.820	2.819	0.002
$5P_{3/2} - 3P_{3/2}$	2.887	2.825	2.824	2.826	2.828	2.824	0.004
$5P_{3/2} - 4P_{1/2}$	36.249	35.593	35.604	35.594	35.606	35.60	0.01
$5P_{3/2} - 4P_{3/2}$	36.394	35.742	35.744	35.743	35.747	35.744	0.003
$5P_{3/2} - 4F_{5/2}$	45.691	46.050	46.054	46.055	46.057	46.054	0.003
$5P_{3/2} - 4F_{7/2}$	111.921	112.801	112.810	112.814	112.812	112.810	0.004
$5P_{3/2} - 5P_{1/2}$	183.356	180.576	180.590	180.581	180.591	180.590	0.009
$6S_{1/2} - 3D_{5/2}$	3.956	3.896	3.895	3.897	3.894	3.895	0.002
$6S_{1/2} - 3D_{3/2}$	3.230	3.181	3.180	3.182	3.183	3.180	0.003
$6S_{1/2} - 4D_{5/2}$	51.803	51.368	51.335	51.361	51.334	51.33	0.02

$6S_{1/2} - 4D_{3/2}$	42.303	41.947	41.909	41.942	41.908	41.91	0.03
$5D_{5/2} - 3S_{1/2}$	0.931	0.908	0.907	0.909	0.910	0.907	0.003
$5D_{5/2} - 4S_{1/2}$	11.281	11.110	11.107	11.111	11.109	11.107	0.004
$5D_{5/2} - 3D_{5/2}$	7.043	6.913	6.912	6.914	6.911	6.912	0.002
$5D_{5/2} - 3D_{3/2}$	3.522	3.457	3.456	3.458	3.455	3.456	0.002
$5D_{5/2} - 5S_{1/2}$	128.245	125.989	126.032	126.012	126.031	126.03	0.02
$5D_{5/2} - 4D_{5/2}$	86.264	85.117	85.109	85.122	85.107	85.11	0.01
$5D_{5/2} - 4D_{3/2}$	43.137	42.563	42.550	42.565	42.549	42.55	0.02
$5D_{5/2} - 6S_{1/2}$	374.904	370.206	370.183	370.216	370.182	370.18	0.03
$5D_{3/2} - 3S_{1/2}$	0.760	0.742	0.741	0.742	0.740	0.741	0.001
$5D_{3/2} - 4S_{1/2}$	9.211	9.072	9.068	9.073	9.069	9.068	0.005
$5D_{3/2} - 3D_{5/2}$	3.521	3.547	3.456	3.458	3.455	3.456	0.002
$5D_{3/2} - 3D_{3/2}$	5.379	5.280	5.279	5.281	5.278	5.279	0.002
$5D_{3/2} - 5S_{1/2}$	104.706	102.864	102.911	102.883	102.910	102.91	0.03
$5D_{3/2} - 4D_{5/2}$	43.128	42.555	42.558	42.559	42.557	42.558	0.001
$5D_{3/2} - 4D_{3/2}$	65.887	65.011	65.001	65.015	65.000	65.00	0.01
$5D_{3/2} - 6S_{1/2}$	306.117	302.280	302.243	302.289	302.242	302.24	0.04
$5D_{3/2} - 5D_{5/2}$	192.806	190.347	190.324	190.350	190.322	190.32	0.02
$5F_{5/2} - 3P_{1/2}$	7.634	7.433	7.435	7.434	7.437	7.435	0.002
$5F_{5/2} - 3P_{3/2}$	4.089	3.982	3.982	3.984	3.985	3.982	0.003
$5F_{5/2} - 4P_{1/2}$	23.865	22.238	22.245	22.233	22.246	22.24	0.01
$5F_{5/2} - 4P_{3/2}$	12.837	11.968	11.967	11.969	11.970	11.967	0.003
$5F_{5/2} - 5P_{1/2}$	241.192	237.463	237.491	237.467	237.492	237.49	0.02
$5F_{5/2} - 5P_{3/2}$	129.081	127.096	127.101	127.098	127.103	127.101	0.003
$5F_{7/2} - 3P_{3/2}$	10.016	9.754	9.755	9.757	9.756	9.755	0.002
$5F_{7/2} - 4P_{3/2}$	31.443	29.316	29.313	29.309	29.312	29.313	0.004
$5F_{7/2} - 5P_{3/2}$	316.184	311.321	311.332	311.326	311.335	311.332	0.006
$5G_{7/2} - 3D_{5/2}$	12.758	12.356	12.353	12.358	12.352	12.353	0.005
$5G_{7/2} - 3D_{3/2}$	38.279	37.071	37.057	37.076	37.055	37.05	0.02
$5G_{7/2} - 4D_{5/2}$	68.082	67.143	67.138	67.145	67.137	67.138	0.007
$5G_{7/2} - 4D_{3/2}$	204.254	201.436	201.406	201.443	201.403	201.40	0.04
$5G_{7/2} - 5D_{5/2}$	90.597	91.028	91.040	91.029	91.039	91.04	0.01
$5G_{7/2} - 5D_{3/2}$	271.788	273.080	273.124	273.084	273.123	273.12	0.04
$5G_{9/2} - 3D_{5/2}$	45.109	43.685	43.675	43.692	43.672	43.67	0.02
$5G_{9/2} - 4D_{5/2}$	240.707	237.387	237.368	237.395	237.365	237.36	0.03
$5G_{9/2} - 5D_{5/2}$	320.312	321.835	321.875	321.839	321.874	321.87	0.03
$6D_{5/2} - 3S_{1/2}$	0.488	0.476	0.476	0.477	0.475	0.476	0.001
$6D_{5/2} - 4S_{1/2}$	5.011	4.948	4.945	4.947	4.946	4.945	0.002

$6D_{5/2} - 3D_{5/2}$	3.498	3.431	3.431	3.433	3.432	3.431	0.002
$6D_{5/2} - 3D_{3/2}$	1.749	1.716	1.716	1.717	1.715	1.716	0.001
$6D_{5/2} - 5S_{1/2}$	30.964	30.594	30.589	30.596	30.590	30.589	0.007
$6D_{5/2} - 4D_{5/2}$	22.523	22.216	22.214	22.217	22.215	22.214	0.003
$6D_{5/2} - 4D_{3/2}$	11.262	11.108	11.109	11.107	11.106	11.109	0.003
$6D_{5/2} - 6S_{1/2}$	276.552	272.465	272.573	272.524	272.572	272.57	0.05
$6D_{5/2} - 5D_{5/2}$	206.455	204.204	204.188	204.210	204.185	204.18	0.02
$6D_{5/2} - 5D_{3/2}$	103.240	102.112	102.081	102.116	102.080	102.08	0.03
$6D_{5/2} - 5G_{7/2}$	19.175	20.121	20.134	20.122	20.133	20.13	0.01
$6D_{5/2} - 5G_{9/2}$	67.796	71.141	71.183	71.143	71.184	71.18	0.04
$6D_{3/2} - 3S_{1/2}$	0.399	0.389	0.388	0.390	0.391	0.388	0.003
$6D_{3/2} - 4S_{1/2}$	4.092	4.040	4.037	4.042	4.038	4.037	0.005
$6D_{3/2} - 3D_{5/2}$	1.749	1.716	1.715	1.717	1.714	1.715	0.002
$6D_{3/2} - 3D_{3/2}$	2.672	2.621	2.620	2.622	2.619	2.620	0.002
$6D_{3/2} - 5S_{1/2}$	25.283	24.981	24.975	24.982	24.974	24.975	0.007
$6D_{3/2} - 4D_{5/2}$	11.261	11.108	11.107	11.109	11.106	11.107	0.002
$6D_{3/2} - 4D_{3/2}$	17.203	16.968	16.966	16.969	16.967	16.966	0.003
$6D_{3/2} - 6S_{1/2}$	225.788	222.453	222.570	222.501	222.569	222.57	0.07
$6D_{3/2} - 5D_{5/2}$	103.218	102.094	102.103	102.097	102.101	102.103	0.006
$6D_{3/2} - 5D_{3/2}$	157.687	155.967	155.945	155.972	155.943	155.94	0.03
$6D_{3/2} - 5G_{7/2}$	57.517	60.356	60.409	60.357	60.410	60.41	0.05
$6D_{3/2} - 6D_{5/2}$	420.728	416.336	416.295	416.339	416.292	416.29	0.04
$6G_{7/2} - 3D_{5/2}$	7.422	7.251	7.250	7.251	7.249	7.250	0.001
$6G_{7/2} - 3D_{3/2}$	22.268	21.754	21.748	21.756	21.747	21.748	0.008
$6G_{7/2} - 4D_{5/2}$	3.658	2.782	2.770	2.783	2.771	2.77	0.01
$6G_{7/2} - 4D_{3/2}$	10.984	8.351	8.302	8.355	8.301	8.30	0.05
$6G_{7/2} - 5D_{5/2}$	158.727	155.796	155.770	155.799	155.769	155.77	0.03
$6G_{7/2} - 5D_{3/2}$	467.209	467.412	467.284	467.421	467.280	467.28	0.14
$6G_{7/2} - 6D_{5/2}$	252.261	253.197	253.227	253.201	253.226	253.22	0.03
$6G_{7/2} - 6D_{3/2}$	756.775	759.584	759.680	759.596	759.688	759.68	0.08
$6G_{9/2} - 3D_{5/2}$	26.241	25.636	25.632	25.638	25.630	25.632	0.006
$6G_{9/2} - 4D_{5/2}$	12.934	9.833	9.793	9.838	9.792	9.79	0.05
$6G_{9/2} - 5D_{5/2}$	561.186	550.823	550.732	550.833	550.728	550.73	0.10
$6G_{9/2} - 6D_{5/2}$	891.885	895.193	895.292	895.207	895.289	895.29	0.09

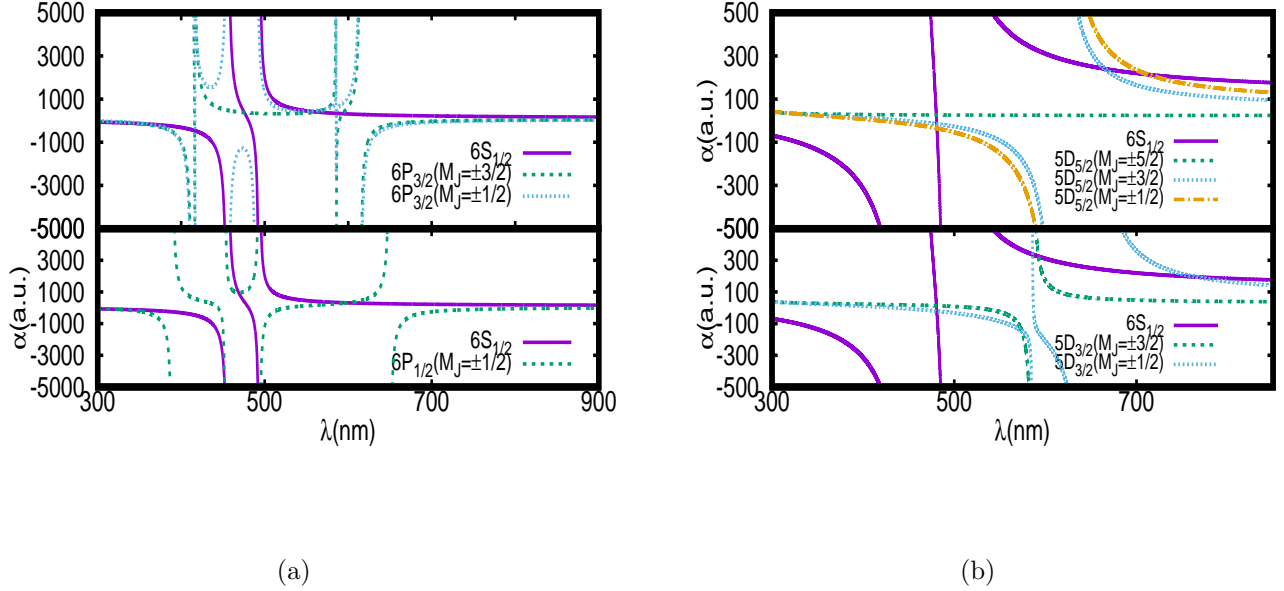


**Fig. 7:** Plots depicting dynamic E1 polarizabilities of (a) the ground  $6S_{1/2}$  and excited  $6P_{3/2,1/2}$  states, and (b) the ground  $6S_{1/2}$  and excited  $5D_{5/2,3/2}$  states in  $\text{Ba}^+$  for the linearly polarized light. The crossings of polarizability curves between two resonances correspond to the magic wavelengths.

Table B: Reduced E2 matrix elements (in a.u.) of  $\text{Ca}^+$  from the DHF, SD and SDpT methods, whereas the label “sc” indicates the scaled values. The second last and the last columns list the recommended  $O^{\text{Final}}$  values of the matrix elements and their absolute uncertainties, respectively.

Transition	$O^{\text{DHF}}$	$O^{\text{SD}}$	$O_{\text{sc}}^{\text{SD}}$	$O^{\text{SDpT}}$	$O_{\text{sc}}^{\text{SDpT}}$	$O^{\text{Final}}$	$\delta$
$3D_{3/2} - 4S_{1/2}$	9.767	7.788	7.945	7.971	7.907	7.94	0.04
$3D_{5/2} - 4S_{1/2}$	11.978	9.561	9.750	9.785	9.704	9.75	0.04
$3D_{5/2} - 3D_{3/2}$	5.018	3.688	3.781	3.794	3.758	3.78	0.02
$4P_{3/2} - 4P_{1/2}$	20.820	19.259	19.366	19.414	19.360	19.36	0.05
$5S_{1/2} - 3D_{3/2}$	6.050	3.736	3.955	3.933	3.864	3.95	0.09
$5S_{1/2} - 3D_{5/2}$	7.427	4.600	4.863	4.841	4.752	4.86	0.11
$4D_{3/2} - 4S_{1/2}$	12.711	12.610	12.704	12.649	12.694	12.70	0.05
$4D_{3/2} - 3D_{3/2}$	8.314	6.183	6.445	6.381	6.352	6.44	0.09
$4D_{3/2} - 3D_{5/2}$	5.454	4.065	4.233	4.194	4.172	4.23	0.06
$4D_{3/2} - 5S_{1/2}$	57.771	52.842	52.958	53.333	52.906	52.95	0.37
$4D_{5/2} - 4S_{1/2}$	15.551	15.426	15.544	15.474	15.531	15.54	0.07
$4D_{5/2} - 3D_{3/2}$	5.437	4.041	4.213	4.171	4.153	4.21	0.06
$4D_{5/2} - 3D_{5/2}$	10.897	8.117	8.454	8.376	8.334	8.45	0.12
$4D_{5/2} - 5S_{1/2}$	70.804	64.776	64.911	65.377	64.849	64.91	0.46
$4D_{5/2} - 4D_{3/2}$	36.537	32.814	32.862	33.163	32.819	32.86	0.30

$5P_{1/2} - 4P_{3/2}$	13.720	12.876	12.951	12.964	12.934	12.95	0.02
$5P_{3/2} - 4P_{1/2}$	13.435	12.587	12.671	12.676	12.654	12.67	0.02
$5P_{3/2} - 4P_{3/2}$	13.614	12.769	12.848	12.857	12.830	12.84	0.02
$5P_{3/2} - 5P_{1/2}$	85.493	81.320	81.594	81.762	81.568	81.59	0.16
$4F_{5/2} - 4P_{1/2}$	28.239	26.009	26.183	26.243	26.164	26.18	0.06
$4F_{5/2} - 4P_{3/2}$	15.212	14.022	14.112	14.147	14.102	14.11	0.03
$4F_{5/2} - 5P_{1/2}$	96.792	93.439	93.659	93.801	93.640	93.65	0.14
$4F_{5/2} - 5P_{3/2}$	51.821	50.039	50.153	50.231	50.143	50.15	0.07
$4F_{7/2} - 4P_{3/2}$	37.262	34.348	34.566	34.653	34.542	34.56	0.08
$4F_{7/2} - 5P_{3/2}$	126.934	122.569	122.849	123.040	122.824	122.84	0.19
$6S_{1/2} - 3D_{3/2}$	1.302	1.014	1.035	1.044	1.038	1.035	0.009
$6S_{1/2} - 3D_{5/2}$	1.597	1.246	1.271	1.282	1.275	1.27	0.01
$6S_{1/2} - 4D_{3/2}$	33.650	27.955	27.923	28.440	27.803	27.92	0.51
$6S_{1/2} - 4D_{5/2}$	41.314	34.348	34.293	34.941	34.146	34.29	0.64
$5D_{3/2} - 4S_{1/2}$	4.531	4.180	4.185	4.217	4.196	4.18	0.03
$5D_{3/2} - 3D_{3/2}$	2.254	1.951	1.962	1.983	1.977	1.96	0.02
$5D_{3/2} - 3D_{5/2}$	1.477	1.280	1.287	1.301	1.297	1.28	0.01
$5D_{3/2} - 5S_{1/2}$	39.635	40.539	40.800	40.547	40.750	40.80	0.25
$5D_{3/2} - 4D_{3/2}$	36.968	33.305	33.366	33.648	33.236	33.36	0.28
$5D_{3/2} - 4D_{5/2}$	24.258	21.867	21.898	22.090	21.813	21.89	0.19
$5D_{3/2} - 6S_{1/2}$	179.817	169.441	169.728	170.525	169.609	169.72	0.79
$5D_{5/2} - 4S_{1/2}$	5.551	5.123	5.129	5.168	5.142	5.13	0.04
$5D_{5/2} - 3D_{3/2}$	1.476	1.278	1.284	1.298	1.294	1.28	0.01
$5D_{5/2} - 3D_{5/2}$	2.956	2.561	2.574	2.602	2.594	2.57	0.03
$5D_{5/2} - 5S_{1/2}$	48.464	49.564	49.894	49.574	49.833	49.89	0.32
$5D_{5/2} - 4D_{3/2}$	24.166	21.765	21.809	21.990	21.725	21.81	0.18
$5D_{5/2} - 4D_{5/2}$	48.445	43.658	43.728	44.105	43.559	43.72	0.37
$5D_{5/2} - 6S_{1/2}$	220.325	207.639	207.976	207.964	207.831	207.97	0.14
$5D_{5/2} - 5D_{3/2}$	117.979	109.562	109.676	110.380	109.563	109.67	0.70
$6P_{1/2} - 4P_{3/2}$	4.259	4.055	4.068	4.077	4.071	4.068	0.009
$6P_{1/2} - 5P_{3/2}$	48.896	46.750	46.912	46.980	46.860	46.91	0.06
$6P_{1/2} - 4F_{5/2}$	62.284	63.136	63.086	63.040	63.068	63.08	0.04
$6P_{3/2} - 4P_{1/2}$	4.222	4.016	4.030	4.038	4.034	4.030	0.008
$6P_{3/2} - 4P_{3/2}$	4.252	4.047	4.060	4.069	4.064	4.060	0.009
$6P_{3/2} - 5P_{1/2}$	47.928	45.759	45.955	45.993	45.903	45.95	0.05
$6P_{3/2} - 5P_{3/2}$	48.506	46.352	46.527	46.583	46.475	46.52	0.05
$6P_{3/2} - 4F_{5/2}$	33.102	33.552	33.532	33.502	33.522	33.53	0.03
$6P_{3/2} - 4F_{7/2}$	81.083	82.185	82.135	82.061	82.112	82.13	0.07

$6P_{3/2} - 6P_{1/2}$	237.205	228.371	228.940	229.324	228.870	228.94	0.38
$5F_{5/2} - 4P_{1/2}$	10.150	9.732	9.755	9.776	9.760	9.75	0.02
$5F_{5/2} - 4P_{3/2}$	5.433	5.213	5.225	5.237	5.228	5.22	0.01
$5F_{5/2} - 5P_{1/2}$	66.210	60.777	61.176	61.364	61.122	61.17	0.18
$5F_{5/2} - 5P_{3/2}$	35.776	32.879	33.079	33.192	33.051	33.07	0.11
$5F_{5/2} - 6P_{1/2}$	294.309	285.470	286.050	286.442	285.989	286.05	0.39
$5F_{5/2} - 6P_{3/2}$	157.611	152.919	153.217	153.435	153.184	153.21	0.21
$5F_{7/2} - 4P_{3/2}$	13.310	12.770	12.799	12.827	12.805	12.79	0.02
$5F_{7/2} - 5P_{3/2}$	87.636	80.539	81.028	81.304	80.957	81.02	0.27
$5F_{7/2} - 6P_{3/2}$	386.064	374.574	375.302	375.836	375.223	375.30	0.53
$5G_{7/2} - 3D_{3/2}$	7.084	4.283	4.530	4.522	4.428	4.53	0.10
$5G_{7/2} - 3D_{5/2}$	2.366	1.434	1.515	1.514	1.481	1.51	0.03
$5G_{7/2} - 4D_{3/2}$	100.787	87.635	87.808	88.901	87.625	87	1
$5G_{7/2} - 4D_{5/2}$	33.641	29.262	29.313	29.683	29.252	29.31	0.37
$5G_{7/2} - 5D_{3/2}$	276.570	267.952	268.150	268.887	267.973	268.15	0.73
$5G_{7/2} - 5D_{5/2}$	92.216	89.353	89.414	89.664	89.355	89.41	0.25
$5G_{9/2} - 3D_{5/2}$	8.367	5.072	5.357	5.353	5.238	5.35	0.12
$5G_{9/2} - 4D_{5/2}$	118.938	103.458	103.637	104.947	103.422	103	1
$5G_{9/2} - 5D_{5/2}$	326.033	315.913	316.128	317.011	315.920	316.12	0.88
$7S_{1/2} - 3D_{3/2}$	0.644	0.533	0.540	0.545	0.544	0.540	0.005
$7S_{1/2} - 3D_{5/2}$	0.790	0.655	0.664	0.670	0.668	0.664	0.006
$7S_{1/2} - 4D_{3/2}$	6.834	6.241	6.244	6.303	6.263	6.24	0.06
$7S_{1/2} - 4D_{5/2}$	8.376	7.654	7.656	7.729	7.680	7.65	0.07
$7S_{1/2} - 5D_{3/2}$	103.471	90.076	89.933	91.233	89.677	89	1
$7S_{1/2} - 5D_{5/2}$	127.010	110.626	110.410	112.039	110.096	110	2
$6D_{3/2} - 4S_{1/2}$	2.476	2.232	2.229	2.256	2.236	2.22	0.02
$6D_{3/2} - 3D_{3/2}$	1.157	1.064	1.060	1.075	1.072	1.06	0.02
$6D_{3/2} - 3D_{5/2}$	0.758	0.698	0.695	0.705	0.703	0.69	0.01
$6D_{3/2} - 5S_{1/2}$	14.222	13.718	13.746	13.784	13.773	13.74	0.04
$6D_{3/2} - 4D_{3/2}$	9.854	9.043	9.049	9.121	9.083	9.04	0.07
$6D_{3/2} - 4D_{5/2}$	6.456	5.926	5.930	5.977	5.952	5.93	0.04
$6D_{3/2} - 6S_{1/2}$	92.879	96.637	97.208	96.491	97.067	97.20	0.71
$6D_{3/2} - 5D_{3/2}$	101.509	94.610	94.726	95.278	94.432	94.72	0.55
$6D_{3/2} - 5D_{5/2}$	66.607	62.105	62.159	62.541	61.966	62.15	0.38
$6D_{3/2} - 5G_{7/2}$	183.977	199.633	199.563	198.071	199.442	199	1
$6D_{3/2} - 7S_{1/2}$	426.859	408.335	408.935	410.333	408.682	408	1
$6D_{5/2} - 4S_{1/2}$	3.036	2.738	2.734	2.767	2.743	2.73	0.03
$6D_{5/2} - 3D_{3/2}$	0.759	0.697	0.694	0.704	0.702	0.69	0.01

Transition	$O^{\text{DHF}}$	$O^{\text{SD}}$	$O_{\text{sc}}^{\text{SD}}$	$O^{\text{SDpT}}$	$O_{\text{sc}}^{\text{SDpT}}$	$O^{\text{Final}}$	$\delta$
$6D_{5/2} - 3D_{5/2}$	1.519	1.396	1.391	1.411	1.406	1.39	0.02
$6D_{5/2} - 5S_{1/2}$	17.415	16.801	16.836	16.882	16.869	16.83	0.04
$6D_{5/2} - 4D_{3/2}$	6.452	5.921	5.925	5.972	5.947	5.92	0.04
$6D_{5/2} - 4D_{5/2}$	12.914	11.854	11.860	11.956	11.905	11.86	0.09
$6D_{5/2} - 6S_{1/2}$	113.534	118.115	118.843	117.939	118.671	118.84	0.90
$6D_{5/2} - 5D_{3/2}$	66.345	61.820	61.910	62.259	61.718	61.91	0.34
$6D_{5/2} - 5D_{5/2}$	132.999	123.978	124.113	124.851	123.729	124.11	0.73
$6D_{5/2} - 5G_{7/2}$	61.261	66.473	66.458	65.953	66.418	66.45	0.50
$6D_{5/2} - 5G_{9/2}$	216.591	235.019	234.965	233.182	234.822	234	2
$6D_{5/2} - 7S_{1/2}$	522.942	500.297	501.006	502.740	500.697	501	2
$6D_{5/2} - 6D_{3/2}$	284.334	268.447	268.679	270.018	268.431	268	1
$6G_{7/2} - 3D_{3/2}$	5.420	3.457	3.629	3.630	3.564	3.62	0.06
$6G_{7/2} - 3D_{5/2}$	1.810	1.157	1.214	1.215	1.192	1.21	0.02
$6G_{7/2} - 4D_{3/2}$	35.252	34.664	34.687	34.766	34.710	34.68	0.07
$6G_{7/2} - 4D_{5/2}$	11.751	11.559	11.566	11.593	11.574	11.56	0.02
$6G_{7/2} - 5D_{3/2}$	169.628	136.505	136.855	139.721	136.493	136	3
$6G_{7/2} - 5D_{5/2}$	56.671	45.638	45.736	46.709	45.616	45.73	0.97
$6G_{7/2} - 6D_{3/2}$	721.485	691.660	692.205	694.877	691.777	692	3
$6G_{7/2} - 6D_{5/2}$	240.594	230.684	230.847	231.752	230.705	230.84	0.90
$6G_{9/2} - 3D_{5/2}$	6.401	4.092	4.291	4.295	4.215	4.29	0.07
$6G_{9/2} - 4D_{5/2}$	41.546	40.868	40.893	40.896	40.920	40.89	0.03
$6G_{9/2} - 5D_{5/2}$	200.359	161.352	161.703	165.138	161.278	161	3
$6G_{9/2} - 6D_{5/2}$	850.630	815.592	816.168	819.370	815.664	816	3

Table C: Reduced E2 matrix elements (in a.u.) of  $\text{Sr}^+$  from the DHF, SD and SDpT methods, whereas the label “sc” indicates the scaled values. The second last and the last columns list the recommended  $O^{\text{Final}}$  values of the matrix elements and their absolute uncertainties, respectively.

Transition	$O^{\text{DHF}}$	$O^{\text{SD}}$	$O_{\text{sc}}^{\text{SD}}$	$O^{\text{SDpT}}$	$O_{\text{sc}}^{\text{SDpT}}$	$O^{\text{Final}}$	$\delta$
$4D_{3/2} - 5S_{1/2}$	12.968	11.009	11.133	11.172	11.100	11.13	0.04
$4D_{5/2} - 5S_{1/2}$	15.972	13.601	13.747	13.797	13.706	13.74	0.05
$4D_{5/2} - 4D_{3/2}$	7.260	5.904	5.978	6.001	5.954	5.97	0.02
$5P_{3/2} - 5P_{1/2}$	25.408	23.257	23.406	23.462	23.393	23.40	0.05
$6S_{1/2} - 4D_{3/2}$	7.969	5.879	6.031	6.041	5.957	6.03	0.07
$6S_{1/2} - 4D_{5/2}$	9.885	7.356	7.531	7.550	7.441	7.53	0.09
$5D_{3/2} - 5S_{1/2}$	13.511	12.865	13.009	12.959	12.987	13.01	0.05
$5D_{3/2} - 4D_{3/2}$	10.061	8.149	8.346	8.317	8.272	8.34	0.07

$5D_{3/2} - 4D_{5/2}$	6.661	5.431	5.553	5.538	5.505	5.55	0.04
$5D_{3/2} - 6S_{1/2}$	68.478	63.419	63.585	63.888	63.532	63.58	0.30
$5D_{5/2} - 5S_{1/2}$	16.444	15.640	15.821	15.757	15.794	15.82	0.06
$5D_{5/2} - 4D_{3/2}$	6.547	5.291	5.421	5.401	5.373	5.42	0.04
$5D_{5/2} - 4D_{5/2}$	13.244	10.776	11.024	10.991	10.928	11.02	0.09
$5D_{5/2} - 6S_{1/2}$	84.103	77.942	78.137	78.513	78.073	78.13	0.37
$6P_{1/2} - 5P_{3/2}$	16.575	15.465	15.569	15.577	15.539	15.56	0.03
$6P_{3/2} - 5P_{1/2}$	15.268	14.121	14.245	14.238	14.214	14.24	0.03
$6P_{3/2} - 5P_{3/2}$	16.077	14.958	15.069	15.072	15.040	15.06	0.03
$6P_{3/2} - 6P_{1/2}$	98.355	92.884	93.249	93.445	93.206	93.24	0.19
$4F_{7/2} - 5P_{3/2}$	47.407	43.588	43.878	43.970	43.841	43.87	0.09
$4F_{7/2} - 6P_{3/2}$	131.267	124.821	125.229	125.534	125.191	125.22	0.30
$4F_{5/2} - 5P_{1/2}$	35.240	32.294	32.530	32.589	32.500	32.53	0.05
$4F_{5/2} - 5P_{3/2}$	19.352	17.794	17.912	17.950	17.897	17.91	0.04
$4F_{5/2} - 6P_{1/2}$	99.930	94.948	95.271	95.500	95.241	95.27	0.23
$4F_{5/2} - 6P_{3/2}$	53.599	50.964	51.132	51.257	51.116	51.13	0.12
$5D_{5/2} - 5D_{3/2}$	44.843	41.152	41.203	41.469	41.162	41.20	0.26
$7S_{1/2} - 4D_{3/2}$	1.727	1.511	1.519	1.528	1.524	1.519	0.009
$7S_{1/2} - 4D_{5/2}$	2.131	1.873	1.883	1.894	1.889	1.88	0.01
$7S_{1/2} - 5D_{3/2}$	43.236	38.457	38.369	38.811	38.262	38.36	0.44
$7S_{1/2} - 5D_{5/2}$	53.540	47.749	47.611	48.172	47.482	47.61	0.56
$6D_{3/2} - 5S_{1/2}$	5.214	4.866	4.883	4.902	4.891	4.88	0.02
$6D_{3/2} - 4D_{3/2}$	2.965	2.674	2.686	2.701	2.694	2.68	0.02
$6D_{3/2} - 4D_{5/2}$	1.953	1.767	1.775	1.785	1.780	1.77	0.01
$6D_{3/2} - 6S_{1/2}$	39.285	38.384	38.766	38.581	38.695	38.76	0.18
$6D_{3/2} - 5D_{3/2}$	42.968	39.478	39.548	39.782	39.439	39.54	0.23
$6D_{3/2} - 5D_{5/2}$	28.448	26.200	26.230	26.394	26.159	26.23	0.16
$6D_{3/2} - 7S_{1/2}$	203.296	192.733	193.144	193.772	193.027	193.14	0.62
$6D_{5/2} - 5S_{1/2}$	6.383	5.958	5.979	6.002	5.989	5.97	0.02
$6D_{5/2} - 4D_{3/2}$	1.942	1.747	1.756	1.766	1.761	1.75	0.01
$6D_{5/2} - 4D_{5/2}$	3.909	3.532	3.548	3.567	3.558	3.54	0.02
$6D_{5/2} - 6S_{1/2}$	47.682	46.537	47.024	46.784	46.937	47.02	0.24
$6D_{5/2} - 5D_{3/2}$	27.923	25.622	25.677	25.824	25.606	25.67	0.15
$6D_{5/2} - 5D_{5/2}$	56.483	51.955	52.032	52.347	51.892	52.03	0.31
$6D_{5/2} - 7S_{1/2}$	249.386	236.513	237.002	237.779	236.860	237.00	0.77
$6D_{5/2} - 6D_{3/2}$	137.329	129.336	129.442	130.052	129.350	129.44	0.61
$7P_{1/2} - 5P_{3/2}$	5.048	4.791	4.806	4.818	4.812	4.80	0.01
$7P_{1/2} - 6P_{3/2}$	56.716	53.990	54.204	54.274	54.124	54.20	0.08

$7P_{1/2} - 4F_{5/2}$	50.308	49.673	49.730	49.784	49.686	49.73	0.05
$7P_{3/2} - 5P_{1/2}$	4.872	4.604	4.623	4.632	4.628	4.623	0.009
$7P_{3/2} - 5P_{3/2}$	5.012	4.753	4.769	4.779	4.774	4.76	0.01
$7P_{3/2} - 6P_{1/2}$	52.456	49.578	49.863	49.880	49.782	49.86	0.08
$7P_{3/2} - 6P_{3/2}$	54.977	52.196	52.438	52.487	52.359	52.43	0.08
$7P_{3/2} - 4F_{7/2}$	63.990	63.100	63.202	63.250	63.146	63.20	0.05
$7P_{3/2} - 4F_{5/2}$	26.136	25.768	25.811	25.831	25.788	25.81	0.02
$7P_{3/2} - 7P_{1/2}$	264.501	253.204	253.934	254.390	253.825	253.93	0.45
$5F_{5/2} - 5P_{1/2}$	10.055	9.486	9.504	9.551	9.519	9.50	0.04
$5F_{5/2} - 5P_{3/2}$	5.333	5.033	5.043	5.067	5.051	5.04	0.02
$5F_{5/2} - 6P_{1/2}$	90.633	84.751	85.215	85.322	85.131	85.21	0.11
$5F_{5/2} - 6P_{3/2}$	50.164	47.082	47.301	47.380	47.258	47.30	0.08
$5F_{5/2} - 7P_{1/2}$	306.465	294.251	295.049	295.616	294.949	295.04	0.56
$5F_{5/2} - 7P_{3/2}$	164.490	158.038	158.448	158.761	158.396	158.44	0.31
$5F_{7/2} - 5P_{3/2}$	13.058	12.326	12.353	12.409	12.372	12.35	0.05
$5F_{7/2} - 6P_{3/2}$	122.911	115.346	115.864	116.081	115.758	115.86	0.22
$5F_{7/2} - 7P_{3/2}$	402.857	387.078	388.114	388.841	387.986	388.11	0.73
$5G_{7/2} - 4D_{3/2}$	10.740	7.601	7.806	7.858	7.715	7.80	0.09
$5G_{7/2} - 4D_{5/2}$	3.620	2.581	2.646	2.666	2.616	2.64	0.03
$5G_{7/2} - 5D_{3/2}$	126.756	114.358	114.504	115.467	114.355	114.50	0.96
$5G_{7/2} - 5D_{5/2}$	42.491	38.391	38.428	38.756	38.379	38.42	0.33
$5G_{7/2} - 6D_{3/2}$	287.395	282.197	282.608	282.752	282.493	282.60	0.14
$5G_{7/2} - 6D_{5/2}$	95.853	94.155	94.288	94.336	94.250	94.28	0.05
$5G_{9/2} - 4D_{5/2}$	12.799	9.126	9.355	9.425	9.250	9.35	0.11
$5G_{9/2} - 5D_{5/2}$	150.232	135.733	135.863	137.024	135.690	135	1
$5G_{9/2} - 6D_{5/2}$	338.892	332.890	333.359	333.530	333.225	333.35	0.17
$8S_{1/2} - 4D_{3/2}$	0.857	0.787	0.788	0.792	0.794	0.788	0.006
$8S_{1/2} - 4D_{5/2}$	1.056	0.974	0.975	0.980	0.979	0.975	0.005
$8S_{1/2} - 5D_{3/2}$	7.990	7.525	7.534	7.570	7.559	7.53	0.03
$8S_{1/2} - 5D_{5/2}$	9.801	9.243	9.255	9.298	9.286	9.25	0.04
$8S_{1/2} - 6D_{3/2}$	129.183	118.979	118.623	119.723	118.403	118	1
$8S_{1/2} - 6D_{5/2}$	159.802	147.445	146.930	148.333	146.664	146	1
$7D_{3/2} - 5S_{1/2}$	2.976	2.770	2.772	2.789	2.779	2.77	0.02
$7D_{3/2} - 4D_{3/2}$	1.575	1.483	1.483	1.493	1.490	1.48	0.01
$7D_{3/2} - 4D_{5/2}$	1.036	0.978	0.978	0.984	0.982	0.978	0.006
$7D_{3/2} - 6S_{1/2}$	15.208	14.609	14.668	14.684	14.686	14.66	0.02
$7D_{3/2} - 5D_{3/2}$	11.640	10.881	10.888	10.948	10.912	10.88	0.06
$7D_{3/2} - 5D_{5/2}$	7.652	7.160	7.163	7.204	7.179	7.16	0.04

$7D_{3/2} - 7S_{1/2}$	88.219	87.368	88.143	87.708	87.974	88.14	0.43
$7D_{3/2} - 6D_{3/2}$	114.789	108.316	108.380	108.898	108.150	108.38	0.52
$7D_{3/2} - 6D_{5/2}$	75.986	71.829	71.826	72.197	71.680	71.82	0.37
$7D_{3/2} - 5G_{7/2}$	146.548	158.999	159.300	157.880	159.221	159	1
$7D_{3/2} - 8S_{1/2}$	469.230	450.304	451.239	452.236	450.996	451.23	0.99
$7D_{5/2} - 5S_{1/2}$	3.652	3.402	3.404	3.425	3.412	3.40	0.02
$7D_{5/2} - 4D_{3/2}$	1.034	0.971	0.971	0.978	0.976	0.971	0.007
$7D_{5/2} - 4D_{5/2}$	2.079	1.958	1.958	1.971	1.967	1.95	0.01
$7D_{5/2} - 6S_{1/2}$	18.569	17.836	17.914	17.929	17.935	17.91	0.02
$7D_{5/2} - 5D_{3/2}$	7.620	7.121	7.125	7.165	7.141	7.12	0.04
$7D_{5/2} - 5D_{5/2}$	15.305	14.318	14.325	14.405	14.356	14.32	0.08
$7D_{5/2} - 7S_{1/2}$	106.892	105.743	106.755	106.175	106.549	106.75	0.58
$7D_{5/2} - 6D_{3/2}$	74.548	70.264	70.338	70.652	70.188	70.33	0.31
$7D_{5/2} - 6D_{5/2}$	150.773	142.362	142.428	143.114	142.131	142.42	0.68
$7D_{5/2} - 5G_{7/2}$	48.524	52.633	52.752	52.666	52.726	52.75	0.08
$7D_{5/2} - 5G_{9/2}$	171.560	186.089	186.506	184.791	186.414	186	2
$7D_{5/2} - 8S_{1/2}$	575.215	552.140	553.260	554.498	552.964	553	1
$7D_{5/2} - 7D_{3/2}$	321.184	306.458	306.717	307.804	306.525	306	1
$8P_{1/2} - 5P_{3/2}$	2.709	2.594	2.598	2.606	2.603	2.598	0.008
$8P_{1/2} - 6P_{3/2}$	15.684	15.001	15.049	15.072	15.071	15.04	0.02
$8P_{1/2} - 4F_{5/2}$	8.418	7.956	7.962	8.008	7.978	7.96	0.04
$8P_{1/2} - 7P_{3/2}$	140.395	135.209	136.489	135.758	136.305	136.48	0.73
$8P_{1/2} - 5F_{5/2}$	159.851	157.671	158.803	158.061	158.649	158.80	0.74
$8P_{3/2} - 5P_{1/2}$	2.654	2.533	2.543	2.546	2.547	2.543	0.004
$8P_{3/2} - 5P_{3/2}$	2.709	2.593	2.600	2.605	2.604	2.600	0.005
$8P_{3/2} - 6P_{1/2}$	15.281	14.574	14.660	14.648	14.679	14.66	0.02
$8P_{3/2} - 6P_{3/2}$	15.606	14.918	14.988	14.990	15.008	14.98	0.02
$8P_{3/2} - 4F_{7/2}$	11.094	10.524	10.529	10.588	10.548	10.52	0.06
$8P_{3/2} - 4F_{5/2}$	4.529	4.297	4.299	4.323	4.307	4.29	0.02
$8P_{3/2} - 7P_{1/2}$	130.011	124.387	126.289	124.986	126.101	126	1
$8P_{3/2} - 7P_{3/2}$	135.972	130.610	132.417	131.179	132.234	132	1
$8P_{3/2} - 5F_{5/2}$	83.081	81.814	82.700	82.033	82.619	82.70	0.66
$8P_{3/2} - 5F_{7/2}$	203.391	200.334	202.573	200.855	202.374	202	2
$8P_{3/2} - 8P_{1/2}$	580.581	560.327	559.879	562.479	559.629	559	3
$6G_{7/2} - 4D_{3/2}$	7.918	5.877	6.014	6.048	5.960	6.01	0.05
$6G_{7/2} - 4D_{5/2}$	2.666	1.992	2.035	2.048	2.018	2.03	0.02
$6G_{7/2} - 5D_{3/2}$	33.283	34.647	34.688	34.565	34.732	34.68	0.12
$6G_{7/2} - 5D_{5/2}$	11.052	11.522	11.537	11.493	11.552	11.53	0.04

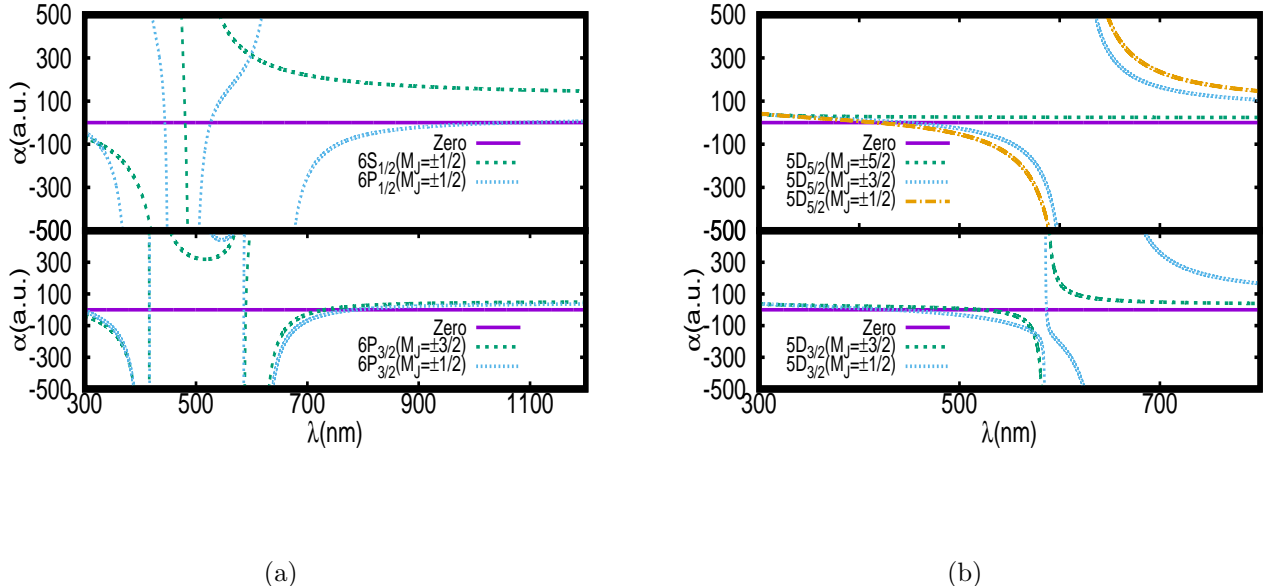
$6G_{7/2} - 6D_{3/2}$	246.562	215.012	215.148	217.846	214.858	215	3
$6G_{7/2} - 6D_{5/2}$	82.897	72.446	72.457	73.381	72.361	72.45	0.92
$6G_{7/2} - 7D_{3/2}$	766.090	748.147	748.846	750.002	748.567	748	1
$6G_{7/2} - 7D_{5/2}$	255.631	249.766	249.977	250.371	249.886	249.97	0.39
$6G_{9/2} - 4D_{5/2}$	9.426	7.043	7.196	7.242	7.134	7.19	0.06
$6G_{9/2} - 5D_{5/2}$	39.078	40.736	40.791	40.635	40.842	40.79	0.15
$6G_{9/2} - 6D_{5/2}$	293.088	256.136	256.176	259.440	255.839	256	3
$6G_{9/2} - 7D_{5/2}$	903.795	883.059	883.801	885.198	883.477	883	1

Table D: Reduced E2 matrix elements (in a.u.) of  $\text{Ba}^+$  from the DHF, SD and SDpT methods, whereas the label “sc” indicates the scaled values. The second last and the last columns list the recommended  $O^{\text{Final}}$  values of the matrix elements and their absolute uncertainties, respectively.

Transition	$O^{\text{DHF}}$	$O^{\text{SD}}$	$O_{\text{sc}}^{\text{SD}}$	$O^{\text{SDpT}}$	$O_{\text{sc}}^{\text{SDpT}}$	$O^{\text{Final}}$	$\delta$
$5D_{3/2} - 6S_{1/2}$	14.763	12.497	12.627	12.740	12.589	12.62	0.11
$5D_{5/2} - 6S_{1/2}$	18.383	15.651	15.803	15.943	15.758	15.80	0.14
$5D_{5/2} - 5D_{3/2}$	8.091	6.649	6.708	6.772	6.686	6.70	0.06
$6P_{3/2} - 6P_{1/2}$	31.319	28.079	28.336	28.472	28.322	28.33	0.13
$7S_{1/2} - 5D_{3/2}$	6.199	4.657	4.741	4.806	4.650	4.74	0.09
$7S_{1/2} - 5D_{5/2}$	7.936	6.075	6.164	6.248	6.056	6.16	0.11
$6D_{3/2} - 6S_{1/2}$	18.133	16.556	16.825	16.797	16.779	16.82	0.04
$6D_{3/2} - 5D_{3/2}$	9.842	8.138	8.296	8.338	8.206	8.29	0.09
$6D_{3/2} - 5D_{5/2}$	6.669	5.578	5.674	5.703	5.617	5.67	0.05
$6D_{3/2} - 7S_{1/2}$	76.978	70.550	70.789	71.327	70.707	70.78	0.53
$6D_{5/2} - 6S_{1/2}$	21.901	19.962	20.297	20.259	20.240	20.29	0.05
$6D_{5/2} - 5D_{3/2}$	6.327	5.207	5.311	5.338	5.253	5.31	0.05
$6D_{5/2} - 5D_{5/2}$	13.104	10.919	11.114	11.171	11.001	11.11	0.11
$6D_{5/2} - 7S_{1/2}$	95.042	87.212	87.497	88.157	87.399	87.49	0.66
$6D_{5/2} - 6D_{3/2}$	49.195	44.857	44.939	45.354	44.886	44.93	0.41
$7P_{1/2} - 6P_{3/2}$	20.696	19.129	19.313	19.330	19.256	19.31	0.05
$7P_{3/2} - 6P_{1/2}$	17.059	15.402	15.620	15.616	15.556	15.62	0.06
$7P_{3/2} - 6P_{3/2}$	19.274	17.688	17.884	17.893	17.826	17.88	0.05
$7P_{3/2} - 7P_{1/2}$	114.206	106.364	106.956	107.385	106.875	106.95	0.42
$8S_{1/2} - 5D_{3/2}$	1.727	1.473	1.482	1.498	1.480	1.48	0.02
$8S_{1/2} - 5D_{5/2}$	2.185	1.889	1.896	1.915	1.895	1.89	0.02
$8S_{1/2} - 6D_{3/2}$	39.868	35.777	35.624	36.174	35.460	35.62	0.55
$8S_{1/2} - 6D_{5/2}$	50.374	45.417	45.193	45.885	44.994	45.19	0.69
$7D_{3/2} - 6S_{1/2}$	6.189	5.669	5.682	5.734	5.704	5.68	0.05

$7D_{3/2} - 5D_{3/2}$	3.248	2.945	2.962	2.987	2.970	2.96	0.02
$7D_{3/2} - 5D_{5/2}$	2.172	1.983	1.993	2.009	1.998	1.99	0.02
$7D_{3/2} - 7S_{1/2}$	51.767	48.892	49.580	49.407	49.438	49.58	0.17
$7D_{3/2} - 6D_{3/2}$	45.067	41.338	41.451	41.779	41.290	41.45	0.32
$7D_{3/2} - 6D_{5/2}$	30.378	27.973	28.028	28.252	27.925	28.02	0.22
$7D_{3/2} - 8S_{1/2}$	224.401	210.800	211.362	212.528	211.161	211	1
$7D_{5/2} - 6S_{1/2}$	7.598	6.962	6.981	7.042	7.007	6.98	0.06
$7D_{5/2} - 5D_{3/2}$	2.116	1.909	1.921	1.938	1.926	1.92	0.02
$7D_{5/2} - 5D_{5/2}$	4.327	3.938	3.958	3.991	3.968	3.95	0.03
$7D_{5/2} - 7S_{1/2}$	62.167	58.616	59.479	59.257	59.306	59.47	0.22
$7D_{5/2} - 6D_{3/2}$	28.937	26.486	26.570	26.779	26.465	26.57	0.21
$7D_{5/2} - 6D_{5/2}$	59.616	54.785	54.916	55.352	54.711	54.91	0.43
$7D_{5/2} - 8S_{1/2}$	276.216	259.639	260.321	261.746	260.077	260	1
$7D_{5/2} - 7D_{3/2}$	147.682	138.371	138.527	139.485	138.392	138.52	0.95
$8P_{1/2} - 6P_{3/2}$	6.093	5.746	5.764	5.792	5.784	5.76	0.03
$8P_{1/2} - 7P_{3/2}$	67.811	64.075	64.439	64.573	64.268	64.43	0.17
$8P_{3/2} - 6P_{1/2}$	5.591	5.211	5.243	5.262	5.256	5.24	0.02
$8P_{3/2} - 6P_{3/2}$	5.993	5.641	5.665	5.688	5.680	5.66	0.02
$8P_{3/2} - 7P_{1/2}$	56.484	52.351	52.825	52.899	52.643	52.82	0.18
$8P_{3/2} - 7P_{3/2}$	63.113	59.232	59.635	59.748	59.465	59.63	0.17
$8P_{3/2} - 8P_{1/2}$	297.318	281.508	282.665	283.616	282.442	282.66	0.95
$5G_{7/2} - 5D_{3/2}$	11.247	8.232	8.411	8.559	8.300	8.41	0.14
$5G_{7/2} - 5D_{5/2}$	3.873	2.872	2.928	2.980	2.892	2.92	0.05
$5G_{7/2} - 6D_{3/2}$	138.368	124.745	125.012	126.387	124.808	125	1
$5G_{7/2} - 6D_{5/2}$	46.755	42.256	42.331	42.794	42.265	42.33	0.46
$5G_{7/2} - 7D_{3/2}$	290.180	283.945	284.293	284.765	284.135	284.29	0.47
$5G_{7/2} - 7D_{5/2}$	96.770	94.764	94.878	95.028	94.827	94.87	0.15
$5G_{9/2} - 5D_{5/2}$	13.697	10.154	10.353	10.534	10.225	10.35	0.18
$5G_{9/2} - 6D_{5/2}$	165.306	149.398	149.664	151.302	149.429	149	2
$5G_{9/2} - 7D_{5/2}$	342.127	335.041	335.442	335.972	335.262	335.44	0.53
$9S_{1/2} - 5D_{3/2}$	0.908	0.812	0.815	0.821	0.816	0.815	0.006
$9S_{1/2} - 5D_{5/2}$	1.146	1.037	1.038	1.045	1.039	1.038	0.007
$9S_{1/2} - 6D_{3/2}$	8.823	8.168	8.163	8.244	8.197	8.16	0.08
$9S_{1/2} - 6D_{5/2}$	10.937	10.154	10.148	10.245	10.193	10.14	0.09
$9S_{1/2} - 7D_{3/2}$	121.055	112.221	111.682	113.053	111.309	111	1
$9S_{1/2} - 7D_{5/2}$	152.377	141.691	140.939	142.669	140.489	140	2
$8D_{3/2} - 6S_{1/2}$	3.405	3.135	3.127	3.166	3.143	3.12	0.04
$8D_{3/2} - 5D_{3/2}$	1.810	1.702	1.705	1.720	1.713	1.70	0.02

$8D_{3/2} - 5D_{5/2}$	1.205	1.140	1.141	1.151	1.146	1.14	0.01
$8D_{3/2} - 7S_{1/2}$	17.831	16.822	16.894	16.967	16.945	16.89	0.07
$8D_{3/2} - 6D_{3/2}$	12.477	11.643	11.654	11.744	11.696	11.65	0.09
$8D_{3/2} - 6D_{5/2}$	8.264	7.726	7.731	7.790	7.760	7.73	0.06
$8D_{3/2} - 8S_{1/2}$	115.302	110.682	112.145	111.622	111.805	112.14	0.52
$8D_{3/2} - 7D_{3/2}$	120.616	113.415	113.603	114.287	113.232	113.60	0.68
$8D_{3/2} - 7D_{5/2}$	81.202	76.569	76.646	77.118	76.407	76.64	0.47
$8D_{3/2} - 5G_{7/2}$	128.817	140.069	140.223	138.652	140.089	140	2
$8D_{3/2} - 9S_{1/2}$	511.407	486.774	487.919	489.996	487.478	487	2
$8D_{5/2} - 6S_{1/2}$	4.208	3.877	3.868	3.915	3.887	3.86	0.04
$8D_{5/2} - 5D_{3/2}$	1.184	1.107	1.110	1.120	1.115	1.11	0.01
$8D_{5/2} - 5D_{5/2}$	2.411	2.272	2.276	2.295	2.286	2.27	0.02
$8D_{5/2} - 7S_{1/2}$	21.762	20.530	20.629	20.710	20.687	20.62	0.08
$8D_{5/2} - 6D_{3/2}$	8.151	7.600	7.608	7.667	7.634	7.60	0.06
$8D_{5/2} - 6D_{5/2}$	16.506	15.422	15.434	15.552	15.488	15.43	0.12
$8D_{5/2} - 8S_{1/2}$	137.988	132.232	134.073	133.409	133.659	134.07	0.66
$8D_{5/2} - 7D_{3/2}$	77.363	72.610	72.761	73.194	72.519	72.76	0.43
$8D_{5/2} - 7D_{5/2}$	159.186	149.838	150.050	150.963	149.574	150.05	0.91
$8D_{5/2} - 5G_{7/2}$	42.129	45.818	45.884	45.357	45.840	45.88	0.53
$8D_{5/2} - 5G_{9/2}$	148.945	161.989	162.223	160.360	162.070	162	2
$8D_{5/2} - 9S_{1/2}$	628.404	598.382	599.785	602.314	599.251	599	3
$8D_{5/2} - 8D_{3/2}$	340.976	323.914	324.186	325.995	323.886	324	2
$6G_{7/2} - 5D_{3/2}$	8.343	6.397	6.511	6.612	6.448	6.51	0.10
$6G_{7/2} - 5D_{5/2}$	2.863	2.221	2.257	2.291	2.236	2.25	0.03
$6G_{7/2} - 6D_{3/2}$	31.314	33.101	33.121	32.925	33.214	33.12	0.19
$6G_{7/2} - 6D_{5/2}$	10.269	10.906	10.916	10.843	10.947	10.91	0.07
$6G_{7/2} - 7D_{3/2}$	284.956	251.086	251.423	255.234	250.971	251	4
$6G_{7/2} - 7D_{5/2}$	96.863	85.650	85.725	87.014	85.577	85	1
$6G_{7/2} - 8D_{3/2}$	778.960	760.268	760.997	762.757	760.580	760	2
$6G_{7/2} - 8D_{5/2}$	260.036	254.034	254.265	254.832	254.130	254.26	0.56
$6G_{9/2} - 5D_{5/2}$	10.123	7.852	7.978	8.101	7.906	7.97	0.12
$6G_{9/2} - 6D_{5/2}$	36.306	38.559	38.595	38.336	38.705	38.59	0.26
$6G_{9/2} - 7D_{5/2}$	342.472	302.824	303.083	307.647	302.562	303	4
$6G_{9/2} - 8D_{5/2}$	919.352	898.141	898.961	900.960	898.484	898	2



**Fig. 8:** Plots for the dynamic E1 polarizabilities of (a) the ground  $6S_{1/2}$  and  $6P_{3/2,1/2}$  states, and (b) the  $5D_{5/2,3/2}$  states in  $\text{Ba}^+$  for the linearly polarized light. The crossings of the dynamic dipole polarizability curves with zero depict the tune-out wavelengths.

Table E: Transition wavelengths ( $\lambda$ ) and electric quadrupole transition properties such as line strengths ( $S_{vk}$ ), transition probabilities ( $A_{vk}$ ) and oscillator strengths ( $f_{kv}$ ) along with their uncertainties between transitions involving an upper energy level (denoted by  $v$ ) and lower energy level (denoted by  $k$ ) of  $\text{Mg}^+$ . Values given in square brackets represent the power of 10.

Levels		$\lambda$	$S_{vk}$	$A_{vk}$	$f_{kv}$
Upper ( $v$ )	Lower ( $k$ )	(in Å)	(in a.u.)	(in $\text{s}^{-1}$ )	
$3P_{3/2}$	$3P_{1/2}$	1092060.718	$1.5151 \pm 0.0007[2]$	$2.732 \pm 0.001[-11]$	$9.769 \pm 0.004[-15]$
$3D_{5/2}$	$3S_{1/2}$	1398.793	$1.4631 \pm 0.0002[2]$	$5.0971 \pm 0.0008[3]$	$4.4860 \pm 0.0007[-6]$
$3D_{5/2}$	$4S_{1/2}$	59338.729	$1.3540 \pm 0.0005[3]$	$3.435 \pm 0.001[-4]$	$5.441 \pm 0.002[-10]$
$3D_{3/2}$	$3S_{1/2}$	1398.776	$9.752 \pm 0.002[1]$	$5.098 \pm 0.001[3]$	$2.9911 \pm 0.0006[-6]$
$3D_{3/2}$	$4S_{1/2}$	59308.112	$9.028 \pm 0.005[2]$	$3.444 \pm 0.002[-4]$	$3.633 \pm 0.002[-10]$
$3D_{3/2}$	$3D_{5/2}$	114942528.736	$2.991 \pm 0.001[2]$	$4.173 \pm 0.002[-21]$	$5.511 \pm 0.003[-21]$
$4P_{1/2}$	$3P_{3/2}$	2229.225	$8.107 \pm 0.005[1]$	$8.245 \pm 0.005[2]$	$3.071 \pm 0.002[-7]$
$4P_{3/2}$	$3P_{1/2}$	2223.175	$7.999 \pm 0.005[1]$	$4.123 \pm 0.003[2]$	$6.111 \pm 0.004[-7]$
$4P_{3/2}$	$3P_{3/2}$	2227.710	$8.069 \pm 0.003[1]$	$4.117 \pm 0.002[2]$	$3.063 \pm 0.001[-7]$
$4P_{3/2}$	$4P_{1/2}$	3276539.973	$3.5822 \pm 0.0006[3]$	$2.6551 \pm 0.0004[-12]$	$8.548 \pm 0.001[-15]$
$5S_{1/2}$	$3D_{5/2}$	4694.765	$1.848 \pm 0.002[2]$	$4.536 \pm 0.006[1]$	$4.997 \pm 0.006[-8]$
$5S_{1/2}$	$3D_{3/2}$	4694.957	$1.232 \pm 0.002[2]$	$3.023 \pm 0.005[1]$	$4.996 \pm 0.009[-8]$
$4D_{5/2}$	$3S_{1/2}$	1071.690	$5.452 \pm 0.004[0]$	$7.191 \pm 0.006[2]$	$3.718 \pm 0.003[-7]$
$4D_{5/2}$	$4S_{1/2}$	4254.298	$2.2532 \pm 0.0005[3]$	$3.0171 \pm 0.0007[2]$	$2.4570 \pm 0.0006[-6]$
$4D_{5/2}$	$3D_{5/2}$	4582.867	$6.834 \pm 0.002[2]$	$6.308 \pm 0.002[1]$	$1.9861 \pm 0.0007[-7]$

$4D_{5/2}$	$3D_{3/2}$	4583.050	$1.708 \pm 0.001[2]$	$1.577 \pm 0.001[1]$	$7.448 \pm 0.004[-8]$
$4D_{5/2}$	$5S_{1/2}$	192278.111	$1.9722 \pm 0.0005[4]$	$1.4003 \pm 0.0004[-5]$	$2.3281 \pm 0.0006[-10]$
$4D_{3/2}$	$3S_{1/2}$	1071.684	$3.633 \pm 0.007[0]$	$7.19 \pm 0.02[2]$	$2.477 \pm 0.005[-7]$
$4D_{3/2}$	$4S_{1/2}$	4254.204	$1.5022 \pm 0.0006[3]$	$3.018 \pm 0.001[2]$	$1.6381 \pm 0.0007[-6]$
$4D_{3/2}$	$3D_{5/2}$	4582.758	$1.7083 \pm 0.0002[2]$	$2.3661 \pm 0.0003[1]$	$4.9670 \pm 0.0007[-8]$
$4D_{3/2}$	$3D_{3/2}$	4582.941	$3.986 \pm 0.002[2]$	$5.519 \pm 0.003[1]$	$1.7381 \pm 0.0008[-7]$
$4D_{3/2}$	$5S_{1/2}$	192086.055	$1.3151 \pm 0.0004[4]$	$1.4073 \pm 0.0004[-5]$	$1.5570 \pm 0.0005[-10]$
$4D_{3/2}$	$4D_{5/2}$	192307692.306	$4.951 \pm 0.002[3]$	$5.269 \pm 0.003[-21]$	$1.948 \pm 0.001[-20]$
$4F_{5/2}$	$3P_{1/2}$	1720.272	$2.171 \pm 0.002[2]$	$2.690 \pm 0.002[3]$	$3.580 \pm 0.003[-6]$
$4F_{5/2}$	$3P_{3/2}$	1722.986	$6.244 \pm 0.003[1]$	$7.674 \pm 0.004[2]$	$5.123 \pm 0.002[-7]$
$4F_{5/2}$	$4P_{1/2}$	7587.178	$6.490 \pm 0.001[3]$	$4.8172 \pm 0.0008[1]$	$1.2471 \pm 0.0002[-6]$
$4F_{5/2}$	$4P_{3/2}$	7604.788	$1.8580 \pm 0.0002[3]$	$1.3631 \pm 0.0001[1]$	$1.7733 \pm 0.0002[-7]$
$4F_{7/2}$	$3P_{3/2}$	1722.983	$3.746 \pm 0.002[2]$	$3.453 \pm 0.001[3]$	$3.074 \pm 0.001[-6]$
$4F_{7/2}$	$4P_{3/2}$	7604.718	$1.11511 \pm 0.00006[4]$	$6.1361 \pm 0.0003[1]$	$1.06401 \pm 0.00006[-6]$
$5P_{1/2}$	$3P_{3/2}$	1620.896	$7.98 \pm 0.01[0]$	$3.996 \pm 0.005[2]$	$7.87 \pm 0.01[-8]$
$5P_{1/2}$	$4P_{3/2}$	5950.574	$1.2841 \pm 0.0004[3]$	$9.636 \pm 0.003[1]$	$2.5572 \pm 0.0007[-7]$
$5P_{1/2}$	$4F_{5/2}$	27356.113	$7.437 \pm 0.002[3]$	$2.7184 \pm 0.0005[-1]$	$1.0163 \pm 0.0002[-8]$
$5P_{3/2}$	$3P_{1/2}$	1618.133	$7.94 \pm 0.01[0]$	$2.005 \pm 0.003[2]$	$1.574 \pm 0.002[-7]$
$5P_{3/2}$	$3P_{3/2}$	1620.534	$7.98 \pm 0.02[0]$	$1.999 \pm 0.005[2]$	$7.87 \pm 0.02[-8]$
$5P_{3/2}$	$4P_{1/2}$	5934.922	$1.2671 \pm 0.0007[3]$	$4.819 \pm 0.002[1]$	$5.090 \pm 0.003[-7]$
$5P_{3/2}$	$4P_{3/2}$	5945.692	$1.2771 \pm 0.0002[3]$	$4.8133 \pm 0.0008[1]$	$2.5512 \pm 0.0004[-7]$
$5P_{3/2}$	$4F_{5/2}$	27253.228	$2.1211 \pm 0.0003[3]$	$3.9494 \pm 0.0005[-2]$	$2.9321 \pm 0.0004[-9]$
$5P_{3/2}$	$4F_{7/2}$	27254.120	$1.2731 \pm 0.0001[4]$	$2.3693 \pm 0.0002[-1]$	$1.3191 \pm 0.0001[-8]$
$5P_{3/2}$	$5P_{1/2}$	7246376.811	$3.2611 \pm 0.0003[4]$	$4.5691 \pm 0.0004[-13]$	$7.1942 \pm 0.0007[-15]$
$6S_{1/2}$	$3D_{5/2}$	3153.921	$1.517 \pm 0.002[1]$	$2.722 \pm 0.003[1]$	$1.353 \pm 0.001[-8]$
$6S_{1/2}$	$3D_{3/2}$	3154.008	$1.011 \pm 0.002[1]$	$1.814 \pm 0.003[1]$	$1.353 \pm 0.002[-8]$
$6S_{1/2}$	$4D_{5/2}$	10115.151	$2.635 \pm 0.002[3]$	$1.393 \pm 0.001[1]$	$7.125 \pm 0.005[-8]$
$6S_{1/2}$	$4D_{3/2}$	10115.683	$1.756 \pm 0.002[3]$	$9.28 \pm 0.02[0]$	$7.12 \pm 0.01[-8]$
$5D_{5/2}$	$3S_{1/2}$	966.934	$8.22 \pm 0.05[-1]$	$1.81 \pm 0.01[2]$	$7.64 \pm 0.05[-8]$
$5D_{5/2}$	$4S_{1/2}$	2974.885	$1.233 \pm 0.001[2]$	$9.882 \pm 0.007[1]$	$3.934 \pm 0.003[-7]$
$5D_{5/2}$	$3D_{5/2}$	3131.899	$4.777 \pm 0.003[1]$	$2.959 \pm 0.001[1]$	$4.352 \pm 0.002[-8]$
$5D_{5/2}$	$3D_{3/2}$	3131.984	$1.194 \pm 0.001[1]$	$7.396 \pm 0.008[0]$	$1.632 \pm 0.002[-8]$
$5D_{5/2}$	$5S_{1/2}$	9408.055	$1.5883 \pm 0.0005[4]$	$4.022 \pm 0.001[1]$	$1.6015 \pm 0.0005[-6]$
$5D_{5/2}$	$4D_{5/2}$	9892.068	$7.244 \pm 0.002[3]$	$1.4273 \pm 0.0003[1]$	$2.0946 \pm 0.0005[-7]$
$5D_{5/2}$	$4D_{3/2}$	9892.577	$1.811 \pm 0.002[3]$	$3.566 \pm 0.003[0]$	$7.850 \pm 0.007[-8]$
$5D_{5/2}$	$6S_{1/2}$	448531.061	$1.3706 \pm 0.0002[5]$	$1.4087 \pm 0.0002[-6]$	$1.2751 \pm 0.0002[-10]$
$5D_{3/2}$	$3S_{1/2}$	966.931	$5.49 \pm 0.01[-1]$	$1.818 \pm 0.005[2]$	$5.09 \pm 0.01[-8]$
$5D_{3/2}$	$4S_{1/2}$	2974.858	$8.223 \pm 0.009[1]$	$9.88 \pm 0.01[1]$	$2.622 \pm 0.003[-7]$

$5D_{3/2}$	$3D_{5/2}$	3131.870	$1.194 \pm 0.001[1]$	$1.109 \pm 0.001[1]$	$1.088 \pm 0.001[-8]$
$5D_{3/2}$	$3D_{3/2}$	3131.955	$2.787 \pm 0.002[1]$	$2.588 \pm 0.002[1]$	$3.807 \pm 0.003[-8]$
$5D_{3/2}$	$5S_{1/2}$	9407.789	$1.059 \pm 0.001[4]$	$4.023 \pm 0.002[1]$	$1.067 \pm 0.001[-6]$
$5D_{3/2}$	$4D_{5/2}$	9891.774	$1.8111 \pm 0.0001[3]$	$5.3542 \pm 0.0002[0]$	$5.2363 \pm 0.0002[-8]$
$5D_{3/2}$	$4D_{3/2}$	9892.283	$4.225 \pm 0.001[3]$	$1.2484 \pm 0.0004[1]$	$1.8322 \pm 0.0005[-7]$
$5D_{3/2}$	$6S_{1/2}$	447928.331	$9.135 \pm 0.002[4]$	$1.4181 \pm 0.0004[-6]$	$8.533 \pm 0.002[-11]$
$5D_{3/2}$	$5D_{5/2}$	333333333.330	$3.6221 \pm 0.0007[4]$	$2.4641 \pm 0.0005[-21]$	$2.7372 \pm 0.0006[-20]$
$5F_{5/2}$	$3P_{1/2}$	1470.144	$5.528 \pm 0.003[1]$	$1.5021 \pm 0.0008[3]$	$1.4604 \pm 0.0008[-6]$
$5F_{5/2}$	$3P_{3/2}$	1472.125	$1.585 \pm 0.002[1]$	$4.280 \pm 0.006[2]$	$2.085 \pm 0.003[-7]$
$5F_{5/2}$	$4P_{1/2}$	4334.566	$4.948 \pm 0.004[2]$	$6.035 \pm 0.005[1]$	$5.100 \pm 0.004[-7]$
$5F_{5/2}$	$4P_{3/2}$	4340.307	$1.4322 \pm 0.0007[2]$	$1.7351 \pm 0.0008[1]$	$7.351 \pm 0.004[-8]$
$5F_{5/2}$	$5P_{1/2}$	16039.161	$5.640 \pm 0.001[4]$	$9.916 \pm 0.002[0]$	$1.1473 \pm 0.0002[-6]$
$5F_{5/2}$	$5P_{3/2}$	16074.741	$1.61521 \pm 0.00007[4]$	$2.8093 \pm 0.0001[0]$	$1.63211 \pm 0.00007[-7]$
$5F_{7/2}$	$3P_{3/2}$	1472.124	$9.516 \pm 0.004[1]$	$1.9261 \pm 0.0007[3]$	$1.2525 \pm 0.0005[-6]$
$5F_{7/2}$	$4P_{3/2}$	4340.296	$8.592 \pm 0.002[2]$	$7.808 \pm 0.002[1]$	$4.411 \pm 0.001[-7]$
$5F_{7/2}$	$5P_{3/2}$	16074.586	$9.6921 \pm 0.0004[4]$	$1.26420 \pm 0.00005[1]$	$9.7943 \pm 0.0004[-7]$
$5G_{7/2}$	$3D_{5/2}$	3104.099	$1.526 \pm 0.001[2]$	$7.412 \pm 0.006[1]$	$1.427 \pm 0.001[-7]$
$5G_{7/2}$	$3D_{3/2}$	3104.183	$1.373 \pm 0.001[3]$	$6.668 \pm 0.007[2]$	$1.927 \pm 0.002[-6]$
$5G_{7/2}$	$4D_{5/2}$	9619.945	$4.5071 \pm 0.0009[3]$	$7.658 \pm 0.002[0]$	$1.4173 \pm 0.0003[-7]$
$5G_{7/2}$	$4D_{3/2}$	9620.426	$4.056 \pm 0.002[4]$	$6.890 \pm 0.003[1]$	$1.9121 \pm 0.0007[-6]$
$5G_{7/2}$	$5D_{5/2}$	349699.259	$8.288 \pm 0.002[3]$	$2.2183 \pm 0.0004[-7]$	$5.424 \pm 0.001[-12]$
$5G_{7/2}$	$5D_{3/2}$	350066.513	$7.459 \pm 0.002[4]$	$1.9861 \pm 0.0005[-6]$	$7.299 \pm 0.002[-11]$
$5G_{9/2}$	$3D_{5/2}$	3104.099	$1.907 \pm 0.002[3]$	$7.412 \pm 0.007[2]$	$1.785 \pm 0.002[-6]$
$5G_{9/2}$	$4D_{5/2}$	9619.945	$5.634 \pm 0.001[4]$	$7.658 \pm 0.002[1]$	$1.7713 \pm 0.0004[-6]$
$5G_{9/2}$	$5D_{5/2}$	349699.259	$1.0364 \pm 0.0002[5]$	$2.2183 \pm 0.0004[-6]$	$6.779 \pm 0.001[-11]$
$6D_{5/2}$	$3S_{1/2}$	918.273	$2.266 \pm 0.009[-1]$	$6.47 \pm 0.03[1]$	$2.45 \pm 0.01[-8]$
$6D_{5/2}$	$4S_{1/2}$	2557.867	$2.445 \pm 0.002[1]$	$4.168 \pm 0.003[1]$	$1.226 \pm 0.001[-7]$
$6D_{5/2}$	$3D_{5/2}$	2673.094	$1.177 \pm 0.001[1]$	$1.609 \pm 0.002[1]$	$1.725 \pm 0.002[-8]$
$6D_{5/2}$	$3D_{3/2}$	2673.156	$2.945 \pm 0.003[0]$	$4.026 \pm 0.005[0]$	$6.471 \pm 0.007[-9]$
$6D_{5/2}$	$5S_{1/2}$	6207.513	$9.357 \pm 0.004[2]$	$1.8956 \pm 0.0008[1]$	$3.284 \pm 0.001[-7]$
$6D_{5/2}$	$4D_{5/2}$	6414.603	$4.935 \pm 0.001[2]$	$8.480 \pm 0.002[0]$	$5.232 \pm 0.001[-8]$
$6D_{5/2}$	$4D_{3/2}$	6414.817	$1.2342 \pm 0.0006[2]$	$2.119 \pm 0.001[0]$	$1.962 \pm 0.001[-8]$
$6D_{5/2}$	$6S_{1/2}$	17533.801	$7.429 \pm 0.002[4]$	$8.367 \pm 0.003[0]$	$1.1573 \pm 0.0004[-6]$
$6D_{5/2}$	$5D_{5/2}$	18247.110	$4.1692 \pm 0.0008[4]$	$3.8464 \pm 0.0007[0]$	$1.9206 \pm 0.0003[-7]$
$6D_{5/2}$	$5D_{3/2}$	18248.109	$1.0423 \pm 0.0006[4]$	$9.612 \pm 0.005[-1]$	$7.198 \pm 0.004[-8]$
$6D_{5/2}$	$5G_{7/2}$	19251.650	$4.054 \pm 0.004[2]$	$2.861 \pm 0.003[-2]$	$1.192 \pm 0.001[-9]$
$6D_{5/2}$	$5G_{9/2}$	19251.650	$5.067 \pm 0.006[3]$	$3.576 \pm 0.004[-1]$	$1.192 \pm 0.001[-8]$
$6D_{3/2}$	$3S_{1/2}$	918.272	$1.51 \pm 0.02[-1]$	$6.45 \pm 0.09[1]$	$1.63 \pm 0.02[-8]$

$6D_{3/2}$	$4S_{1/2}$	2557.855	$1.629 \pm 0.004[1]$	$4.16 \pm 0.01[1]$	$8.17 \pm 0.02[-8]$
$6D_{3/2}$	$3D_{5/2}$	2673.081	$2.941 \pm 0.006[0]$	$6.03 \pm 0.02[0]$	$4.31 \pm 0.01[-9]$
$6D_{3/2}$	$3D_{3/2}$	2673.144	$6.86 \pm 0.01[0]$	$1.408 \pm 0.002[1]$	$1.508 \pm 0.002[-8]$
$6D_{3/2}$	$5S_{1/2}$	6207.444	$6.237 \pm 0.003[2]$	$1.895 \pm 0.001[1]$	$2.189 \pm 0.001[-7]$
$6D_{3/2}$	$4D_{5/2}$	6414.529	$1.2332 \pm 0.0004[2]$	$3.180 \pm 0.001[0]$	$1.3081 \pm 0.0005[-8]$
$6D_{3/2}$	$4D_{3/2}$	6414.743	$2.878 \pm 0.001[2]$	$7.419 \pm 0.003[0]$	$4.577 \pm 0.002[-8]$
$6D_{3/2}$	$6S_{1/2}$	17533.247	$4.954 \pm 0.003[4]$	$8.369 \pm 0.005[0]$	$7.716 \pm 0.004[-7]$
$6D_{3/2}$	$5D_{5/2}$	18246.510	$1.0434 \pm 0.0001[4]$	$1.4431 \pm 0.0002[0]$	$4.8021 \pm 0.0005[-8]$
$6D_{3/2}$	$5D_{3/2}$	18247.509	$2.4325 \pm 0.0009[4]$	$3.365 \pm 0.001[0]$	$1.6801 \pm 0.0006[-7]$
$6D_{3/2}$	$5G_{7/2}$	19250.983	$3.649 \pm 0.006[3]$	$3.864 \pm 0.006[-1]$	$1.074 \pm 0.001[-8]$
$6D_{3/2}$	$6D_{5/2}$	555555555.577	$1.7332 \pm 0.0003[5]$	$9.168 \pm 0.002[-22]$	$2.8282 \pm 0.0005[-20]$
$6G_{7/2}$	$3D_{5/2}$	2660.858	$5.256 \pm 0.001[1]$	$5.516 \pm 0.001[1]$	$7.807 \pm 0.002[-8]$
$6G_{7/2}$	$3D_{3/2}$	2660.919	$4.729 \pm 0.003[2]$	$4.963 \pm 0.003[2]$	$1.0537 \pm 0.0007[-6]$
$6G_{7/2}$	$4D_{5/2}$	6344.589	$7.67 \pm 0.05[0]$	$1.045 \pm 0.007[-1]$	$8.41 \pm 0.06[-10]$
$6G_{7/2}$	$4D_{3/2}$	6344.799	$6.89 \pm 0.08[1]$	$9.38 \pm 0.11[-1]$	$1.13 \pm 0.01[-8]$
$6G_{7/2}$	$5D_{5/2}$	17691.756	$2.4264 \pm 0.0009[4]$	$1.9597 \pm 0.0007[0]$	$1.2262 \pm 0.0004[-7]$
$6G_{7/2}$	$5D_{3/2}$	17692.695	$2.183 \pm 0.001[5]$	$1.763 \pm 0.001[1]$	$1.6548 \pm 0.0009[-6]$
$6G_{7/2}$	$6D_{5/2}$	581293.960	$6.412 \pm 0.001[4]$	$1.3524 \pm 0.0003[-7]$	$9.135 \pm 0.002[-12]$
$6G_{7/2}$	$6D_{3/2}$	581902.822	$5.771 \pm 0.001[5]$	$1.2108 \pm 0.0002[-6]$	$1.2294 \pm 0.0002[-10]$
$6G_{9/2}$	$3D_{5/2}$	2660.858	$6.569 \pm 0.003[2]$	$5.516 \pm 0.002[2]$	$9.759 \pm 0.004[-7]$
$6G_{9/2}$	$4D_{5/2}$	6344.589	$9.58 \pm 0.09[1]$	$1.04 \pm 0.01[0]$	$1.05 \pm 0.01[-8]$
$6G_{9/2}$	$5D_{5/2}$	17691.756	$3.033 \pm 0.001[5]$	$1.9597 \pm 0.0007[1]$	$1.5327 \pm 0.0005[-6]$
$6G_{9/2}$	$6D_{5/2}$	581293.960	$8.015 \pm 0.002[5]$	$1.3525 \pm 0.0003[-6]$	$1.1419 \pm 0.0002[-10]$

Table F: Transition wavelengths ( $\lambda$ ) and electric quadrupole transition properties such as line strengths ( $S_{vk}$ ), transition probabilities ( $A_{vk}$ ) and oscillator strengths ( $f_{kv}$ ) along with their uncertainties between transitions involving an upper energy level (denoted by  $v$ ) and lower energy level (denoted by  $k$ ) of  $\text{Ca}^+$ . Values given in square brackets represent the power of 10.

Levels		$\lambda$	$S_{vk}$	$A_{vk}$	$f_{kv}$
Upper ( $v$ )	Lower ( $k$ )	(in Å)	(in a.u.)	(in $\text{s}^{-1}$ )	
$3D_{3/2}$	$4S_{1/2}$	7325.905	$6.31 \pm 0.06[1]$	$0.838 \pm 0.008[0]$	$1.35 \pm 0.01[-8]$
$3D_{5/2}$	$4S_{1/2}$	7293.477	$9.51 \pm 0.07[1]$	$0.860 \pm 0.007[0]$	$2.05 \pm 0.02[-8]$
$3D_{5/2}$	$3D_{3/2}$	1647717.911	$1.43 \pm 0.01[1]$	$2.19 \pm 0.02[-13]$	$1.34 \pm 0.01[-16]$
$4P_{3/2}$	$4P_{1/2}$	448651.801	$3.75 \pm 0.02[2]$	$5.77 \pm 0.03[-9]$	$3.48 \pm 0.02[-13]$
$5S_{1/2}$	$3D_{3/2}$	2596.273	$1.56 \pm 0.07[1]$	$7.42 \pm 0.34[1]$	$3.75 \pm 0.17[-8]$
$5S_{1/2}$	$3D_{5/2}$	2600.371	$2.36 \pm 0.11[1]$	$1.11 \pm 0.05[2]$	$3.763 \pm 0.17[-8]$

$4D_{3/2}$	$4S_{1/2}$	1759.347	$1.61 \pm 0.01[2]$	$2.68 \pm 0.02[3]$	$2.48 \pm 0.02[-6]$
$4D_{3/2}$	$3D_{3/2}$	2315.401	$4.15 \pm 0.12[1]$	$1.74 \pm 0.05[2]$	$1.41 \pm 0.04[-7]$
$4D_{3/2}$	$3D_{5/2}$	2318.659	$1.79 \pm 0.05[1]$	$7.48 \pm 0.21[1]$	$4.02 \pm 0.11[-8]$
$4D_{3/2}$	$5S_{1/2}$	21402.643	$2.81 \pm 0.04[3]$	$1.75 \pm 0.02[-1]$	$2.40 \pm 0.03[-8]$
$4D_{5/2}$	$4S_{1/2}$	1758.753	$2.42 \pm 0.02[2]$	$2.67 \pm 0.02[3]$	$3.73 \pm 0.03[-6]$
$4D_{5/2}$	$3D_{3/2}$	2314.371	$1.77 \pm 0.05[1]$	$4.98 \pm 0.14[1]$	$6.01 \pm 0.17[-8]$
$4D_{5/2}$	$3D_{5/2}$	2317.627	$7.15 \pm 0.20[1]$	$5.00 \pm 0.14[1]$	$1.61 \pm 0.05[-7]$
$4D_{5/2}$	$5S_{1/2}$	21315.008	$4.21 \pm 0.06[3]$	$1.78 \pm 0.03[-1]$	$3.65 \pm 0.05[-8]$
$4D_{5/2}$	$4D_{3/2}$	5205622.071	$1.08 \pm 0.02[3]$	$5.27 \pm 0.09[-14]$	$3.21 \pm 0.06[-16]$
$5P_{1/2}$	$4P_{3/2}$	2847.492	$1.677 \pm 0.005[2]$	$5.02 \pm 0.02[2]$	$3.049 \pm 0.009[-7]$
$5P_{3/2}$	$4P_{1/2}$	2823.282	$1.605 \pm 0.005[2]$	$2.505 \pm 0.008[2]$	$5.98 \pm 0.02[-7]$
$5P_{3/2}$	$4P_{3/2}$	2841.161	$1.651 \pm 0.005[2]$	$2.496 \pm 0.007[2]$	$3.021 \pm 0.009[-7]$
$5P_{3/2}$	$5P_{1/2}$	1277791.975	$6.66 \pm 0.03[3]$	$5.47 \pm 0.02[-10]$	$2.67 \pm 0.01[-13]$
$4F_{5/2}$	$4P_{1/2}$	2332.883	$6.85 \pm 0.03[2]$	$1.851 \pm 0.008[3]$	$4.53 \pm 0.02[-6]$
$4F_{5/2}$	$4P_{3/2}$	2345.077	$1.991 \pm 0.008[2]$	$5.24 \pm 0.02[2]$	$6.48 \pm 0.03[-7]$
$4F_{5/2}$	$5P_{1/2}$	13290.997	$8.77 \pm 0.03[3]$	$3.95 \pm 0.01[0]$	$3.136 \pm 0.009[-7]$
$4F_{5/2}$	$5P_{3/2}$	13430.696	$2.515 \pm 0.007[3]$	$1.074 \pm 0.003[0]$	$4.35 \pm 0.01[-8]$
$4F_{7/2}$	$4P_{3/2}$	2345.077	$1.195 \pm 0.005[3]$	$2.36 \pm 0.01[3]$	$3.88 \pm 0.02[-6]$
$4F_{7/2}$	$5P_{3/2}$	13430.696	$1.509 \pm 0.004[4]$	$4.83 \pm 0.01[0]$	$2.614 \pm 0.008[-7]$
$6S_{1/2}$	$3D_{3/2}$	1753.542	$1.07 \pm 0.02[0]$	$3.62 \pm 0.06[1]$	$8.34 \pm 0.15[-9]$
$6S_{1/2}$	$3D_{5/2}$	1755.410	$1.62 \pm 0.03[0]$	$5.43 \pm 0.08[1]$	$8.35 \pm 0.13[-9]$
$6S_{1/2}$	$4D_{3/2}$	7226.284	$7.79 \pm 0.28[2]$	$2.21 \pm 0.08[1]$	$8.67 \pm 0.32[-8]$
$6S_{1/2}$	$4D_{5/2}$	7236.329	$1.17 \pm 0.04[3]$	$3.32 \pm 0.12[1]$	$8.68 \pm 0.32[-8]$
$5D_{3/2}$	$4S_{1/2}$	1375.095	$1.75 \pm 0.03[1]$	$9.97 \pm 0.14[2]$	$5.65 \pm 0.08[-7]$
$5D_{3/2}$	$3D_{3/2}$	1692.848	$3.85 \pm 0.08[0]$	$7.75 \pm 0.16[1]$	$3.33 \pm 0.07[-8]$
$5D_{3/2}$	$3D_{5/2}$	1694.589	$1.65 \pm 0.03[0]$	$3.32 \pm 0.05[1]$	$9.52 \pm 0.15[-9]$
$5D_{3/2}$	$5S_{1/2}$	4864.925	$1.66 \pm 0.02[3]$	$1.71 \pm 0.02[2]$	$1.21 \pm 0.01[-6]$
$5D_{3/2}$	$4D_{3/2}$	6296.047	$1.11 \pm 0.02[3]$	$3.15 \pm 0.05[1]$	$1.87 \pm 0.03[-7]$
$5D_{3/2}$	$4D_{5/2}$	6303.671	$4.79 \pm 0.08[2]$	$1.35 \pm 0.02[1]$	$5.35 \pm 0.09[-8]$
$5D_{3/2}$	$6S_{1/2}$	48909.082	$2.88 \pm 0.03[4]$	$2.88 \pm 0.03[-2]$	$2.06 \pm 0.02[-8]$
$5D_{5/2}$	$4S_{1/2}$	1374.930	$2.63 \pm 0.04[1]$	$9.99 \pm 0.15[2]$	$8.49 \pm 0.13[-7]$
$5D_{5/2}$	$3D_{3/2}$	1692.598	$1.65 \pm 0.02[0]$	$2.22 \pm 0.03[1]$	$1.43 \pm 0.02[-8]$
$5D_{5/2}$	$3D_{5/2}$	1694.339	$6.63 \pm 0.15[0]$	$8.85 \pm 0.21[1]$	$3.81 \pm 0.08[-8]$
$5D_{5/2}$	$5S_{1/2}$	4862.867	$2.48 \pm 0.03[3]$	$1.71 \pm 0.02[2]$	$1.82 \pm 0.02[-6]$
$5D_{5/2}$	$4D_{3/2}$	6292.601	$4.75 \pm 0.08[2]$	$8.99 \pm 0.15[0]$	$8.01 \pm 0.13[-8]$
$5D_{5/2}$	$4D_{5/2}$	6300.216	$1.91 \pm 0.03[3]$	$3.59 \pm 0.06[1]$	$2.14 \pm 0.04[-7]$
$5D_{5/2}$	$6S_{1/2}$	48701.852	$4.33 \pm 0.06[4]$	$2.95 \pm 0.04[-2]$	$3.14 \pm 0.04[-8]$
$5D_{5/2}$	$5D_{3/2}$	11494252.873	$1.20 \pm 0.02[4]$	$1.12 \pm 0.01[-14]$	$3.32 \pm 0.04[-16]$

$6P_{1/2}$	$4P_{3/2}$	2037.883	$1.655 \pm 0.007[1]$	$2.64 \pm 0.01[2]$	$8.21 \pm 0.04[-8]$
$6P_{1/2}$	$5P_{3/2}$	7207.913	$2.201 \pm 0.005[3]$	$6.33 \pm 0.02[1]$	$2.466 \pm 0.006[-7]$
$6P_{1/2}$	$4F_{5/2}$	15556.914	$3.979 \pm 0.005[3]$	$2.445 \pm 0.003[0]$	$2.957 \pm 0.004[-8]$
$6P_{3/2}$	$4P_{1/2}$	2027.154	$1.624 \pm 0.006[1]$	$1.328 \pm 0.005[2]$	$1.636 \pm 0.006[-7]$
$6P_{3/2}$	$4P_{3/2}$	2036.355	$1.648 \pm 0.007[1]$	$1.317 \pm 0.006[2]$	$8.19 \pm 0.04[-8]$
$6P_{3/2}$	$5P_{1/2}$	7148.611	$2.112 \pm 0.004[3]$	$3.167 \pm 0.007[1]$	$4.85 \pm 0.01[-7]$
$6P_{3/2}$	$5P_{3/2}$	7188.829	$2.165 \pm 0.004[3]$	$3.156 \pm 0.007[1]$	$2.445 \pm 0.005[-7]$
$6P_{3/2}$	$4F_{5/2}$	15468.286	$1.124 \pm 0.002[3]$	$3.554 \pm 0.006[-1]$	$8.50 \pm 0.02[-9]$
$6P_{3/2}$	$4F_{7/2}$	15468.286	$6.74 \pm 0.01[3]$	$2.133 \pm 0.004[0]$	$3.825 \pm 0.006[-8]$
$6P_{3/2}$	$6P_{1/2}$	2715177.844	$5.24 \pm 0.02[4]$	$9.94 \pm 0.03[-11]$	$2.197 \pm 0.007[-13]$
$5F_{5/2}$	$4P_{1/2}$	1892.402	$9.52 \pm 0.04[1]$	$7.32 \pm 0.03[2]$	$1.178 \pm 0.005[-6]$
$5F_{5/2}$	$4P_{3/2}$	1900.418	$2.73 \pm 0.01[1]$	$2.055 \pm 0.008[2]$	$1.669 \pm 0.006[-7]$
$5F_{5/2}$	$5P_{1/2}$	5713.838	$3.74 \pm 0.02[3]$	$1.147 \pm 0.007[2]$	$1.684 \pm 0.009[-6]$
$5F_{5/2}$	$5P_{3/2}$	5739.503	$1.094 \pm 0.007[3]$	$3.28 \pm 0.02[1]$	$2.43 \pm 0.01[-7]$
$5F_{5/2}$	$6P_{1/2}$	28173.220	$8.18 \pm 0.02[4]$	$8.60 \pm 0.02[-1]$	$3.071 \pm 0.008[-7]$
$5F_{5/2}$	$6P_{3/2}$	28468.616	$2.347 \pm 0.006[4]$	$2.343 \pm 0.006[-1]$	$4.27 \pm 0.01[-8]$
$5F_{7/2}$	$4P_{3/2}$	1900.418	$1.638 \pm 0.005[2]$	$9.25 \pm 0.03[2]$	$1.002 \pm 0.003[-6]$
$5F_{7/2}$	$5P_{3/2}$	5739.503	$6.56 \pm 0.04[3]$	$1.475 \pm 0.009[2]$	$1.457 \pm 0.009[-6]$
$5F_{7/2}$	$6P_{3/2}$	28468.616	$1.408 \pm 0.004[5]$	$1.054 \pm 0.003[0]$	$2.562 \pm 0.007[-7]$
$5G_{7/2}$	$3D_{3/2}$	1550.038	$2.05 \pm 0.09[1]$	$3.21 \pm 0.14[2]$	$2.31 \pm 0.10[-7]$
$5G_{7/2}$	$3D_{5/2}$	1551.497	$2.29 \pm 0.09[0]$	$3.57 \pm 0.14[1]$	$1.72 \pm 0.07[-8]$
$5G_{7/2}$	$4D_{3/2}$	4689.228	$7.71 \pm 0.17[3]$	$4.76 \pm 0.11[2]$	$3.14 \pm 0.07[-6]$
$5G_{7/2}$	$4D_{5/2}$	4693.456	$8.59 \pm 0.22[2]$	$5.28 \pm 0.13[1]$	$2.33 \pm 0.06[-7]$
$5G_{7/2}$	$5D_{3/2}$	18373.941	$7.19 \pm 0.04[4]$	$4.81 \pm 0.02[0]$	$4.86 \pm 0.02[-7]$
$5G_{7/2}$	$5D_{5/2}$	18403.361	$7.99 \pm 0.04[3]$	$5.30 \pm 0.03[-1]$	$3.58 \pm 0.02[-8]$
$5G_{9/2}$	$3D_{5/2}$	1551.497	$2.87 \pm 0.13[1]$	$3.57 \pm 0.16[2]$	$2.15 \pm 0.09[-7]$
$5G_{9/2}$	$4D_{5/2}$	4693.456	$1.07 \pm 0.02[4]$	$5.28 \pm 0.10[2]$	$2.91 \pm 0.05[-6]$
$5G_{9/2}$	$5D_{5/2}$	18403.361	$9.99 \pm 0.05[4]$	$5.30 \pm 0.03[0]$	$4.48 \pm 0.02[-7]$
$7S_{1/2}$	$3D_{3/2}$	1519.800	$2.92 \pm 0.05[-1]$	$2.01 \pm 0.04[1]$	$3.48 \pm 0.06[-9]$
$7S_{1/2}$	$3D_{5/2}$	1521.204	$4.41 \pm 0.08[-1]$	$3.03 \pm 0.05[1]$	$3.50 \pm 0.06[-9]$
$7S_{1/2}$	$4D_{3/2}$	4423.011	$3.89 \pm 0.07[1]$	$1.28 \pm 0.02[1]$	$1.89 \pm 0.03[-8]$
$7S_{1/2}$	$4D_{5/2}$	4426.772	$5.86 \pm 0.11[1]$	$1.93 \pm 0.03[1]$	$1.89 \pm 0.03[-8]$
$7S_{1/2}$	$5D_{3/2}$	14867.567	$8.08 \pm 0.18[3]$	$6.23 \pm 0.14[0]$	$1.03 \pm 0.02[-7]$
$7S_{1/2}$	$5D_{5/2}$	14886.823	$1.22 \pm 0.04[4]$	$9.33 \pm 0.34[0]$	$1.03 \pm 0.03[-7]$
$6D_{3/2}$	$4S_{1/2}$	1241.903	$4.96 \pm 0.09[0]$	$4.71 \pm 0.08[2]$	$2.17 \pm 0.04[-7]$
$6D_{3/2}$	$3D_{3/2}$	1495.408	$1.12 \pm 0.04[0]$	$4.21 \pm 0.15[1]$	$1.41 \pm 0.05[-8]$
$6D_{3/2}$	$3D_{5/2}$	1496.767	$4.83 \pm 0.14[-1]$	$1.80 \pm 0.05[1]$	$4.03 \pm 0.12[-9]$
$6D_{3/2}$	$5S_{1/2}$	3526.764	$1.88 \pm 0.01[2]$	$9.69 \pm 0.05[1]$	$3.62 \pm 0.02[-7]$

$6D_{3/2}$	$4D_{3/2}$	4222.566	$8.18 \pm 0.13[1]$	$1.71 \pm 0.03[1]$	$4.56 \pm 0.07[-8]$
$6D_{3/2}$	$4D_{5/2}$	4225.994	$3.52 \pm 0.05[1]$	$7.30 \pm 0.09[0]$	$1.30 \pm 0.02[-8]$
$6D_{3/2}$	$6S_{1/2}$	10158.565	$9.45 \pm 0.14[3]$	$2.44 \pm 0.03[1]$	$7.56 \pm 0.11[-7]$
$6D_{3/2}$	$5D_{3/2}$	12821.663	$8.97 \pm 0.10[3]$	$7.25 \pm 0.08[0]$	$1.78 \pm 0.02[-7]$
$6D_{3/2}$	$5D_{5/2}$	12835.981	$3.86 \pm 0.04[3]$	$3.10 \pm 0.03[0]$	$5.11 \pm 0.06[-8]$
$6D_{3/2}$	$5G_{7/2}$	42430.234	$3.98 \pm 0.04[4]$	$8.11 \pm 0.08[-2]$	$1.09 \pm 0.01[-8]$
$6D_{3/2}$	$7S_{1/2}$	93174.935	$1.672 \pm 0.008[5]$	$6.66 \pm 0.03[-3]$	$1.735 \pm 0.008[-8]$
$6D_{5/2}$	$4S_{1/2}$	1241.832	$7.47 \pm 0.16[0]$	$4.72 \pm 0.10[2]$	$3.27 \pm 0.07[-7]$
$6D_{5/2}$	$3D_{3/2}$	1495.305	$4.82 \pm 0.14[-1]$	$1.20 \pm 0.03[1]$	$6.05 \pm 0.17[-9]$
$6D_{5/2}$	$3D_{5/2}$	1496.663	$1.94 \pm 0.05[0]$	$4.81 \pm 0.14[1]$	$1.62 \pm 0.04[-8]$
$6D_{5/2}$	$5S_{1/2}$	3526.180	$2.84 \pm 0.01[2]$	$9.70 \pm 0.05[1]$	$5.43 \pm 0.03[-7]$
$6D_{5/2}$	$4D_{3/2}$	4221.741	$3.51 \pm 0.05[1]$	$4.88 \pm 0.06[0]$	$1.96 \pm 0.03[-8]$
$6D_{5/2}$	$4D_{5/2}$	4225.167	$1.41 \pm 0.02[2]$	$1.95 \pm 0.03[1]$	$5.22 \pm 0.08[-8]$
$6D_{5/2}$	$6S_{1/2}$	10153.789	$1.41 \pm 0.02[4]$	$2.44 \pm 0.03[1]$	$1.13 \pm 0.01[-6]$
$6D_{5/2}$	$5D_{3/2}$	12814.056	$3.83 \pm 0.04[3]$	$2.07 \pm 0.02[0]$	$7.64 \pm 0.08[-8]$
$6D_{5/2}$	$5D_{5/2}$	12828.357	$1.54 \pm 0.01[4]$	$8.27 \pm 0.09[0]$	$2.042 \pm 0.02[-7]$
$6D_{5/2}$	$5G_{7/2}$	42347.042	$4.42 \pm 0.06[3]$	$6.05 \pm 0.09[-3]$	$1.22 \pm 0.02[-9]$
$6D_{5/2}$	$5G_{9/2}$	42347.042	$5.52 \pm 0.09[4]$	$7.56 \pm 0.13[-2]$	$1.22 \pm 0.02[-8]$
$6D_{5/2}$	$7S_{1/2}$	92774.705	$2.51 \pm 0.02[5]$	$6.82 \pm 0.05[-3]$	$2.64 \pm 0.02[-8]$
$6D_{5/2}$	$6D_{3/2}$	21598272.138	$7.22 \pm 0.05[4]$	$2.86 \pm 0.02[-15]$	$3.01 \pm 0.02[-16]$
$6G_{7/2}$	$3D_{3/2}$	1430.823	$1.32 \pm 0.04[1]$	$3.07 \pm 0.10[2]$	$1.88 \pm 0.06[-7]$
$6G_{7/2}$	$3D_{5/2}$	1432.067	$1.47 \pm 0.05[0]$	$3.43 \pm 0.11[1]$	$1.40 \pm 0.05[-8]$
$6G_{7/2}$	$4D_{3/2}$	3745.213	$1.203 \pm 0.005[3]$	$2.285 \pm 0.009[2]$	$9.61 \pm 0.04[-7]$
$6G_{7/2}$	$4D_{5/2}$	3747.909	$1.337 \pm 0.004[2]$	$2.532 \pm 0.008[1]$	$7.11 \pm 0.02[-8]$
$6G_{7/2}$	$5D_{3/2}$	9244.049	$1.87 \pm 0.08[4]$	$3.88 \pm 0.17[1]$	$9.95 \pm 0.44[-7]$
$6G_{7/2}$	$5D_{5/2}$	9251.489	$2.09 \pm 0.08[3]$	$4.32 \pm 0.18[0]$	$7.39 \pm 0.31[-8]$
$6G_{7/2}$	$6D_{3/2}$	33129.366	$4.79 \pm 0.04[5]$	$1.68 \pm 0.01[0]$	$5.53 \pm 0.05[-7]$
$6G_{7/2}$	$6D_{5/2}$	33180.261	$5.33 \pm 0.04[4]$	$1.85 \pm 0.01[-1]$	$4.08 \pm 0.03[-8]$
$6G_{9/2}$	$3D_{5/2}$	1432.067	$1.84 \pm 0.06[1]$	$3.42 \pm 0.11[2]$	$1.75 \pm 0.06[-7]$
$6G_{9/2}$	$4D_{5/2}$	3747.909	$1.672 \pm 0.002[3]$	$2.532 \pm 0.003[2]$	$8.88 \pm 0.01[-7]$
$6G_{9/2}$	$5D_{5/2}$	9251.489	$2.62 \pm 0.09[4]$	$4.32 \pm 0.16[-1]$	$9.24 \pm 0.34[-7]$
$6G_{9/2}$	$6D_{5/2}$	33180.261	$6.66 \pm 0.05[5]$	$1.85 \pm 0.01[0]$	$5.10 \pm 0.04[-7]$

Table G: Transition wavelengths ( $\lambda$ ) and electric quadrupole transition properties such as line strengths ( $S_{vk}$ ), transition probabilities ( $A_{vk}$ ) and oscillator strengths ( $f_{kv}$ ) along with their uncertainties between transitions involving an upper energy level (denoted by  $v$ ) and lower energy level (denoted by  $k$ ) of  $\text{Sr}^+$ . Values given in square brackets represent the power of 10.

Levels	$\lambda$	$S_{vk}$	$A_{vk}$	$f_{kv}$
--------	-----------	----------	----------	----------

Upper ( $v$ )	Lower ( $k$ )	(in Å)	(in a.u.)	(in $s^{-1}$ )
$4D_{3/2}$	$5S_{1/2}$	6870.066	$1.239 \pm 0.009[2]$	$2.26 \pm 0.01[0]$
$4D_{5/2}$	$5S_{1/2}$	6740.252	$1.88 \pm 0.01[2]$	$2.53 \pm 0.02[0]$
$4D_{5/2}$	$4D_{3/2}$	356709.709	$3.57 \pm 0.02[1]$	$1.155 \pm 0.007[-9]$
$5P_{3/2}$	$5P_{1/2}$	124772.290	$5.47 \pm 0.02[2]$	$5.07 \pm 0.02[-6]$
$6S_{1/2}$	$4D_{3/2}$	3013.806	$3.64 \pm 0.08[1]$	$8.19 \pm 0.19[1]$
$6S_{1/2}$	$4D_{5/2}$	3039.486	$5.67 \pm 0.14[1]$	$1.22 \pm 0.03[2]$
$5D_{3/2}$	$5S_{1/2}$	1876.624	$1.69 \pm 0.01[2]$	$2.04 \pm 0.02[3]$
$5D_{3/2}$	$4D_{3/2}$	2581.950	$6.96 \pm 0.12[1]$	$1.69 \pm 0.03[2]$
$5D_{3/2}$	$4D_{5/2}$	2600.775	$3.08 \pm 0.04[1]$	$7.25 \pm 0.10[1]$
$5D_{3/2}$	$6S_{1/2}$	18018.732	$4.04 \pm 0.04[3]$	$5.95 \pm 0.05[-1]$
$5D_{5/2}$	$5S_{1/2}$	1873.607	$2.50 \pm 0.02[2]$	$2.02 \pm 0.01[3]$
$5D_{5/2}$	$4D_{3/2}$	2576.186	$2.94 \pm 0.04[1]$	$4.83 \pm 0.07[1]$
$5D_{5/2}$	$4D_{5/2}$	2594.926	$1.22 \pm 0.02[2]$	$1.93 \pm 0.03[2]$
$5D_{5/2}$	$6S_{1/2}$	17741.695	$6.11 \pm 0.06[3]$	$6.48 \pm 0.06[-1]$
$6P_{1/2}$	$5P_{3/2}$	3199.687	$2.424 \pm 0.009[2]$	$4.04 \pm 0.02[2]$
$6P_{3/2}$	$5P_{1/2}$	3091.886	$2.029 \pm 0.008[2]$	$2.010 \pm 0.008[2]$
$6P_{3/2}$	$5P_{3/2}$	3170.451	$2.271 \pm 0.009[2]$	$1.984 \pm 0.008[2]$
$6P_{3/2}$	$6P_{1/2}$	346981.263	$8.69 \pm 0.04[3]$	$4.84 \pm 0.02[-7]$
$4F_{7/2}$	$5P_{3/2}$	2741.724	$1.925 \pm 0.008[3]$	$1.739 \pm 0.007[3]$
$4F_{7/2}$	$6P_{3/2}$	20275.174	$1.568 \pm 0.007[4]$	$6.41 \pm 0.03[-1]$
$4F_{5/2}$	$5P_{1/2}$	2682.680	$1.058 \pm 0.004[3]$	$1.421 \pm 0.005[3]$
$4F_{5/2}$	$5P_{3/2}$	2741.627	$3.21 \pm 0.01[2]$	$3.86 \pm 0.02[2]$
$4F_{5/2}$	$6P_{1/2}$	19151.071	$9.07 \pm 0.04[3]$	$6.57 \pm 0.03[-1]$
$4F_{5/2}$	$6P_{3/2}$	20269.832	$2.61 \pm 0.01[3]$	$1.426 \pm 0.007[-1]$
$5D_{5/2}$	$5D_{3/2}$	1153934.918	$1.69 \pm 0.02[3]$	$1.55 \pm 0.02[-10]$
$7S_{1/2}$	$4D_{3/2}$	1983.804	$2.31 \pm 0.03[0]$	$4.21 \pm 0.05[1]$
$7S_{1/2}$	$4D_{5/2}$	1994.898	$3.55 \pm 0.04[0]$	$6.28 \pm 0.07[1]$
$7S_{1/2}$	$5D_{3/2}$	8563.264	$1.47 \pm 0.03[3]$	$1.79 \pm 0.04[1]$
$7S_{1/2}$	$5D_{5/2}$	8627.286	$2.27 \pm 0.05[3]$	$2.65 \pm 0.06[1]$
$6D_{3/2}$	$5S_{1/2}$	1480.979	$2.38 \pm 0.02[1]$	$9.37 \pm 0.07[2]$
$6D_{3/2}$	$4D_{3/2}$	1887.969	$7.22 \pm 0.11[0]$	$8.42 \pm 0.13[1]$
$6D_{3/2}$	$4D_{5/2}$	1898.015	$3.15 \pm 0.03[0]$	$3.58 \pm 0.04[1]$
$6D_{3/2}$	$6S_{1/2}$	5053.991	$1.50 \pm 0.01[3]$	$1.27 \pm 0.01[2]$
$6D_{3/2}$	$5D_{3/2}$	7024.168	$1.56 \pm 0.02[3]$	$2.56 \pm 0.03[1]$
$6D_{3/2}$	$5D_{5/2}$	7067.187	$6.88 \pm 0.08[2]$	$1.09 \pm 0.01[1]$
$6D_{3/2}$	$7S_{1/2}$	39081.277	$3.73 \pm 0.02[4]$	$1.146 \pm 0.007[-1]$
$6D_{5/2}$	$5S_{1/2}$	1480.096	$3.57 \pm 0.02[1]$	$9.39 \pm 0.06[2]$

$6D_{5/2}$	$4D_{3/2}$	1886.534	$3.08 \pm 0.04[0]$	$2.41 \pm 0.03[1]$	$1.93 \pm 0.02[-8]$
$6D_{5/2}$	$4D_{5/2}$	1896.564	$1.26 \pm 0.01[1]$	$9.57 \pm 0.11[1]$	$5.16 \pm 0.06[-8]$
$6D_{5/2}$	$6S_{1/2}$	5043.724	$2.21 \pm 0.02[3]$	$1.26 \pm 0.01[2]$	$1.44 \pm 0.01[-6]$
$6D_{5/2}$	$5D_{3/2}$	7004.351	$6.59 \pm 0.07[2]$	$7.29 \pm 0.08[0]$	$8.05 \pm 0.09[-8]$
$6D_{5/2}$	$5D_{5/2}$	7047.126	$2.71 \pm 0.03[3]$	$2.91 \pm 0.03[1]$	$2.16 \pm 0.02[-7]$
$6D_{5/2}$	$7S_{1/2}$	38475.596	$5.62 \pm 0.03[4]$	$1.243 \pm 0.008[-1]$	$8.27 \pm 0.05[-8]$
$6D_{5/2}$	$6D_{3/2}$	2482621.648	$1.67 \pm 0.02[4]$	$3.32 \pm 0.03[-11]$	$4.59 \pm 0.04[-14]$
$7P_{1/2}$	$5P_{3/2}$	2264.354	$2.309 \pm 0.009[1]$	$2.172 \pm 0.009[2]$	$8.35 \pm 0.03[-8]$
$7P_{1/2}$	$6P_{3/2}$	7923.026	$2.938 \pm 0.008[3]$	$5.27 \pm 0.02[1]$	$2.479 \pm 0.007[-7]$
$7P_{1/2}$	$4F_{5/2}$	13007.284	$2.473 \pm 0.005[3]$	$3.718 \pm 0.007[0]$	$3.144 \pm 0.006[-8]$
$7P_{3/2}$	$5P_{1/2}$	2217.200	$2.137 \pm 0.008[1]$	$1.116 \pm 0.004[2]$	$1.645 \pm 0.006[-7]$
$7P_{3/2}$	$5P_{3/2}$	2257.312	$2.274 \pm 0.009[1]$	$1.086 \pm 0.004[2]$	$8.29 \pm 0.03[-8]$
$7P_{3/2}$	$6P_{1/2}$	7664.350	$2.486 \pm 0.008[3]$	$2.632 \pm 0.008[1]$	$4.64 \pm 0.01[-7]$
$7P_{3/2}$	$6P_{3/2}$	7837.469	$2.749 \pm 0.008[3]$	$2.603 \pm 0.008[1]$	$2.397 \pm 0.007[-7]$
$7P_{3/2}$	$4F_{7/2}$	12776.156	$3.994 \pm 0.006[3]$	$3.285 \pm 0.005[0]$	$4.019 \pm 0.006[-8]$
$7P_{3/2}$	$4F_{5/2}$	12778.278	$6.66 \pm 0.01[2]$	$5.474 \pm 0.008[-1]$	$8.93 \pm 0.01[-9]$
$7P_{3/2}$	$7P_{1/2}$	725794.745	$6.45 \pm 0.02[4]$	$8.96 \pm 0.03[-8]$	$1.415 \pm 0.005[-11]$
$5F_{5/2}$	$5P_{1/2}$	2111.905	$9.03 \pm 0.07[1]$	$4.01 \pm 0.03[2]$	$8.05 \pm 0.07[-7]$
$5F_{5/2}$	$5P_{3/2}$	2148.266	$2.54 \pm 0.02[1]$	$1.037 \pm 0.008[2]$	$1.076 \pm 0.008[-7]$
$5F_{5/2}$	$6P_{1/2}$	6537.614	$7.26 \pm 0.02[3]$	$1.135 \pm 0.003[2]$	$2.181 \pm 0.006[-6]$
$5F_{5/2}$	$6P_{3/2}$	6663.157	$2.237 \pm 0.007[3]$	$3.18 \pm 0.01[1]$	$3.17 \pm 0.01[-7]$
$5F_{5/2}$	$7P_{1/2}$	41903.069	$8.71 \pm 0.03[4]$	$1.257 \pm 0.005[-1]$	$9.93 \pm 0.04[-8]$
$5F_{5/2}$	$7P_{3/2}$	44470.533	$2.511 \pm 0.009[4]$	$2.69 \pm 0.01[-2]$	$1.198 \pm 0.005[-8]$
$5F_{7/2}$	$5P_{3/2}$	2148.266	$1.53 \pm 0.01[2]$	$4.67 \pm 0.04[2]$	$6.46 \pm 0.05[-7]$
$5F_{7/2}$	$6P_{3/2}$	6663.157	$1.342 \pm 0.005[4]$	$1.431 \pm 0.005[2]$	$1.904 \pm 0.007[-6]$
$5F_{7/2}$	$7P_{3/2}$	44470.533	$1.506 \pm 0.006[5]$	$1.212 \pm 0.005[-1]$	$7.18 \pm 0.03[-8]$
$5G_{7/2}$	$4D_{3/2}$	1760.504	$6.09 \pm 0.14[1]$	$5.04 \pm 0.12[2]$	$4.68 \pm 0.11[-7]$
$5G_{7/2}$	$4D_{5/2}$	1769.236	$7.00 \pm 0.16[0]$	$5.65 \pm 0.13[1]$	$3.54 \pm 0.08[-8]$
$5G_{7/2}$	$5D_{3/2}$	5533.578	$1.31 \pm 0.02[4]$	$3.54 \pm 0.06[2]$	$3.25 \pm 0.05[-6]$
$5G_{7/2}$	$5D_{5/2}$	5560.241	$1.47 \pm 0.03[3]$	$3.88 \pm 0.07[1]$	$2.40 \pm 0.04[-7]$
$5G_{7/2}$	$6D_{3/2}$	26076.095	$7.986 \pm 0.008[4]$	$9.272 \pm 0.009[-1]$	$1.891 \pm 0.002[-7]$
$5G_{7/2}$	$6D_{5/2}$	26352.891	$8.890 \pm 0.009[3]$	$9.79 \pm 0.01[-2]$	$1.359 \pm 0.001[-8]$
$5G_{9/2}$	$4D_{5/2}$	1769.236	$8.75 \pm 0.21[1]$	$5.56 \pm 0.13[2]$	$4.42 \pm 0.10[-7]$
$5G_{9/2}$	$5D_{5/2}$	5560.241	$1.84 \pm 0.03[4]$	$3.89 \pm 0.06[2]$	$3.01 \pm 0.04[-6]$
$5G_{9/2}$	$6D_{5/2}$	26352.891	$1.111 \pm 0.001[6]$	$9.791 \pm 0.009[-1]$	$1.698 \pm 0.002[-7]$
$8S_{1/2}$	$4D_{3/2}$	1704.123	$6.21 \pm 0.09[-1]$	$2.42 \pm 0.04[1]$	$5.27 \pm 0.08[-9]$
$8S_{1/2}$	$4D_{5/2}$	1712.303	$9.51 \pm 0.09[-1]$	$3.62 \pm 0.04[1]$	$5.29 \pm 0.06[-9]$
$8S_{1/2}$	$5D_{3/2}$	5012.332	$5.67 \pm 0.05[1]$	$1.005 \pm 0.008[1]$	$1.89 \pm 0.02[-8]$

$8S_{1/2}$	$5D_{5/2}$	5034.199	$8.56 \pm 0.07[1]$	$1.48 \pm 0.01[1]$	$1.88 \pm 0.02[-8]$
$8S_{1/2}$	$6D_{3/2}$	17500.171	$1.40 \pm 0.02[4]$	$4.79 \pm 0.08[0]$	$1.10 \pm 0.02[-7]$
$8S_{1/2}$	$6D_{5/2}$	17624.406	$2.16 \pm 0.03[4]$	$7.11 \pm 0.09[0]$	$1.10 \pm 0.02[-7]$
$7D_{3/2}$	$5S_{1/2}$	1340.099	$7.68 \pm 0.11[0]$	$4.97 \pm 0.07[2]$	$2.68 \pm 0.04[-7]$
$7D_{3/2}$	$4D_{3/2}$	1664.852	$2.19 \pm 0.03[0]$	$4.81 \pm 0.07[1]$	$2.01 \pm 0.03[-8]$
$7D_{3/2}$	$4D_{5/2}$	1672.658	$9.56 \pm 0.12[-1]$	$2.05 \pm 0.03[1]$	$5.72 \pm 0.07[-9]$
$7D_{3/2}$	$6S_{1/2}$	3719.578	$2.152 \pm 0.006[2]$	$8.46 \pm 0.02[1]$	$3.509 \pm 0.009[-7]$
$7D_{3/2}$	$5D_{3/2}$	4687.136	$1.18 \pm 0.01[2]$	$1.46 \pm 0.02[1]$	$4.83 \pm 0.05[-8]$
$7D_{3/2}$	$5D_{5/2}$	4706.252	$5.13 \pm 0.06[1]$	$6.22 \pm 0.07[0]$	$1.37 \pm 0.02[-8]$
$7D_{3/2}$	$7S_{1/2}$	10354.968	$7.77 \pm 0.08[3]$	$1.83 \pm 0.02[1]$	$5.87 \pm 0.06[-7]$
$7D_{3/2}$	$6D_{3/2}$	14087.622	$1.17 \pm 0.01[4]$	$5.93 \pm 0.06[0]$	$1.76 \pm 0.02[-7]$
$7D_{3/2}$	$6D_{5/2}$	14168.018	$5.16 \pm 0.05[3]$	$2.53 \pm 0.03[0]$	$5.07 \pm 0.05[-8]$
$7D_{3/2}$	$5G_{7/2}$	30641.948	$2.53 \pm 0.03[4]$	$2.62 \pm 0.03[-1]$	$1.85 \pm 0.02[-8]$
$7D_{3/2}$	$8S_{1/2}$	72243.895	$2.036 \pm 0.009[5]$	$2.89 \pm 0.01[-2]$	$4.53 \pm 0.02[-8]$
$7D_{5/2}$	$5S_{1/2}$	1339.708	$1.16 \pm 0.01[1]$	$5.01 \pm 0.06[2]$	$4.04 \pm 0.05[-7]$
$7D_{5/2}$	$4D_{3/2}$	1664.247	$9.43 \pm 0.14[-1]$	$1.38 \pm 0.02[1]$	$8.59 \pm 0.12[-9]$
$7D_{5/2}$	$4D_{5/2}$	1672.048	$3.83 \pm 0.04[0]$	$5.47 \pm 0.06[1]$	$2.29 \pm 0.02[-8]$
$7D_{5/2}$	$6S_{1/2}$	3716.564	$3.209 \pm 0.007[2]$	$8.44 \pm 0.02[1]$	$5.25 \pm 0.01[-7]$
$7D_{5/2}$	$5D_{3/2}$	4682.351	$5.07 \pm 0.06[1]$	$4.21 \pm 0.05[0]$	$2.07 \pm 0.02[-8]$
$7D_{5/2}$	$5D_{5/2}$	4701.428	$2.05 \pm 0.02[2]$	$1.66 \pm 0.01[1]$	$5.53 \pm 0.06[-8]$
$7D_{5/2}$	$7S_{1/2}$	10331.645	$1.14 \pm 0.01[4]$	$1.81 \pm 0.02[1]$	$8.67 \pm 0.09[-7]$
$7D_{5/2}$	$6D_{3/2}$	14044.490	$4.95 \pm 0.04[3]$	$1.69 \pm 0.01[0]$	$7.49 \pm 0.06[-8]$
$7D_{5/2}$	$6D_{5/2}$	14124.393	$2.03 \pm 0.02[4]$	$6.74 \pm 0.06[0]$	$2.01 \pm 0.02[-7]$
$7D_{5/2}$	$5G_{7/2}$	30438.620	$2.732 \pm 0.008[3]$	$1.951 \pm 0.006[-2]$	$2.033 \pm 0.006[-9]$
$7D_{5/2}$	$5G_{9/2}$	30438.620	$3.42 \pm 0.07[4]$	$2.44 \pm 0.05[-1]$	$2.03 \pm 0.04[-8]$
$7D_{5/2}$	$8S_{1/2}$	71123.755	$3.06 \pm 0.01[5]$	$3.13 \pm 0.01[-2]$	$7.14 \pm 0.03[-8]$
$7D_{5/2}$	$7D_{3/2}$	4587155.963	$9.41 \pm 0.06[4]$	$8.64 \pm 0.05[-12]$	$4.09 \pm 0.03[-14]$
$8P_{1/2}$	$5P_{3/2}$	1971.369	$6.75 \pm 0.04[0]$	$1.269 \pm 0.008[2]$	$3.69 \pm 0.02[-8]$
$8P_{1/2}$	$6P_{3/2}$	5212.432	$2.265 \pm 0.006[2]$	$3.295 \pm 0.008[1]$	$6.71 \pm 0.02[-8]$
$8P_{1/2}$	$4F_{5/2}$	7016.825	$6.34 \pm 0.06[1]$	$2.08 \pm 0.02[0]$	$5.13 \pm 0.05[-9]$
$8P_{1/2}$	$7P_{3/2}$	15562.555	$1.86 \pm 0.02[4]$	$1.14 \pm 0.01[1]$	$2.07 \pm 0.02[-7]$
$8P_{1/2}$	$5F_{5/2}$	23940.627	$2.52 \pm 0.02[4]$	$1.79 \pm 0.01[0]$	$5.14 \pm 0.05[-8]$
$8P_{3/2}$	$5P_{1/2}$	1938.111	$6.47 \pm 0.02[0]$	$6.62 \pm 0.02[1]$	$7.45 \pm 0.03[-8]$
$8P_{3/2}$	$5P_{3/2}$	1968.691	$6.76 \pm 0.03[0]$	$6.39 \pm 0.03[1]$	$3.72 \pm 0.01[-8]$
$8P_{3/2}$	$6P_{1/2}$	5117.157	$2.149 \pm 0.006[2]$	$1.715 \pm 0.005[1]$	$1.346 \pm 0.004[-7]$
$8P_{3/2}$	$6P_{3/2}$	5193.753	$2.246 \pm 0.006[2]$	$1.664 \pm 0.004[1]$	$6.73 \pm 0.02[-8]$
$8P_{3/2}$	$4F_{7/2}$	6982.382	$1.11 \pm 0.01[2]$	$1.87 \pm 0.02[0]$	$6.83 \pm 0.08[-9]$
$8P_{3/2}$	$4F_{5/2}$	6983.016	$1.85 \pm 0.02[1]$	$3.12 \pm 0.03[-1]$	$1.52 \pm 0.01[-9]$

$8P_{3/2}$	$7P_{1/2}$	15077.362	$1.59 \pm 0.03[4]$	$5.73 \pm 0.09[0]$	$3.91 \pm 0.06[-7]$
$8P_{3/2}$	$7P_{3/2}$	15397.217	$1.75 \pm 0.02[4]$	$5.67 \pm 0.08[0]$	$2.02 \pm 0.03[-7]$
$8P_{3/2}$	$5F_{5/2}$	23551.578	$6.84 \pm 0.11[3]$	$2.64 \pm 0.04[-1]$	$1.46 \pm 0.02[-8]$
$8P_{3/2}$	$5F_{7/2}$	23551.578	$4.10 \pm 0.08[4]$	$1.58 \pm 0.03[0]$	$6.59 \pm 0.13[-8]$
$8P_{3/2}$	$8P_{1/2}$	1449275.362	$3.13 \pm 0.03[5]$	$1.37 \pm 0.01[-8]$	$8.64 \pm 0.09[-12]$
$6G_{7/2}$	$4D_{3/2}$	1608.187	$3.62 \pm 0.06[1]$	$4.71 \pm 0.08[2]$	$3.65 \pm 0.06[-7]$
$6G_{7/2}$	$4D_{5/2}$	1615.470	$4.14 \pm 0.08[0]$	$5.27 \pm 0.11[1]$	$2.75 \pm 0.05[-8]$
$6G_{7/2}$	$5D_{3/2}$	4264.139	$1.203 \pm 0.008[3]$	$1.195 \pm 0.008[2]$	$6.51 \pm 0.04[-7]$
$6G_{7/2}$	$5D_{5/2}$	4279.955	$1.331 \pm 0.009[2]$	$1.297 \pm 0.009[1]$	$4.75 \pm 0.03[-8]$
$6G_{7/2}$	$6D_{3/2}$	10852.072	$4.63 \pm 0.13[4]$	$4.31 \pm 0.12[1]$	$1.52 \pm 0.04[-6]$
$6G_{7/2}$	$6D_{5/2}$	10899.717	$5.25 \pm 0.13[3]$	$4.77 \pm 0.12[0]$	$1.13 \pm 0.03[-7]$
$6G_{7/2}$	$7D_{3/2}$	47250.047	$5.60 \pm 0.01[5]$	$3.333 \pm 0.008[-1]$	$2.230 \pm 0.006[-7]$
$6G_{7/2}$	$7D_{5/2}$	47741.812	$6.27 \pm 0.02[4]$	$3.54 \pm 0.01[-2]$	$1.612 \pm 0.005[-8]$
$6G_{9/2}$	$4D_{5/2}$	1615.470	$5.17 \pm 0.08[1]$	$5.27 \pm 0.08[2]$	$3.43 \pm 0.06[-7]$
$6G_{9/2}$	$5D_{5/2}$	4279.955	$1.66 \pm 0.01[3]$	$1.297 \pm 0.009[2]$	$5.94 \pm 0.04[-7]$
$6G_{9/2}$	$6D_{5/2}$	10899.717	$6.56 \pm 0.15[4]$	$4.77 \pm 0.11[1]$	$1.42 \pm 0.03[-6]$
$6G_{9/2}$	$7D_{5/2}$	47741.812	$7.83 \pm 0.02[5]$	$3.537 \pm 0.008[-1]$	$2.015 \pm 0.004[-7]$

Table H: Transition wavelengths ( $\lambda$ ) and electric quadrupole transition properties such as line strengths ( $S_{vk}$ ), transition probabilities ( $A_{vk}$ ) and oscillator strengths ( $f_{kv}$ ) along with their uncertainties between transitions involving an upper energy level (denoted by  $v$ ) and lower energy level (denoted by  $k$ ) of  $\text{Ba}^+$ . Values given in square brackets represent the power of 10.

Levels		$\lambda$	$S_{vk}$	$A_{vk}$	$f_{kv}$
Upper ( $v$ )	Lower ( $k$ )	(in Å)	(in a.u.)	(in $\text{s}^{-1}$ )	
$5D_{3/2}$	$6S_{1/2}$	20517.652	$1.59 \pm 0.03[2]$	$1.23 \pm 0.02[-2]$	$1.55 \pm 0.03[-9]$
$5D_{5/2}$	$6S_{1/2}$	17621.744	$2.49 \pm 0.04[2]$	$2.74 \pm 0.05[-2]$	$3.83 \pm 0.07[-9]$
$5D_{5/2}$	$5D_{3/2}$	124850.959	$4.49 \pm 0.08[1]$	$2.77 \pm 0.05[-7]$	$9.70 \pm 0.17[-13]$
$6P_{3/2}$	$6P_{1/2}$	59142.096	$8.03 \pm 0.07[2]$	$3.11 \pm 0.03[-4]$	$3.25 \pm 0.03[-10]$
$7S_{1/2}$	$5D_{3/2}$	2667.995	$2.25 \pm 0.08[1]$	$9.31 \pm 0.34[1]$	$4.97 \pm 0.19[-8]$
$7S_{1/2}$	$5D_{5/2}$	2726.254	$3.79 \pm 0.14[1]$	$1.41 \pm 0.05[2]$	$5.25 \pm 0.19[-8]$
$6D_{3/2}$	$6S_{1/2}$	2176.303	$2.83 \pm 0.01[2]$	$1.623 \pm 0.007[3]$	$2.31 \pm 0.01[-6]$
$6D_{3/2}$	$5D_{3/2}$	2434.534	$6.88 \pm 0.15[1]$	$2.25 \pm 0.05[2]$	$2.01 \pm 0.04[-7]$
$6D_{3/2}$	$5D_{5/2}$	2482.950	$3.22 \pm 0.06[1]$	$9.55 \pm 0.17[1]$	$5.88 \pm 0.10[-8]$
$6D_{3/2}$	$7S_{1/2}$	27821.852	$5.01 \pm 0.08[3]$	$8.42 \pm 0.13[-2]$	$1.95 \pm 0.03[-8]$
$6D_{5/2}$	$6S_{1/2}$	2166.619	$4.12 \pm 0.02[2]$	$1.61 \pm 0.08[3]$	$3.40 \pm 0.01[-6]$
$6D_{5/2}$	$5D_{3/2}$	2422.422	$2.82 \pm 0.05[1]$	$6.31 \pm 0.12[1]$	$8.33 \pm 0.16[-8]$
$6D_{5/2}$	$5D_{5/2}$	2470.353	$1.23 \pm 0.02[2]$	$2.51 \pm 0.05[2]$	$2.29 \pm 0.04[-7]$
$6D_{5/2}$	$7S_{1/2}$	26318.061	$7.65 \pm 0.12[3]$	$1.13 \pm 0.02[-1]$	$3.53 \pm 0.05[-8]$

$6D_{5/2}$	$6D_{3/2}$	486914.181	$2.02 \pm 0.04[3]$	$1.37 \pm 0.02[-8]$	$7.34 \pm 0.13[-13]$
$7P_{1/2}$	$6P_{3/2}$	3644.657	$3.73 \pm 0.02[2]$	$3.24 \pm 0.01[2]$	$3.23 \pm 0.01[-7]$
$7P_{3/2}$	$6P_{1/2}$	3361.369	$2.44 \pm 0.02[2]$	$1.59 \pm 0.01[2]$	$5.39 \pm 0.04[-7]$
$7P_{3/2}$	$6P_{3/2}$	3563.927	$3.19 \pm 0.02[2]$	$1.557 \pm 0.008[2]$	$2.96 \pm 0.01[-7]$
$7P_{3/2}$	$7P_{1/2}$	160896.385	$1.144 \pm 0.009[4]$	$2.97 \pm 0.02[-5]$	$2.31 \pm 0.01[-10]$
$8S_{1/2}$	$5D_{3/2}$	1881.419	$2.19 \pm 0.06[0]$	$5.22 \pm 0.14[1]$	$1.38 \pm 0.04[-8]$
$8S_{1/2}$	$5D_{5/2}$	1910.205	$3.59 \pm 0.07[0]$	$7.91 \pm 0.16[1]$	$1.44 \pm 0.03[-8]$
$8S_{1/2}$	$6D_{3/2}$	8281.066	$1.27 \pm 0.04[3]$	$1.83 \pm 0.05[1]$	$9.38 \pm 0.29[-8]$
$8S_{1/2}$	$6D_{5/2}$	8424.341	$2.04 \pm 0.06[3]$	$2.69 \pm 0.08[1]$	$9.56 \pm 0.29[-8]$
$7D_{3/2}$	$6S_{1/2}$	1672.233	$3.23 \pm 0.06[1]$	$6.91 \pm 0.12[2]$	$5.79 \pm 0.10[-7]$
$7D_{3/2}$	$5D_{3/2}$	1820.618	$8.77 \pm 0.12[0]$	$1.23 \pm 0.02[2]$	$6.10 \pm 0.08[-8]$
$7D_{3/2}$	$5D_{5/2}$	1847.559	$3.97 \pm 0.08[0]$	$5.16 \pm 0.11[1]$	$1.76 \pm 0.03[-8]$
$7D_{3/2}$	$7S_{1/2}$	5732.275	$2.46 \pm 0.01[3]$	$1.112 \pm 0.007[2]$	$1.096 \pm 0.007[-6]$
$7D_{3/2}$	$6D_{3/2}$	7219.808	$1.72 \pm 0.02[3]$	$2.45 \pm 0.04[1]$	$1.92 \pm 0.03[-7]$
$7D_{3/2}$	$6D_{5/2}$	7328.473	$7.85 \pm 0.12[2]$	$1.04 \pm 0.02[1]$	$5.58 \pm 0.08[-8]$
$7D_{3/2}$	$8S_{1/2}$	56336.663	$4.47 \pm 0.04[4]$	$2.20 \pm 0.02[-2]$	$2.09 \pm 0.02[-8]$
$7D_{5/2}$	$6S_{1/2}$	1669.590	$4.87 \pm 0.08[1]$	$7.01 \pm 0.12[2]$	$8.79 \pm 0.15[-7]$
$7D_{5/2}$	$5D_{3/2}$	1817.485	$3.69 \pm 0.08[0]$	$3.47 \pm 0.07[1]$	$2.58 \pm 0.05[-8]$
$7D_{5/2}$	$5D_{5/2}$	1844.333	$1.56 \pm 0.02[1]$	$1.37 \pm 0.02[2]$	$6.98 \pm 0.11[-8]$
$7D_{5/2}$	$7S_{1/2}$	5701.334	$3.54 \pm 0.03[3]$	$1.096 \pm 0.008[2]$	$1.60 \pm 0.01[-6]$
$7D_{5/2}$	$6D_{3/2}$	7170.794	$7.06 \pm 0.11[2]$	$6.95 \pm 0.11[0]$	$8.03 \pm 0.13[-8]$
$7D_{5/2}$	$6D_{5/2}$	7277.977	$3.02 \pm 0.05[3]$	$2.75 \pm 0.04[1]$	$2.18 \pm 0.03[-7]$
$7D_{5/2}$	$8S_{1/2}$	53484.029	$6.77 \pm 0.05[4]$	$2.89 \pm 0.02[-2]$	$3.72 \pm 0.03[-8]$
$7D_{5/2}$	$7D_{3/2}$	1056256.205	$1.92 \pm 0.03[4]$	$2.72 \pm 0.04[-9]$	$6.83 \pm 0.09[-13]$
$8P_{1/2}$	$6P_{3/2}$	2538.902	$3.32 \pm 0.03[1]$	$1.76 \pm 0.02[2]$	$8.52 \pm 0.09[-8]$
$8P_{1/2}$	$7P_{3/2}$	8827.558	$4.15 \pm 0.02[3]$	$4.33 \pm 0.02[1]$	$2.53 \pm 0.01[-7]$
$8P_{3/2}$	$6P_{1/2}$	2416.601	$2.75 \pm 0.02[1]$	$9.34 \pm 0.07[1]$	$1.64 \pm 0.01[-7]$
$8P_{3/2}$	$6P_{3/2}$	2519.552	$3.21 \pm 0.02[1]$	$8.85 \pm 0.06[1]$	$8.42 \pm 0.06[-8]$
$8P_{3/2}$	$7P_{1/2}$	8161.814	$2.79 \pm 0.02[3]$	$2.15 \pm 0.01[1]$	$4.31 \pm 0.03[-7]$
$8P_{3/2}$	$7P_{3/2}$	8597.964	$3.55 \pm 0.02[3]$	$2.12 \pm 0.01[1]$	$2.35 \pm 0.01[-7]$
$8P_{3/2}$	$8P_{1/2}$	330578.512	$7.98 \pm 0.05[4]$	$5.66 \pm 0.04[-6]$	$1.85 \pm 0.01[-10]$
$5G_{7/2}$	$5D_{3/2}$	1719.605	$7.07 \pm 0.24[1]$	$6.58 \pm 0.22[2]$	$5.84 \pm 0.19[-7]$
$5G_{7/2}$	$5D_{5/2}$	1743.621	$8.57 \pm 0.29[0]$	$7.45 \pm 0.25[1]$	$4.53 \pm 0.15[-8]$
$5G_{7/2}$	$6D_{3/2}$	5855.742	$1.56 \pm 0.02[4]$	$3.18 \pm 0.05[2]$	$3.26 \pm 0.05[-6]$
$5G_{7/2}$	$6D_{5/2}$	5927.022	$1.79 \pm 0.04[3]$	$3.43 \pm 0.07[1]$	$2.41 \pm 0.05[-7]$
$5G_{7/2}$	$7D_{3/2}$	30993.615	$8.08 \pm 0.03[4]$	$3.95 \pm 0.01[-1]$	$1.139 \pm 0.004[-7]$
$5G_{7/2}$	$7D_{5/2}$	31930.549	$9.00 \pm 0.03[3]$	$3.79 \pm 0.01[-2]$	$7.74 \pm 0.02[-9]$
$5G_{9/2}$	$5D_{5/2}$	1743.621	$1.07 \pm 0.04[2]$	$7.45 \pm 0.26[2]$	$5.65 \pm 0.19[-7]$

$5G_{9/2}$	$6D_{5/2}$	5927.022	$2.24 \pm 0.06[4]$	$3.43 \pm 0.09[2]$	$3.01 \pm 0.08[-6]$
$5G_{9/2}$	$7D_{5/2}$	31930.549	$1.125 \pm 0.003[5]$	$3.79 \pm 0.01[-1]$	$9.67 \pm 0.03[-8]$
$9S_{1/2}$	$5D_{3/2}$	1644.472	$6.64 \pm 0.09[-1]$	$3.09 \pm 0.05[1]$	$6.27 \pm 0.09[-9]$
$9S_{1/2}$	$5D_{5/2}$	1666.422	$1.07 \pm 0.01[0]$	$4.69 \pm 0.06[1]$	$6.51 \pm 0.09[-9]$
$9S_{1/2}$	$6D_{3/2}$	5067.352	$6.66 \pm 0.13[1]$	$1.12 \pm 0.02[1]$	$2.15 \pm 0.04[-8]$
$9S_{1/2}$	$6D_{5/2}$	5120.643	$1.03 \pm 0.02[2]$	$1.64 \pm 0.03[1]$	$2.14 \pm 0.04[-8]$
$9S_{1/2}$	$7D_{3/2}$	16996.997	$1.25 \pm 0.02[4]$	$4.92 \pm 0.08[0]$	$1.06 \pm 0.02[-7]$
$9S_{1/2}$	$7D_{5/2}$	17274.982	$1.98 \pm 0.06[4]$	$7.23 \pm 0.21[0]$	$1.08 \pm 0.03[-7]$
$8D_{3/2}$	$6S_{1/2}$	1499.842	$9.78 \pm 0.25[0]$	$3.61 \pm 0.09[2]$	$2.43 \pm 0.06[-7]$
$8D_{3/2}$	$5D_{3/2}$	1618.128	$2.91 \pm 0.07[0]$	$7.34 \pm 0.17[1]$	$2.88 \pm 0.07[-8]$
$8D_{3/2}$	$5D_{5/2}$	1639.375	$1.30 \pm 0.02[0]$	$3.07 \pm 0.05[1]$	$8.27 \pm 0.15[-9]$
$8D_{3/2}$	$7S_{1/2}$	4112.099	$2.85 \pm 0.02[2]$	$6.79 \pm 0.06[1]$	$3.44 \pm 0.03[-7]$
$8D_{3/2}$	$6D_{3/2}$	4825.282	$1.36 \pm 0.02[2]$	$1.45 \pm 0.02[1]$	$5.07 \pm 0.08[-8]$
$8D_{3/2}$	$6D_{5/2}$	4873.578	$5.97 \pm 0.09[1]$	$6.08 \pm 0.09[0]$	$1.44 \pm 0.02[-8]$
$8D_{3/2}$	$8S_{1/2}$	11562.778	$1.26 \pm 0.01[4]$	$1.70 \pm 0.02[1]$	$6.83 \pm 0.06[-7]$
$8D_{3/2}$	$7D_{3/2}$	14548.846	$1.29 \pm 0.01[4]$	$5.54 \pm 0.06[0]$	$1.76 \pm 0.02[-7]$
$8D_{3/2}$	$7D_{5/2}$	14752.041	$5.87 \pm 0.07[3]$	$2.35 \pm 0.03[0]$	$5.12 \pm 0.06[-8]$
$8D_{3/2}$	$5G_{7/2}$	27420.353	$1.96 \pm 0.05[4]$	$3.55 \pm 0.10[-1]$	$2.00 \pm 0.05[-8]$
$8D_{3/2}$	$9S_{1/2}$	101009.590	$2.38 \pm 0.02[5]$	$6.34 \pm 0.05[-3]$	$1.94 \pm 0.01[-8]$
$8D_{5/2}$	$6S_{1/2}$	1498.675	$1.49 \pm 0.03[1]$	$3.69 \pm 0.08[2]$	$3.73 \pm 0.08[-7]$
$8D_{5/2}$	$5D_{3/2}$	1616.769	$1.23 \pm 0.02[0]$	$2.08 \pm 0.04[1]$	$1.22 \pm 0.02[-8]$
$8D_{5/2}$	$5D_{5/2}$	1637.981	$5.18 \pm 0.09[0]$	$8.19 \pm 0.14[1]$	$3.29 \pm 0.06[-8]$
$8D_{5/2}$	$7S_{1/2}$	4103.335	$4.25 \pm 0.03[2]$	$6.83 \pm 0.05[1]$	$5.17 \pm 0.04[-7]$
$8D_{5/2}$	$6D_{3/2}$	4813.218	$5.78 \pm 0.09[1]$	$4.18 \pm 0.06[0]$	$2.18 \pm 0.03[-8]$
$8D_{5/2}$	$6D_{5/2}$	4861.273	$2.38 \pm 0.04[2]$	$1.64 \pm 0.02[1]$	$5.80 \pm 0.09[-8]$
$8D_{5/2}$	$8S_{1/2}$	11493.751	$1.79 \pm 0.02[4]$	$1.67 \pm 0.02[1]$	$9.94 \pm 0.09[-7]$
$8D_{5/2}$	$7D_{3/2}$	14439.731	$5.29 \pm 0.06[3]$	$1.57 \pm 0.02[0]$	$7.38 \pm 0.08[-8]$
$8D_{5/2}$	$7D_{5/2}$	14639.867	$2.25 \pm 0.03[4]$	$6.25 \pm 0.07[0]$	$2.01 \pm 0.02[-7]$
$8D_{5/2}$	$5G_{7/2}$	27035.312	$2.11 \pm 0.05[3]$	$2.72 \pm 0.06[-2]$	$2.23 \pm 0.05[-9]$
$8D_{5/2}$	$5G_{9/2}$	27035.312	$2.63 \pm 0.06[4]$	$3.40 \pm 0.08[-1]$	$2.24 \pm 0.05[-8]$
$8D_{5/2}$	$9S_{1/2}$	95974.355	$3.59 \pm 0.03[5]$	$8.24 \pm 0.08[-3]$	$3.42 \pm 0.03[-8]$
$8D_{5/2}$	$8D_{3/2}$	1925298.421	$1.05 \pm 0.01[5]$	$7.42 \pm 0.09[-10]$	$6.18 \pm 0.07[-13]$
$6G_{7/2}$	$5D_{3/2}$	1573.508	$4.24 \pm 0.13[1]$	$6.15 \pm 0.19[2]$	$4.56 \pm 0.14[-7]$
$6G_{7/2}$	$5D_{5/2}$	1593.592	$5.09 \pm 0.14[0]$	$6.94 \pm 0.19[1]$	$3.52 \pm 0.09[-8]$
$6G_{7/2}$	$6D_{3/2}$	4449.066	$1.09 \pm 0.01[3]$	$8.81 \pm 0.11[1]$	$5.23 \pm 0.06[-7]$
$6G_{7/2}$	$6D_{5/2}$	4490.094	$1.19 \pm 0.01[2]$	$9.14 \pm 0.12[0]$	$3.68 \pm 0.05[-8]$
$6G_{7/2}$	$7D_{3/2}$	11593.072	$6.32 \pm 0.20[4]$	$4.22 \pm 0.13[1]$	$1.70 \pm 0.05[-6]$
$6G_{7/2}$	$7D_{5/2}$	11721.725	$7.35 \pm 0.17[3]$	$4.65 \pm 0.11[0]$	$1.27 \pm 0.03[-7]$

$6G_{7/2}$	$8D_{3/2}$	57063.164	$5.79 \pm 0.03[5]$	$1.339 \pm 0.007[-1]$	$1.308 \pm 0.007[-7]$
$6G_{7/2}$	$8D_{5/2}$	58806.095	$6.46 \pm 0.03[4]$	$1.287 \pm 0.006[-2]$	$8.89 \pm 0.04[-9]$
$6G_{9/2}$	$5D_{5/2}$	1593.592	$6.36 \pm 0.19[1]$	$6.94 \pm 0.21[2]$	$4.40 \pm 0.13[-7]$
$6G_{9/2}$	$6D_{5/2}$	4490.094	$1.49 \pm 0.02[3]$	$9.14 \pm 0.12[1]$	$4.60 \pm 0.06[-7]$
$6G_{9/2}$	$7D_{5/2}$	11721.725	$9.18 \pm 0.25[4]$	$4.65 \pm 0.12[1]$	$1.59 \pm 0.04[-6]$
$6G_{9/2}$	$8D_{5/2}$	58806.095	$8.08 \pm 0.04[5]$	$1.287 \pm 0.006[-1]$	$1.112 \pm 0.005[-7]$

Table I: Comparison of transition probabilities  $A_{vk}$  (in  $\text{s}^{-1}$ ) of the E2 forbidden transitions involving upper level ( $v$ ) and lower level ( $k$ ) in  $\text{Mg}^+$  from different works. Values given in square brackets represent the power of 10.

Transition		$A_{vk}$			
Upper ( $v$ )	Lower ( $k$ )	Present	[55]	[56]	[57]
$3D_{5/2}$	$3S_{1/2}$	$5.0971 \pm 0.0008[3]$	4.94[3]	5.010[3]	8.77[3]
$3D_{3/2}$	$3S_{1/2}$	$5.098 \pm 0.001[3]$	4.94[3]	5.010[3]	
$4D_{5/2}$	$3S_{1/2}$	$7.191 \pm 0.006[2]$	7.01[2]	6.580[2]	1.04[3]
$4D_{3/2}$	$3S_{1/2}$	$7.19 \pm 0.02[2]$	7.01[2]	6.590[2]	
$3P_{3/2}$	$3P_{1/2}$	$2.732 \pm 0.001[-11]$	2.99[-11]	3.050[-11]	3.81[-11]
$4P_{1/2}$	$3P_{3/2}$	$8.245 \pm 0.005[2]$	7.60[2]	7.901[2]	8.37[2]
$4P_{3/2}$	$3P_{1/2}$	$4.123 \pm 0.003[2]$	3.85[2]	3.970[2]	4.22[2]
$4P_{3/2}$	$3P_{3/2}$	$4.117 \pm 0.002[2]$	3.82[2]	3.750[2]	4.19[2]
$4P_{3/2}$	$4P_{1/2}$	$2.6551 \pm 0.0004[-12]$		2.960[-12]	
$5P_{1/2}$	$3P_{3/2}$	$3.996 \pm 0.005[2]$	3.05[2]	2.86[2]	
$5P_{1/2}$	$4P_{3/2}$	$9.636 \pm 0.003[1]$	8.63[1]	8.840[1]	
$5P_{3/2}$	$3P_{1/2}$	$2.005 \pm 0.003[2]$	1.53[2]	1.440[2]	
$5P_{3/2}$	$3P_{3/2}$	$1.999 \pm 0.005[2]$	1.53[2]	1.300[2]	
$5P_{3/2}$	$4P_{1/2}$	$4.819 \pm 0.002[1]$	4.31[1]	4.440[1]	4.44[1]
$5P_{3/2}$	$4P_{3/2}$	$4.8133 \pm 0.0008[1]$	4.31[1]	4.140[1]	4.14[1]
$5P_{3/2}$	$5P_{1/2}$	$4.5691 \pm 0.0004[-13]$	4.70[-13]	5.350[-13]	5.35[-13]
$4F_{5/2}$	$3P_{1/2}$	$2.690 \pm 0.002[3]$	2.86[3]	2.620[3]	
$4F_{5/2}$	$3P_{3/2}$	$7.674 \pm 0.004[2]$	8.12[2]	7.460[2]	
$4F_{5/2}$	$4P_{1/2}$	$4.8172 \pm 0.0008[1]$	4.66[1]	4.730[1]	
$4F_{5/2}$	$4P_{3/2}$	$1.3631 \pm 0.0001[1]$	1.32[1]	1.340[1]	
$4F_{7/2}$	$3P_{3/2}$	$3.453 \pm 0.001[3]$	3.65[3]	3.360[3]	
$4F_{7/2}$	$4P_{3/2}$	$6.1361 \pm 0.0003[1]$	5.94[1]	6.020[1]	
$5P_{1/2}$	$4F_{5/2}$	$2.7184 \pm 0.0005[-1]$		1.010[1]	
$5P_{3/2}$	$4F_{5/2}$	$3.9494 \pm 0.0005[-2]$		2.71[-2]	

$5P_{3/2}$	$4F_{7/2}$	$2.3693 \pm 0.0002[-1]$		1.220[-1]	
$5F_{5/2}$	$3P_{1/2}$	$1.5021 \pm 0.0008[3]$	1.37[3]	1.170[3]	
$5F_{5/2}$	$3P_{3/2}$	$4.280 \pm 0.006[2]$	3.90[2]	3.330[2]	
$5F_{5/2}$	$4P_{1/2}$	$6.035 \pm 0.005[1]$	4.80[1]	4.810[1]	
$5F_{5/2}$	$4P_{3/2}$	$1.7351 \pm 0.0008[1]$	1.38[1]	1.37[1]	
$5F_{5/2}$	$5P_{1/2}$	$0.9911 \pm 0.0002[1]$	1.02[1]	1.16[3]	1.16[3]
$5F_{5/2}$	$5P_{3/2}$	$2.8093 \pm 0.0001[0]$	2.88[0]	2.860[0]	2.86[0]
$5F_{7/2}$	$3P_{3/2}$	$1.9261 \pm 0.0007[3]$	1.76[3]	1.50[3]	
$5F_{7/2}$	$4P_{3/2}$	$7.808 \pm 0.002[1]$	6.21[1]	6.180[1]	
$5F_{7/2}$	$5P_{3/2}$	$1.26420 \pm 0.00005[1]$	1.30[1]	1.290[1]	1.29[1]
$4D_{5/2}$	$4S_{1/2}$	$3.017 \pm 0.0007[2]$	3.00[2]	2.930[2]	
$4D_{3/2}$	$4S_{1/2}$	$3.018 \pm 0.001[2]$	3.00[2]	2.930[2]	
$5D_{5/2}$	$3S_{1/2}$	$0.181 \pm 0.001[3]$		0.443[3]	
$5D_{3/2}$	$3S_{1/2}$	$0.1818 \pm 0.0005[3]$		0.443[3]	
$5D_{5/2}$	$4S_{1/2}$	$0.9882 \pm 0.0007[2]$	1.02[2]	1.250[2]	1.25[2]
$5D_{3/2}$	$4S_{1/2}$	$0.988 \pm 0.001[2]$	1.02[2]	1.250[2]	1.25[2]
$5D_{5/2}$	$5S_{1/2}$	$4.022 \pm 0.001[1]$	4.32[1]	4.220[1]	4.22[1]
$5D_{3/2}$	$5S_{1/2}$	$4.023 \pm 0.002[1]$	4.32[1]	4.220[1]	4.22[1]
$3D_{3/2}$	$3D_{5/2}$	$4.173 \pm 0.002[-21]$		0.138[-21]	
$4D_{5/2}$	$3D_{5/2}$	$6.308 \pm 0.002[1]$	6.36[1]		6.30[1]
$4D_{5/2}$	$3D_{3/2}$	$1.577 \pm 0.001[1]$	1.59[1]	1.550[1]	
$4D_{3/2}$	$3D_{5/2}$	$2.3661 \pm 0.0003[1]$	2.38[1]	1.56[1]	2.36[1]
$4D_{3/2}$	$3D_{3/2}$	$5.519 \pm 0.003[1]$	5.56[1]		5.51[1]
$5D_{5/2}$	$3D_{5/2}$	$2.959 \pm 0.001[1]$	2.98[1]		
$5D_{5/2}$	$3D_{3/2}$	$7.396 \pm 0.008[0]$	7.46[0]	5.150[0]	
$5D_{3/2}$	$3D_{5/2}$	$1.109 \pm 0.001[1]$	1.12[2]	0.534[-2]	
$5D_{3/2}$	$3D_{3/2}$	$2.588 \pm 0.002[1]$	2.67[1]		
$5D_{5/2}$	$4D_{5/2}$	$1.4273 \pm 0.0003[1]$	1.43[1]		
$5D_{5/2}$	$4D_{3/2}$	$3.566 \pm 0.003[0]$	3.57[0]	3.390[0]	
$5D_{3/2}$	$4D_{5/2}$	$5.3542 \pm 0.0002[0]$	5.36[0]	3.420[0]	
$5D_{3/2}$	$4D_{3/2}$	$1.2484 \pm 0.0004[1]$	1.25[1]		
$6D_{5/2}$	$3D_{5/2}$	$1.609 \pm 0.002[1]$	1.63[1]		
$6D_{5/2}$	$3D_{3/2}$	$4.026 \pm 0.005[0]$	4.07[0]		
$6D_{3/2}$	$3D_{5/2}$	$6.03 \pm 0.02[0]$	6.11[0]		
$6D_{3/2}$	$3D_{3/2}$	$1.408 \pm 0.002[1]$	1.43[1]		
$6D_{5/2}$	$4D_{5/2}$	$8.480 \pm 0.002[0]$	8.47[0]		
$6D_{5/2}$	$4D_{3/2}$	$2.119 \pm 0.001[0]$	2.12[0]		
$6D_{3/2}$	$4D_{5/2}$	$3.180 \pm 0.001[0]$	3.18[0]		

$6D_{3/2}$	$4D_{3/2}$	$7.419 \pm 0.003[0]$	$7.42[0]$
------------	------------	----------------------	-----------

Table J: Comparison of the transition probabilities  $A_{vk}$  (in  $s^{-1}$ ) and absorption oscillator strengths  $f_{kv}$  in the  $\text{Ca}^+$ ,  $\text{Sr}^+$  and  $\text{Ba}^+$  alkaline earth metal ions with different works. Values given in parentheses represent the power of 10.

Transition		$A_{vk}$		$f_{kv}$	
Upper ( $v$ )	Lower ( $k$ )	Present	Others(Th, Exp)	Present	Others(Th, Exp)
Ca <sup>+</sup>					
$3D_{3/2}$	$4S_{1/2}$	$0.838 \pm 0.008(0)$	$0.8662 \pm 0.0049(0)$ [58]	$1.35 \pm 0.01(-8)$	$1.393 \pm 0.007(-8)$ [58]
			$1.3(0)$ [77]		$2.092(-8)$ [77]
$3D_{5/2}$	$4S_{1/2}$	$0.860 \pm 0.007(0)$	$0.8567 \pm 0.0108(0)$ [79]	$2.05 \pm 0.02(-8)$	$2.049 \pm 0.025(-8)$ [79]
			$0.8892 \pm 0.0049(0)$ [58]		$2.127 \pm 0.012(-8)$ [58]
			$0.853 \pm 0.002(0)$ [59]		$2.041 \pm 0.005(-8)$ [59]
			$1.3(0)$ [77]		$3.110(-8)$ [77]
$3D_{5/2}$	$3D_{3/2}$	$2.19 \pm 0.02(-13)$	$2.207 \pm 0.028(-13)$ [58]	$1.34 \pm 0.01(-16)$	$1.347 \pm 0.017(-16)$ [58]
Sr <sup>+</sup>					
$4D_{3/2}$	$5S_{1/2}$	$2.26 \pm 0.01(0)$	$2.245 \pm 0.018(0)$ [58]	$3.21 \pm 0.02(-8)$	$3.177 \pm 0.025(-8)$ [58]
			$2.299(0)$ [77]		$3.253(-8)$ [77]
$4D_{5/2}$	$5S_{1/2}$	$2.53 \pm 0.02(0)$	$2.509 \pm 0.020(0)$ [58]	$5.18 \pm 0.04(-8)$	$5.126 \pm 0.041(-8)$ [58]
			$2.559(0)$ [77]		$5.228(-8)$ [77]
$4D_{5/2}$	$4D_{3/2}$	$1.155 \pm 0.007(-9)$	$1.130 \pm 0.019(-9)$ [58]	$3.30 \pm 0.02(-14)$	$3.233 \pm 0.054(-14)$ [58]
Ba <sup>+</sup>					
$5D_{3/2}$	$6S_{1/2}$	$1.23 \pm 0.02(-2)$	$1.192 \pm 0.003(-2)$ [58]	$1.55 \pm 0.03(-9)$	$1.504 \pm 0.004(-9)$ [58]
			$1.219(-2)$ [60]		$1.538(-9)$ [60]
$5D_{5/2}$	$6S_{1/2}$	$2.74 \pm 0.05(-2)$	$2.662 \pm 0.005(-2)$ [58]	$3.83 \pm 0.07(-9)$	$3.717 \pm 0.007(-9)$ [58]
			$2.607(-2)$ [60]		$3.641(-9)$ [60]
$5D_{5/2}$	$5D_{3/2}$	$2.77 \pm 0.05(-7)$	$2.622 \pm 0.010(-7)$ [58]	$9.70 \pm 0.17(-13)$	$9.191 \pm 0.035(-13)$ [58]
			$2.649(-7)$ [60]		$9.285(-13)$ [60]

Table K: Static dipole polarizabilities (in a.u.) of the ground and excited states of  $\text{Mg}^+$  with core correlation contribution  $0.43 \pm 0.02$  a.u. from the present work. The valence correlation contributions are given as ‘Main’ and ‘Tail’, whereas the core-valence correlation contributions are given under ‘vc’. Other literature values are also quoted for the comparison. The core-valence correlation contributions to the tensor components of the polarizabilities are not quoted here due to their negligible magnitudes.

State	$\alpha_{d,0}^J$				$\alpha_{d,2}^J$			
	Main	Tail	vc	Total	Main	Tail	Total	

$3S_{1/2}$	$34.5 \pm 0.9$	$0.07 \pm 0.03$	-0.01	$35 \pm 1$ $35.05 [14]$			
$4S_{1/2}$	$552.7 \pm 0.4$	$0.17 \pm 0.08$	-0.01	$553.3 \pm 0.4$			
$5S_{1/2}$	$3757 \pm 5$	$1.8 \pm 0.9$	-0.01	$3759 \pm 5$			
$3P_{1/2}$	$30.9 \pm 0.5$	$0.2 \pm 0.1$	$\sim 0$	$31.5 \pm 0.5$ $31.60 [14]$			
$3P_{3/2}$	$31.2 \pm 0.6$	$0.2 \pm 0.1$	$\sim 0$	$31.8 \pm 0.6$ $31.88 [14]$	$1.3 \pm 0.5$	$-0.17 \pm 0.08$	$1.1 \pm 0.5$ $1.156 [14]$
$4P_{1/2}$	$105.8 \pm 0.3$	$3 \pm 1$	$\sim 0$	$109 \pm 1$			
$4P_{3/2}$	$110.4 \pm 0.2$	$3 \pm 1$	$\sim 0$	$114 \pm 1$	$78.4 \pm 0.2$	$-1.8 \pm 0.9$	$76.6 \pm 0.9$
$5P_{1/2}$	$-379 \pm 3$	$37 \pm 19$	$\sim 0$	$-342 \pm 19$			
$5P_{3/2}$	$-347 \pm 2$	$37 \pm 19$	$\sim 0$	$-310 \pm 19$	$727 \pm 2$	$-25 \pm 13$	$702 \pm 13$
$3D_{3/2}$	$185.3 \pm 0.2$	$3 \pm 2$	$\sim 0$	$189 \pm 2$ $189.3 [14]$	$-78.37 \pm 0.09$	$-0.7 \pm 0.4$	$-79.1 \pm 0.4$ $-79.15 [14]$
$3D_{5/2}$	$184.7 \pm 0.3$	$3 \pm 2$	$\sim 0$	$188 \pm 2$ $188.6 [14]$	$-111.1 \pm 0.3$	$-1.0 \pm 0.5$	$-112.1 \pm 0.6$ $-112.2 [14]$
$4D_{3/2}$	$12703 \pm 2$	$67 \pm 33$	$\sim 0$	$12770 \pm 33$	$-2929.7 \pm 0.8$	$-15 \pm 8$	$-2945 \pm 8$
$4D_{5/2}$	$12683 \pm 2$	$67 \pm 33$	$\sim 0$	$12750 \pm 33$	$-4172.3 \pm 0.8$	$-22 \pm 11$	$-4194 \pm 11$

Table L: Static dipole polarizabilities (in a.u.) of the ground and excited states of  $\text{Ca}^+$  with core correlation contribution  $3.2 \pm 0.2$  a.u. from the present work. The valence correlation contributions are given as ‘Main’ and ‘Tail’, whereas the core-valence correlation contributions are given under ‘vc’. Other literature values are also quoted for the comparison. The core-valence correlation contributions to the tensor components of the polarizabilities are not quoted here due to their negligible magnitudes.

State	$\alpha_{d,0}^J$				$\alpha_{d,2}^J$		
	Main	Tail	vc	Total	Main	Tail	Total
$4S_{1/2}$	$72.8 \pm 0.6$	$0.06 \pm 0.03$	-0.08	$76.0 \pm 0.6$ $76.1 \pm 0.5 [30]$ $75.28 [15]$ $73.0 \pm 1.5 [17]$ $75.49 [16]$ $75.3 \pm 0.4 [18]$			
$5S_{1/2}$	$975 \pm 3$	$0.16 \pm 0.08$	-0.08	$978 \pm 3$			
$6S_{1/2}$	$5878 \pm 12$	$3 \pm 1$	-0.08	$5884 \pm 12$			
$4P_{1/2}$	$-5.3 \pm 0.6$	$1.7 \pm 0.8$	$\sim 0$	$-0.4 \pm 1.0$ $-0.75 \pm 0.70 [30]$ $-2.032 [16]$ $-2.774 [15]$			

$4P_{3/2}$	-3.4±0.6	1.7±0.8	~0	1.5±1.0 1.02±0.64 [30] -2.032 [16] -0.931 [15]	10.7±0.3	-0.4±0.2	10.3±0.4 10.31±0.28 [30] 10.47 [16] 10.12 [15]
$5P_{1/2}$	-938±18	15±7	~0	-920±19			
$5P_{3/2}$	-903±14	15±7	~0	-885±16 262±3 -4±2	262±3	-4±2	258±4
$6P_{1/2}$	-7710±94	165±83	~0	-7542±125			
$6P_{3/2}$	-7481±87	166±83	~0	-7312±120 1897±20 -49±24	1897±20	-49±24	1848±31
$3D_{3/2}$	27.1±0.2	3±1	~0	33±1 32.0±0.3 [30] 32.99 [15] 28.5±1.0 [17] 32.73 [16]	-17.1±0.2 -17.43±0.23 [30] -17.88 [15] -15.8±0.7 [17] -25.20 [16]	-0.6±0.3	-17.7±0.3
$3D_{5/2}$	26.9±0.3	3±1	-0.01	33±1 31.8±0.3 [30] 32.81 [15] 29.5±1.0 [17] 32.73 [16]	-23.9±0.3 -24.51±0.29 [30] -25.16 [15] -22.45±0.05 [17] -25.20 [16]	-0.9±0.4	-24.8±0.5
$4D_{3/2}$	1049±10	5±2	~0	1057±10 -528±9 -0.9±0.5	-528±9	-0.9±0.5	-529±9
$4D_{5/2}$	1041±10	5±2	-0.01	1049±10 -740±9 -1.3±0.7	-740±9	-1.3±0.7	-741±9
$5D_{3/2}$	6508±56	10±5	~0	6521±56 -3604±47 -3±1	-3604±47	-3±1	-3607±47
$5D_{5/2}$	6449±63	9±5	-0.01	6461±63 -5037±57 -4±2	-5037±57	-4±2	-5041±57

Table M: Static dipole polarizabilities (in a.u.) of the ground and excited states of  $\text{Sr}^+$  with core correlation contribution  $5.8\pm0.3$  a.u. from the present work. The valence correlation contributions are given as ‘Main’ and ‘Tail’, whereas the core-valence correlation contributions are given under ‘vc’. Other literature values are also quoted for the comparison. The core-valence correlation contributions to the tensor components of the polarizabilities are not quoted here due to their negligible magnitudes.

State	$\alpha_{d,0}^J$				$\alpha_{d,2}^J$		
	Main	Tail	vc	Total	Main	Tail	Total
$5S_{1/2}$	85.7±0.9	0.02±0.01	-0.19	91.3±0.9 92.2±0.7 [22] 91.30 [20] 89.88 [21] 88.29±1.00 [19] 87.5 [23] 90.100±0.127 [31] 86±11 [24]			

$6S_{1/2}$	$1076 \pm 3$	$0.05 \pm 0.02$	-0.19	$1082 \pm 3$ $1082 \pm 4$ [22] $1089$ [21]			
$7S_{1/2}$	$6160 \pm 12$	$0.5 \pm 0.2$	-0.19	$6166 \pm 12$ $6235 \pm 39$ [22]			
$8S_{1/2}$	$24635 \pm 84$	$33 \pm 16$	-0.19	$24673 \pm 85$ $24463 \pm 148$ [22]			
$5P_{1/2}$	$-40 \pm 2$	$2 \pm 1$	$\sim 0$	$-32 \pm 2$ $-32.2 \pm 0.9$ [22] $-31.29 \pm 0.49$ [31] $-23.13$ [21] $-38.4$ [23]			
$5P_{3/2}$	$-29 \pm 2$	$2 \pm 1$	$\sim 0$	$-21 \pm 2$ $-21.4 \pm 0.8$ [22] $-23.13$ [21] $-20.92 \pm 0.70$ [31] $-38.4$ [23]	$11.1 \pm 0.5$	$-0.6 \pm 0.3$	$10.5 \pm 0.6$ $10.74 \pm 0.23$ [22] $10.58$ [21] $9.836 \pm 0.147$ [31]
$6P_{1/2}$	$-2013 \pm 21$	$19 \pm 10$	$\sim 0$	$-1988 \pm 23$ $-1990 \pm 5$ [22] $-2056$ [21]			
$6P_{3/2}$	$-1769 \pm 19$	$19 \pm 10$	$\sim 0$	$-1744 \pm 21$ $-1745 \pm 5$ [22] $-2056$ [21]	$332 \pm 5$	$-5 \pm 2$	$327 \pm 5$ $326.9 \pm 3.5$ [22] $363.5$ [21]
$7P_{1/2}$	$-15026 \pm 99$	$190 \pm 95$	$\sim 0$	$-14830 \pm 137$ $-15438 \pm 72$ [22]			
$7P_{3/2}$	$-13371 \pm 98$	$194 \pm 97$	$\sim 0$	$-13171 \pm 138$ $-13539 \pm 42$ [22]	$2366 \pm 22$	$-57 \pm 29$	$2309 \pm 36$ $2376 \pm 17$ [22]
$4D_{3/2}$	$54.2 \pm 0.8$	$6 \pm 3$	-0.02	$66 \pm 3$ $63.3 \pm 0.9$ [22] $63.12 \pm 0.82$ [31] $61.43 \pm 0.52$ [19] $51.2$ [23]	$-34.8 \pm 0.8$	$-1.2 \pm 0.6$	$-36 \pm 1$ $-35.5 \pm 0.6$ [22] $-35.11 \pm 0.50$ [31] $35.42 \pm 0.25$ [19]
$4D_{5/2}$	$54.4 \pm 0.9$	$4 \pm 2$	-0.03	$64 \pm 2$ $61.77$ [21] $62.87 \pm 0.75$ [19] $62.0 \pm 0.9$ [22] $62.0 \pm 0.5$ [20] $61.99 \pm 0.72$ [31]	$-47.1 \pm 0.9$	$-1.1 \pm 0.6$	$-48 \pm 1$ $-47.20$ [21] $-48.83 \pm 0.30$ [19] $-47.7 \pm 0.8$ [22] $-47.7 \pm 0.3$ [20] $-47.38 \pm 0.67$ [31]

				51.2 [23]			
$5D_{3/2}$	$1957 \pm 11$	$16 \pm 8$	-0.02	$1979 \pm 14$	$-1051 \pm 10$	$-3 \pm 2$	$-1054 \pm 10$
				$1975 \pm 2$ [22]			$-1053 \pm 10$ [22]
$5D_{5/2}$	$1889 \pm 13$	$16 \pm 8$	-0.03	$1911 \pm 15$	$-1369 \pm 13$	$-5 \pm 2$	$-1374 \pm 13$
				$1907 \pm 2$ [22]			$-1373 \pm 13$ [22]
$6D_{3/2}$	$13359 \pm 55$	$46 \pm 23$	-0.02	$13411 \pm 60$	$-7289 \pm 50$	$-10 \pm 5$	$-7299 \pm 50$
				$13678 \pm 38$ [22]			$-7528 \pm 27$ [22]
$6D_{5/2}$	$12854 \pm 69$	$49 \pm 25$	-0.03	$12909 \pm 73$	$-9455 \pm 65$	$-14 \pm 7$	$-9469 \pm 65$
				$13071 \pm 45$ [22]			$-9643 \pm 45$ [22]

Table N: Static dipole polarizabilities (in a.u.) of the ground and excited states of  $\text{Ba}^+$  with core correlation contribution  $10.6 \pm 0.5$  a.u. from the present work. The valence correlation contributions are given as ‘Main’ and ‘Tail’, whereas the core-valence correlation contributions are given under ‘vc’. Other literature values are also quoted for the comparison. The core-valence correlation contributions to the tensor components of the polarizabilities are not quoted here due to their negligible magnitudes.

State	$\alpha_{d,0}^J$				$\alpha_{d,2}^J$		
	Main	Tail	vc	Total	Main	Tail	Total
$6S_{1/2}$	$114 \pm 2$	$0.016 \pm 0.008$	-0.38	$124 \pm 2$			
				$124.26 \pm 1.00$ [19]			
				$123.7 \pm 0.5$ [25]			
				$124.15$ [26]			
				$123.88 \pm 0.05$ [27]			
				$125.50 \pm 0.10$ [28]			
$7S_{1/2}$	$1355 \pm 6$	$0.15 \pm 0.08$	-0.38	$1365 \pm 6$			
$8S_{1/2}$	$7400 \pm 22$	$10 \pm 5$	-0.38	$7420 \pm 23$			
$6P_{1/2}$	$7 \pm 1$	$3 \pm 1$	$\sim 0$	$21 \pm 2$			
$6P_{3/2}$	$33 \pm 1$	$3 \pm 1$	$\sim 0$	$46 \pm 2$	$5.3 \pm 0.9$	$-0.8 \pm 0.4$	$4.5 \pm 0.9$
$7P_{1/2}$	$-1383 \pm 24$	$21 \pm 11$	$\sim 0$	$-1351 \pm 26$			
$7P_{3/2}$	$-971 \pm 19$	$21 \pm 11$	$\sim 0$	$-939 \pm 22$	$273 \pm 5$	$-6 \pm 3$	$267 \pm 6$
$8P_{1/2}$	$-11340 \pm 121$	$224 \pm 112$	$\sim 0$	$-11105 \pm 165$			
$8P_{3/2}$	$-8680 \pm 102$	$232 \pm 116$	$\sim 0$	$-8437 \pm 154$	$2010 \pm 24$	$-69 \pm 35$	$1941 \pm 42$
$5D_{3/2}$	$38.5 \pm 0.9$	$3 \pm 2$	-0.02	$52 \pm 2$	$-21.9 \pm 0.3$	$-0.7 \pm 0.3$	$-22.6 \pm 0.4$
				$48.81 \pm 0.46$ [19]			$-24.62 \pm 0.28$ [19]
$5D_{5/2}$	$39 \pm 1$	$3 \pm 2$	-0.04	$53 \pm 2$	$-29.5 \pm 0.5$	$-1.0 \pm 0.5$	$-30.5 \pm 0.7$
				$50.6 \pm 1.2$ [25]			$-29.8 \pm 0.7$ [25]
				$50.67 \pm 0.58$ [19]			$-30.85 \pm 0.31$ [19]

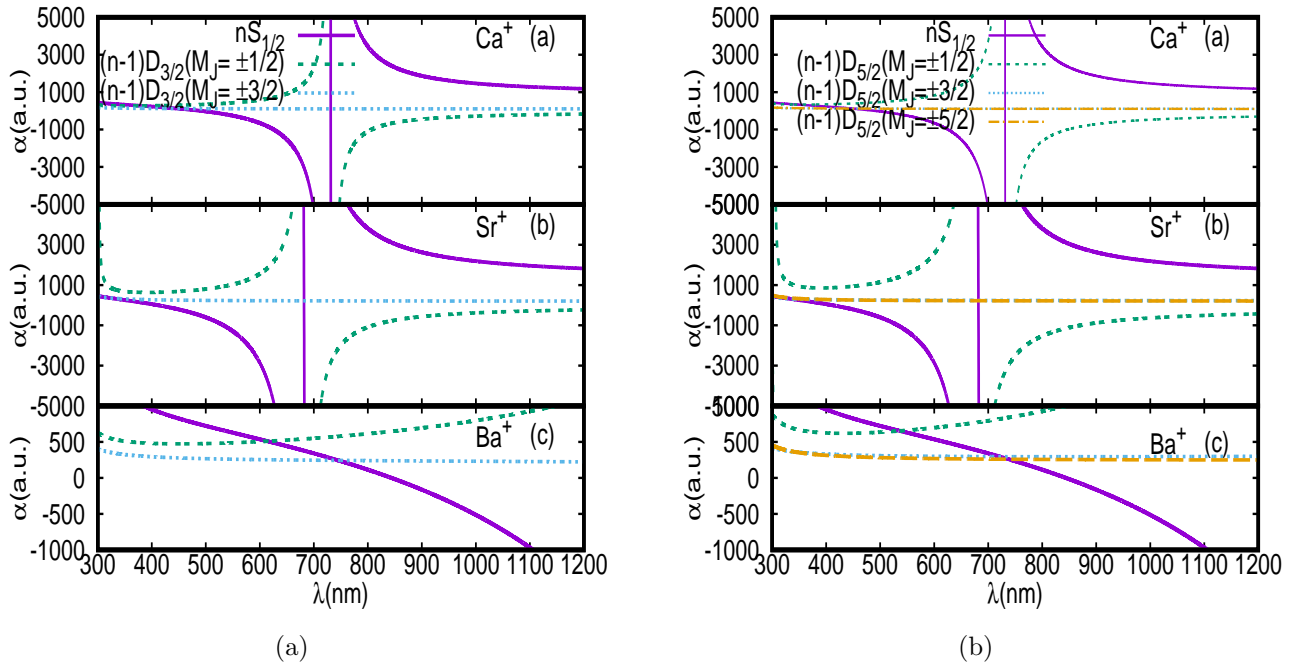


**Fig. 9:** Plots depicting dynamic E2 polarizabilities of (a) ground and metastable  $(n-1)D_{3/2}$  states in  $\text{Ca}^+$ ( $n=4$ ),  $\text{Sr}^+$ ( $n=5$ ) and  $\text{Ba}^+$ ( $n=6$ ) (b) of ground and the metastable  $(n-1)D_{5/2}$  states in  $\text{Ca}^+$ ( $n=4$ ),  $\text{Sr}^+$ ( $n=5$ ) and  $\text{Ba}^+$ ( $n=6$ ) for wavelength range 300 – 1300 nm for the linearly polarized light.

Table O: Static quadrupole polarizabilities (in a.u.) of the ground and excited states of  $Mg^+$  with core correlation contribution  $0.52\pm0.03$  a.u. from the present work. The valence correlation contributions are given as ‘Main’ and ‘Tail’, whereas the core-valence correlation contributions are given under ‘vc’. Other literature values are also quoted for the comparison. The core-valence correlation contributions to the tensor components of the polarizabilities are not quoted here due to their negligible magnitudes.

State	$\alpha_{q,0}^J$				$\alpha_{q,2}^J$			$\alpha_{q,4}^J$		
	Main	Tail	vc	Total	Main	Tail	Total	Main	Tail	Total
$3S_{1/2}$	$154.69\pm0.02$	$0.8\pm0.4$	$\sim 0$	$156.0\pm0.4$						
					$156.1$ [16]					
					$156.02\pm1.27$ [29]					
$3P_{1/2}$	$72947\pm35$	$58\pm29$	$\sim 0$	$73005\pm45$						
$3P_{3/2}$	$-36046\pm18$	$58\pm29$	$\sim 0$	$-35987\pm34$	$36261\pm18$	$-10\pm5$	$36251\pm18$			
$3D_{3/2}$	$-7555049\pm4363$	$797\pm399$	$\sim 0$	$-7554251\pm4381$	$-5377735\pm3116$	$-227\pm114$	$-5377962\pm3118$			
$3D_{5/2}$	$5019851\pm2909$	$797\pm399$	$\sim 0$	$5020648\pm2936$	$-2549856\pm1484$	$-324\pm162$	$-2550180\pm1493$	$-1234286\pm712$	$3\pm 1$	$-1234283\pm712$

Table P: Static quadrupole polarizabilities (in a.u.) of the ground and excited states of  $\text{Ca}^+$  with core correlation contribution  $6.9 \pm 0.3$  a.u. from the present work. The valence correlation contributions are given as ‘Main’ and ‘Tail’, whereas the core-valence correlation contributions are given under ‘vc’. Other literature values are also quoted for the comparison. The core-valence correlation contributions to the tensor components of the polarizabilities are not quoted here due to their negligible magnitudes.

State	$\alpha_{q,0}^J$				$\alpha_{q,2}^J$			$\alpha_{q,4}^J$		
	Main	Tail	vc	Total	Main	Tail	Total	Main	Tail	Total
$4S_{1/2}$	$852 \pm 4$	$15 \pm 8$	$\sim 0$	$874 \pm 9$						
					$871 \pm 4$ [30]					
					$875.1$ [16]					
					$875 \pm 10$ [38]					
$4P_{1/2}$	$74854 \pm 381$	$66 \pm 33$	$\sim 0$	$74927 \pm 382$						
$4P_{3/2}$	$-35910 \pm 191$	$66 \pm 33$	$\sim 0$	$-35837 \pm 194$	$36703 \pm 191$	$-14 \pm 7$	$36689 \pm 191$			
$3D_{3/2}$	$5122 \pm 55$	$66 \pm 33$	$\sim 0$	$5195 \pm 64$	$3788 \pm 39$	$-18 \pm 9$	$3770 \pm 40$			
				$5225 \pm 103$ [38]			$3797 \pm 71$ [38]			
$3D_{5/2}$	$-3494 \pm 36$	$66 \pm 33$	$\sim 0$	$-3421 \pm 49$	$1895 \pm 19$	$-26 \pm 13$	$1869 \pm 23$	$826 \pm 9$	$0.2 \pm 0.1$	$826 \pm 9$
				$-3450 \pm 72$ [38]			$1883 \pm 36$ [38]			$831 \pm 16$ [38]

Table Q: Static quadrupole polarizabilities (in a.u.) of the ground and excited states of  $\text{Sr}^+$  with core correlation contribution  $17.1 \pm 0.9$  a.u. from the present work. The valence correlation contributions are given as ‘Main’ and ‘Tail’, whereas the core-valence correlation contributions are given under ‘vc’. Other literature values are also quoted for the comparison. The core-valence correlation contributions to the tensor components of the polarizabilities are not quoted here due to their negligible magnitudes.

State	$\alpha_{q,0}^J$				$\alpha_{q,2}^J$			$\alpha_{q,4}^J$		
	Main	Tail	vc	Total	Main	Tail	Total	Main	Tail	Total
$5S_{1/2}$	1328±5	30±15	~0	1375±16						
				1370±28 [22]						
				1379±17 [38]						
				1346 [21]						
				1356.300±0.315 [31]						
				1100±10 [24]						
$5P_{1/2}$	31636±128	48±24	~0	31701±130						
				31596±455 [31]						
$\infty$	$5P_{3/2}$	-13210±64	47±23	~0	-13146±68	14613±64	-11±5	14602±64		
				-13099±225 [31]						
$4D_{3/2}$	2734±19	122±61	~0	2873±64	2163±13	-34±17	2129±21			
				2713±44 [31]						
				2884±70 [38]			2148±35 [38]			
$4D_{5/2}$	-1924±13	124±62	~0	-1783±63	1184±7	-49±24	1135±25	426±3	0.5±0.2	427±3
				-1728±23 [31]						
				-1807±62 [38]			1147±27 [38]			430±7 [38]

Table R: Static quadrupole polarizabilities (in a.u.) of the ground and excited states of  $\text{Ba}^+$  with core correlation contribution  $46\pm 2$  a.u. from the present work. The valence correlation contributions are given as ‘Main’ and ‘Tail’, whereas the core-valence correlation contributions are given under ‘vc’. Other literature values are also quoted for the comparison. The core-valence correlation contributions to the tensor components of the polarizabilities are not quoted here due to their negligible magnitudes.

State	$\alpha_{q,0}^J$				$\alpha_{q,2}^J$			$\alpha_{q,4}^J$		
	Main	Tail	vc	Total	Main	Tail	Total	Main	Tail	Total
$6S_{1/2}$	4106±42	40±20	~0	4192±47						
				4182±34 [26]						
				4270±27 [32]						
				4251±61 [38]						
				4091.5 [80]						
				4420±250 [27]						
$5D_{3/2}$	629±25	138±69	~0	813±73	1585±20	-38±19	1547±28			
				835±32 [32]						
				820±72 [38]			1579±33 [38]			
$5D_{5/2}$	-1341±19	144±72	~0	-1151±74	1316±18	-56±28	1260±33	70±4	0.6±0.3	71±4
				-1201±36 [32]						
				-1182±69 [38]			1286±35 [38]			72±6 [38]

Table S: Magic wavelengths  $\lambda_{\text{magic}}$  (in nm) and corresponding polarizability values (in a.u.) for the  $3S - 3P_{3/2,1/2}$  and  $3S - 3D_{5/2,3/2}$  transitions of  $\text{Mg}^+$  using the linearly polarized light. The resonant wavelengths (in nm) for the transitions contributing to the  $nP_J$  and  $nD_J$  ac polarizabilities are listed as  $\lambda_{\text{res}}$ .

Resonances	$\lambda_{\text{res}}$	$ M_J $	$\lambda_{\text{magic}}$	$\alpha_d^J(\lambda_{\text{magic}})$
Transition			<u><math>3S - 3P_{1/2}</math></u>	
		1/2	276.1±0.7	-1266
$3P_{1/2}-3D_{3/2}$	279.160			
$3P_{1/2}-3S_{1/2}$	280.353			
$3P_{1/2}-4S_{1/2}$	292.948			
		1/2	307±2	202
Transition			<u><math>3S - 3P_{3/2}</math></u>	
$3P_{3/2}-3D_{3/2}$	279.875			
$3P_{3/2}-3D_{5/2}$	279.882			
$3P_{3/2}-3S_{1/2}$	279.635			
$3P_{3/2}-4S_{1/2}$	293.736			
		1/2	324±3	137
Transition			<u><math>3S - 3D_{3/2}</math></u>	
$3D_{3/2}-5F_{5/2}$	310.570			

		1/2	$313.7 \pm 0.1$	169
		3/2	$314.2 \pm 0.2$	167
$3D_{3/2} - 5P_{3/2}$	384.943			
		3/2	$385.011 \pm 0.003$	73
$3D_{3/2} - 5P_{1/2}$	385.147			
		1/2	$385.376 \pm 0.003$	73
$3D_{3/2} - 4F_{5/2}$	448.258			
		1/2	$705 \pm 1$	41
		3/2	$901 \pm 3$	39
$3D_{3/2} - 4P_{3/2}$	1091.827			
$3D_{3/2} - 4P_{1/2}$	1095.477			
Transition		<u><math>3S - 3D_{5/2}</math></u>		
$3D_{5/2} - 5F_{7/2}$	310.561			
$3D_{5/2} - 5F_{5/2}$	310.562			
		1/2	$313.67 \pm 0.07$	170
		3/2	$313.80 \pm 0.08$	169
		5/2	$314.4 \pm 0.2$	167
$3D_{5/2} - 5P_{3/2}$	384.930			
		3/2	$385.121 \pm 0.003$	73
		1/2	$385.170 \pm 0.003$	74
$3D_{5/2} - 4F_{7/2}$	448.238			
$3D_{5/2} - 4F_{5/2}$	448.241			
		1/2	$699 \pm 1$	42
		3/2	$737 \pm 2$	41
$3D_{5/2} - 4P_{3/2}$	1091.723			

Table T: Magic wavelengths  $\lambda_{\text{magic}}$  (in nm) and corresponding polarizability values (in a.u.) for the  $4S - 4P_{3/2,1/2}$  and  $4S - 3D_{5/2,3/2}$  transitions of  $\text{Ca}^+$  using the linearly polarized light. The resonant wavelengths (in nm) for the transitions contributing to the  $nP_J$  and  $nD_J$  ac polarizabilities are listed as  $\lambda_{\text{res}}$ .

Resonances	$\lambda_{\text{res}}$	$ M_J $	$\lambda_{\text{magic}}$	$\alpha_d^J(\lambda_{\text{magic}})$
Transition		<u><math>4S - 4P_{1/2}</math></u>		
$4P_{1/2} - 4D_{3/2}$	315.978			
		1/2	$368.08 \pm 0.04$	-485
			368.0149	-477.2554
			$368.0221 \pm 0.1412$ [33]	[15]
$4P_{1/2} - 5S_{1/2}$	370.707			
		1/2	$395.18 \pm 0.02$	2935

			395.1807	2896.7954	[15]
			395.1788±0.0377 [33]		
$4P_{1/2} - 4S_{1/2}$	396.959				
		1/2	693±2	111	
			690.817	110.0849	[15]
			691.24±12.29 [33]		
$4P_{1/2} - 3D_{3/2}$	866.452				
Transition			<u><math>4S - 4P_{3/2}</math></u>		
$4P_{3/2} - 4D_{5/2}$	318.025				
		3/2	318.04±0.01	-131	
$4P_{3/2} - 4D_{3/2}$	318.219				
		1/2	369.75±0.05	-521	
			369.6393	-512.1655	[15]
			369.6523±0.1849 [33]		
$4P_{3/2} - 5S_{1/2}$	373.796				
$4P_{3/2} - 4S_{1/2}$	393.477				
		3/2	395.77±0.02	127	
			395.774	123.4906	[15]
			395.7729±0.0019 [33]		
		1/2	396.23±0.01	-3119	
			396.2315	-3077.3881	[15]
			396.2297±0.0218 [33]		
$4S_{1/2} - 4P_{1/2}$	396.959				
		3/2	674±4	114	
			672.508	113.0150	[15]
			672.89±15.33 [33]		
		1/2	690±3	111	
			687.022	110.6606	[15]
			687.51±10.33 [33]		
$4P_{3/2} - 3D_{3/2}$	850.035				
		1/2	850.117±0.006	96	
			850.1164±0.0001 [33]		
		3/2	850.92±0.02	95	
			850.9217±0.0015 [33]		
$4P_{3/2} - 3D_{5/2}$	854.443				
Transition			<u><math>4S - 3D_{3/2}</math></u>		
$4S_{1/2} - 4P_{3/2}$	393.477				
		1/2	395.79±0.01	3	

		395.7981	1.1711	[15]
		395.7962±0.0001 [33]		
	3/2	395.79±0.01	8	
		395.7970	7.1019	[15]
		395.7951±0.0001 [33]		
$4S_{1/2} - 4P_{1/2}$	396.959			
$3D_{3/2} - 4P_{3/2}$	850.035			
	1/2	850.33±0.02	95	
		850.335	95.0011	[15]
		850.3301±0.0018 [33]		
$3D_{3/2} - 4P_{1/2}$	866.452			
	3/2	886±1	94	
		887.382	92.9908	[15]
		887.28±3.52 [33]		
	1/2	1288±3	84	
		1308.590	82.4644	[15]
		1307.60±96.20 [33]		
<hr/>				
Transition		<u><math>4S - 3D_{5/2}</math></u>		
$4S_{1/2} - 4P_{3/2}$	393.477			
	1/2	395.79±0.01	2	
		395.7982	0.5371	[15]
		395.7963±0.0001 [33]		
	3/2	395.79±0.01	5	
		395.7978	3.1792	[15]
		395.7958±0.0001 [33]		
	5/2	395.79±0.01	9	
		395.7968	8.4633	[15]
		395.7949±0.0001 [33]		
$4S_{1/2} - 4P_{1/2}$	396.959			
$3D_{5/2} - 4P_{3/2}$	854.443			
	3/2	1065±3	88	
		1074.336	86.4837	[15]
		1073.80±31.61 [33]		
	1/2	1312±2	83	
		1338.474	82.1167	[15]
		1337.30±115.38 [33]		
<hr/> <hr/>				

Table U: Magic wavelengths  $\lambda_{\text{magic}}$  (in nm) and corresponding polarizability values (in a.u.) for the  $5S - 5P_{3/2,1/2}$  and  $5S - 4D_{5/2,3/2}$  transitions of  $\text{Sr}^+$  using the linearly polarized light. The resonant wavelengths (in nm) for the transitions contributing to the  $nP_J$  and  $nD_J$  ac polarizabilities are listed as  $\lambda_{\text{res}}$ .

Resonances	$\lambda_{\text{res}}$	$ M_J $	$\lambda_{\text{magic}}$	$\alpha_d^J(\lambda_{\text{magic}})$
<u>Transition</u>				
<u><math>5S - 5P_{1/2}</math></u>				
$5P_{1/2} - 5D_{3/2}$	338.167			
$5P_{1/2} - 6S_{1/2}$	416.296			
$5P_{1/2} - 5S_{1/2}$	421.670			
		1/2	$767 \pm 2$	127
			764.238 [31]	
$5P_{1/2} - 4D_{3/2}$	1091.787			
<u>Transition</u>				
<u><math>5S - 5P_{3/2}</math></u>				
$5P_{3/2} - 5D_{5/2}$	346.544			
		3/2	$347.383 \pm 0.003$	-205
		1/2	$347.570 \pm 0.001$	-206
$5P_{3/2} - 5D_{3/2}$	347.588			
$5P_{3/2} - 5S_{1/2}$	407.886			
		3/2	$416.6 \pm 0.1$	168
		1/2	$419.31 \pm 0.04$	-1526
$5S_{1/2} - 5P_{1/2}$	421.670			
$5P_{3/2} - 6S_{1/2}$	430.665			
		1/2	$438.5 \pm 0.2$	815
			438.00 [31]	
		1/2	$713 \pm 2$	135
			709 [31]	
		3/2	$722 \pm 2$	133
			721 [31]	
$5P_{3/2} - 4D_{3/2}$	1003.940			
		1/2	$1004.47 \pm 0.05$	109
			1004 [31]	
		3/2	$1009.8 \pm 0.1$	109
			1009 [31]	
$5P_{3/2} - 4D_{5/2}$	1033.014			
<u>Transition</u>				
<u><math>5S - 4D_{3/2}</math></u>				
$5S_{1/2} - 5P_{3/2}$	407.886			
		3/2	$416.99 \pm 0.06$	18
		1/2	$417.01 \pm 0.06$	15

$5S_{1/2} - 5P_{1/2}$	421.670			
$4D_{3/2} - 5P_{3/2}$	1003.940			
		1/2	$1005.3 \pm 0.1$	108
		3/2	$1085 \pm 2$	106
			1083 [31]	
$4D_{3/2} - 5P_{1/2}$	1091.787			
Transition			<u><math>5S - 4D_{5/2}</math></u>	
$5S_{1/2} - 5P_{3/2}$	407.886			
		5/2	$416.99 \pm 0.06$	19
		3/2	$417.01 \pm 0.06$	15
		1/2	$417.01 \pm 0.06$	12
$5S_{1/2} - 5P_{1/2}$	421.670			
$4D_{5/2} - 5P_{3/2}$	1033.014			

Table V: Magic wavelengths  $\lambda_{\text{magic}}$  (in nm) and corresponding polarizability values (in a.u.) for the  $6S - 6P_{3/2,1/2}$  and  $6S - 5D_{5/2,3/2}$  transitions of  $\text{Ba}^+$  using the linearly polarized light. The resonant wavelengths (in nm) for the transitions contributing to the  $nP_J$  and  $nD_J$  ac polarizabilities are listed as  $\lambda_{\text{res}}$ .

Resonances	$\lambda_{\text{res}}$	$ M_J $	$\lambda_{\text{magic}}$	$\alpha_d^J(\lambda_{\text{magic}})$
Transition			<u><math>6S - 6P_{1/2}</math></u>	
$6P_{1/2} - 8S_{1/2}$	264.805	1/2	$323 \pm 2$	-93
$6P_{1/2} - 6D_{3/2}$	389.288	1/2	$451.72 \pm 0.04$	-4557
$6P_{1/2} - 7S_{1/2}$	452.619	1/2	$468.9 \pm 0.3$	958
$6P_{1/2} - 6S_{1/2}$	493.545	1/2	$599 \pm 1$	312
$6P_{1/2} - 5D_{3/2}$	649.869			
Transition			<u><math>6S - 6P_{3/2}</math></u>	
$6P_{3/2} - 8S_{1/2}$	277.217	3/2	$348 \pm 2$	-133
		1/2	$360 \pm 2$	-158
$6P_{3/2} - 6D_{5/2}$	413.181			
$6P_{3/2} - 6D_{3/2}$	416.717	1/2	$416.660 \pm 0.006$	-467
		3/2	$416.06 \pm 0.01$	-460
$6P_{3/2} - 6S_{1/2}$	455.531			

		3/2	475.7±0.5	375
$6P_{3/2} - 7S_{1/2}$	490.129	1/2	552±2	445
		3/2	561±1	407
$6S_{1/2} - 6P_{1/2}$	493.545			
$6P_{3/2} - 5D_{3/2}$	585.529	1/2	586.23±0.08	336
		3/2	593.4±0.3	322
$6P_{3/2} - 5D_{5/2}$	614.341			
Transition			<u><math>6S - 5D_{3/2}</math></u>	
$6S_{1/2} - 6P_{3/2}$	455.531	3/2	480.5±0.3	13
		1/2	480.9±0.3	-21
$6S_{1/2} - 6P_{1/2}$	493.545			
$5D_{3/2} - 6P_{3/2}$	585.529	1/2	585.99±0.05	337
		3/2	592.5±0.2	324
$5D_{3/2} - 6P_{1/2}$	649.869	1/2	766±4	195
Transition			<u><math>6S - 5D_{5/2}</math></u>	
$6S_{1/2} - 6P_{3/2}$	455.531	5/2	480.3±0.3	26
		3/2	480.8±0.3	-15
		1/2	481.0±0.3	-36
$6S_{1/2} - 6P_{1/2}$	493.545			
$5D_{5/2} - 6P_{3/2}$	614.341	3/2	665±2	240
		1/2	713±3	214

Table W: The tune-out wavelengths ( $\lambda_T$ ) in nm for  $Mg^+$ ,  $Ca^+$ ,  $Sr^+$ ,  $Ba^+$  using the linearly polarized light

$3/2$        $787 \pm 2$

$5/2$        $324.36 \pm 0.72$

---

---

#### 4. Conclusion

By applying the relativistic all-order method with single and double excitations and also incorporating the partial triple excitations, the E2 matrix elements are evaluated for a large number of transitions between many excited states of the singly charged magnesium, calcium, strontium and barium alkaline earth-metal ions. This includes 114, 114, 130 and 96 transitions in  $Mg^+$ ,  $Ca^+$ ,  $Sr^+$  and  $Ba^+$  respectively and electric quadrupole transition properties are also calculated for these transitions. In addition, the results of the static as well as dynamic dipole and quadrupole polarizabilities of the ground and low-lying metastable states of the above ions are enlisted. The magic and tune-out wavelengths inferred by plotting the dynamic polarizabilities these state of the considered alkaline earth-metal ions are also tabulated. We have also quoted the estimated uncertainties to our calculations, and compare them with the available literature data. Many of the reported quadrupole transition properties associated with the high-lying excited states are presented for the first time. These data will be useful for both the atomic spectroscopy analyses and interpreting astrophysical observations. The listed magic and tune-out wavelengths will of immense interest for suitably designing ionic traps to conduct high-precision experiments.

#### Acknowledgments

The work of B.A. is supported by DST-SERB(India) Grant No. EMR/2016/001228. The employed all order method was developed in the group of Professor M. S. Safranova of the University of Delaware, USA.

#### References

- [1] D. Nigg, M. Müller, E. A. Martinez, P. Schindler, M. Hennrich, T. Monz, M. A. Martin-Delgado, R. Blatt, *Science* 345 (2014) 302.
- [2] A. C. Wilson, Y. Colombe, K. R. Brown, E. Knill, D. Leibfried, D. J. Wineland, *Nature* 512 (2014) 57.
- [3] C. W. Chou, D. Hume, T. Rosenband, D. J. Wineland, *Science* 329 (2010) 1630.
- [4] R.F. Garcia Ruiz et al., *Nature Phys.* 12 (2016) 594.
- [5] C. Shi, F. Gebert, C. Gorges, S. Kaufmann, W. Nörtershäuser, B. K. Sahoo, A. Surzhykov, V. A. Yerokhin, J. C. Berengut, F. Wolf, J. C. Heip, P. O. Schmidt, *Appl. Phys. B* 123 (2017) 2.
- [6] N. Fortson, *Phys. Rev. Lett.* 70 (1993) 2383.
- [7] C.S. Wood, S. C. Bennet, D. Cho, B. P. Masterson, J. L. Roberts, C. E. Tanner, C. E. Wieman, *Science* 275 (1997) 1759.
- [8] T. G. Tiecke, J. D. Thompson, N. P. de Leon, L. R. Liu, V. Vuletic, M. D. Lukin, *Nature* 508 (2014) 241.
- [9] Y. Huang, H. Guan, P. Liu, W. Bian, L. Ma, K. Liang, T. Li, K. Gao, *Phys. Rev. Lett.* 116 (2016) 013001.
- [10] C. Champenois, M. Houssin, C. Lisowski, M. Knoop, G. Hagel, M. Vedel, F. Vedel, *Phys. Lett. A* 331 (2004) 298.
- [11] G. P. Barwood, P. Gill, G. Huang, H. A. Klein, *Measurement Sci. Tech.* 23 (2012) 055201.
- [12] T. Fordell, T. Lindvall, P. Dub'e, A. A. Madej, A. E. Wallin, M. Merimaa, *Opt. Lett.* 40 (2015) 1822.

- [13] P. Dub'e, A. A. Madej, Z. Zhou, J. E. Bernard, Phys. Rev. A 87 (2013) 023806.
- [14] J. Mitroy, M. S. Safronova, Phys. Rev. A 79 (2009) 012513.
- [15] Y. B. Tang, H. X. Qiao, T. Y. Shi, J. Mitroy, Phys. Rev. A 87 (2013) 042517.
- [16] J. Mitroy, J.Y. Zhang, Eur. Phys. J. D 46 (2008) 415.
- [17] B. K. Sahoo, B. P. Das, D. Mukherjee, Phys. Rev. A 79 (2009) 052511.
- [18] E. S. Chang, J. Phys. B: At. Mol. Opt. Phys. 16 (1983) L539.
- [19] B. K. Sahoo, R. G. E. Timmermans, B. P. Das, D. Mukherjee, Phys. Rev. A 80 (2009) 062506.
- [20] D. Jiang, B. Arora, M. S. Safronova, C. W. Clark, J. Phys. B: At. Mol. Opt. Phys. 42 (2009) 154020.
- [21] J. Mitroy, J. Y. Zhang, M. W. J. Bromley, Phys. Rev. A 77 (2008) 032512.
- [22] U. I. Safronova, Phys. Rev. A 82 (2010) 022504.
- [23] P. S. Barklem, B. J. O'Mara, Mon. Not. R. Astron. Soc. 311 (2000) 535.
- [24] J. Nunkaew, E. S. Shuman, T. F. Gallagher, Phys. Rev. A 79 (2009) 054501.
- [25] M. D. Barrett, K. J. Arnold, M. S. Safronova, Phys. Rev. A 100 (2019) 043418.
- [26] E. I.-Tchoukova, M. S. Safronova, Phys. Rev. A 78 (2008) 012508.
- [27] E. L. Snow, S. R. Lundeen, Phys. Rev. A 76 (2007) 052505.
- [28] T. F. Gallagher, R. Kachru, N. H. Tran, Phys. Rev. A 26 (1982) 2611.
- [29] B. K. Sahoo, Chem. Phys. Lett. 448 (2007) 144.
- [30] M. S. Safronova, U. I. Safronova, Phys. Rev. A 83 (2011) 012503.
- [31] J. Jiang, J. Mitroy, Y. Cheng, M. W. J. Bromley, Phys. Rev. A 94 (2016) 062514.
- [32] B. K. Sahoo, B. P. Das, Phys. Rev. A 86 (2012) 022506.
- [33] J. Jiang, L. Jiang, X. Wang, P. Shaw, D. -H. Zhang, L. Y. Xie, C. Z. Dong, IOP Conf. Series: Journal of Physics: Conf. Series 875 (2017) 122003.
- [34] P. -L. Liu, Y. Huang, W. Bian, H. Shao, H. Guan, Y.-B. Tang, C.-B. Li, J. Mitroy, K.-L. Gao, Phys. Rev. Lett. 114 (2015) 223001.
- [35] J. Kaur, Theoretical study of atomic properties of alkaline earth metal ions for various applications (PhD thesis).
- [36] T. Rosenband et al. Phys. Rev. Lett. 98 (2007) 220801.
- [37] M. Hobein, A. Solders, M. Suhonen, Y. Liu, R. Schuch, Phys. Rev. Lett. 106 (2011) 013002.
- [38] S. Singh, M. Kaur, B. Arora, B. K. Sahoo, Phys. Rev. A 98 (2018) 013406.
- [39] R. W. Wood, R. Fortrat, Astrophys. J. 43 (1916) 73.
- [40] J. Borsenberger, F. Praderie, G. Michaud, ApJ 243 (1981) 533.
- [41] L. Mashonkina, T. Gehren, L. Bikmaev, Astron. Astrophys. 343 (1999) 519.

- [42] L. Mashonkina, G. Zhao, T. Gehren, W. Aoki, M. Bergemann, K. Noguchi, J.R Shi, M. T. Hidai, H. W. Zhang, *Astron. Astrophys.* 478 (2008) 529.
- [43] M. Murga, G. Zhu, B. Menard, T. -W. Lan, *Mon. Not. R. Astron. Soc.* 452 (2015) 511.
- [44] S. M. Andrievsky, F. spite, S. A. Korotin, P. Francois, M. Spite, P. Bonifacio, R. Cayrel, V. Hill, *Astron. Astrophys.* 530 (2011) A105.
- [45] L. Mashonkina, T. Gehren, *Astron. Astrophys.* 376 (2001) 232.
- [46] D. E. Welty, D. C. Mortan, L. M. Hobbs, *Astrophys. J. Suppl.* 106 (1996) 533.
- [47] J. Kwan, W. Fischer, *Mon. Not. R. Astron. Soc.* 411 (2011) 2383.
- [48] G. D. Sandlin, G. E. Bruckner, V. E. Scherrev, R. Tousey, *Astrophys. J.* 205 (1976) L47.
- [49] B. Edlen, *Phys. Scr. T* 8 (1984) 5.
- [50] C. F. Roos, M. Chwalla, K. Kim, M. Riebe, R. Blatt, *Nature (London)* 443 (2006) 316.
- [51] J. Benhelm, G. Kirchmair, C. F. Roos, R. Blatt, *Nat. Phys.* 4 (2008) 463.
- [52] B. K. Sahoo, M. R. Islam, B. P. Das, R. Chaudhuri, D. Mukherjee, *Phys. Rev. A* 74 (2006) 062504.
- [53] B. K. Sahoo, B. P. Das, *Mol. Phys.* 115 (2017) 2765.
- [54] R. Cote, A. Dalgarno, *Phys. Rev. A* 62 (2000) 012709.
- [55] G. Celik, D. Doğan, S. Ates, M. Taser, *J. Quant. Spectr. Radiat. Transfer* 113 (2012) 1601.
- [56] S. Majumder, G. Gopakumar, R.K. Chaudhuri, B.P. Das, H. Merlitz, U.S. Mahapatra, D. Mukherjee, *Eur. Phys. J. D* 28 (2004) 3.
- [57] C. F. Fischer, <http://nlte.nist.gov/MCHF/view.html>.
- [58] L. Filippin, S. Schiffmann, J. Dohet-Eraly, D. Baye, M. Godefroid, *Phys. Rev. A* 97 (2018) 012506.
- [59] H. Guan, H. Shao, Y. Qian, Y. Huang, P. Liu, W. Bian, C.-B. Li, B. K. Sahoo, K.-L. Gao, *Phys. Rev. A* 91 (2015) 022511.
- [60] J. Gurell, E. Biémont, K. Blagoev, V. Fivet, P. Lundin, S. Mannervik, L.-O. Norlin, P. Quinet, D. Rostohar, P. Royen, P. Schef, *Phys. Rev. A* 75 (2007) 052506.
- [61] M. Kaur, D. F. Dar, B. K. Sahoo, B. Arora, *At. Data Nuc. Data Tables* 137 (2021) 101381.
- [62] S. A. Blundell, W. R. Johnson, J. Sapirstein, *Phys. Rev. A* 43 (1991) 3407.
- [63] M. S. Safranova, W. R. Johnson, *Adv. At. Mol. Opt. Phys.* 55 (2008) 191.
- [64] B. K. Sahoo, D. K. Nandy, B. P. Das and Y. Sakemi, *Phys. Rev. A* 91 (2015) 042507.
- [65] B. K. Sahoo, B. P. Das, *Phys. Rev. A* 92 (2015) 052511.
- [66] M. S. Safranova, High-Precision Calculation of Atomic Properties and Parity Nonconservation in Systems With One Valence Electron (PhD Thesis).
- [67] D. Jiang, B. Arora, M. S. Safranova, *Phys. Rev. A* 78 (2008) 022514.

- [68] D. E. kelleher, L. I. Podobedova, J. Phys. Chem. Ref. Data 37 (2008) 267.
- [69] P. J. Mohr, David B. Newell, B. N. Taylor, Journal of Physical and Chemical Reference Data 45, 043102 (2016).
- [70] I. I. Sobelman, Aatomic Spectra and Radiative Transitions, Springer, Verlag (1979).
- [71] K. Bonin, V. V. Kresin, Electric-dipole Polarizabilities of Atoms, Molecules and Clusters (World Scientific-Singapore, 1997).
- [72] N. Manakov, V. Ovsianikov, L. Rapoport, Physics Reports 141 (1986) 320.
- [73] K. Beloy, Theory of the ac stark effect on the atomic hyperfine structure and applications to microwave atomic clocks, ph.d. thesis (2009).
- [74] S. Singh, K. Kaur, B. K. Sahoo, B. Arora, J. Phys. B: At. Mol. Opt. Phys. 49 (2016) 145005.
- [75] B. Arora, D. K. Nandy, B. K. Sahoo, Phys. Rev. A 85 (2012) 012506.
- [76] J. Kaur, D. K. Nandy, B. Arora, B. K. Sahoo, Phys. Rev. A 91 (2015) 012705.
- [77] A. Kramida, Yu.- Ralchenko, J. Reader, NIST ASD Team (2018). NIST Atomic Spectra Database (ver. 5.6.1), [Online]. Available: <https://physics.nist.gov/asd> [2019, August 29]. National Institute of Standards and Technology, Gaithersburg, MD. DOI: <https://doi.org/10.18434/T4W30F>.
- [78] B. K. Sahoo, Phys. Rev. A 93 (2016) 022503.
- [79] H. Shao, Y. Hxuang, H. Guan, C. Li, T. Shi, K. Gao, Phys. Rev. A 95 (2017) 053415.
- [80] U. I. Safronova, Phys. Rev. A 81 (2010) 052506.

This figure "preview-micro.jpg" is available in "jpg" format from:

<http://arxiv.org/ps/2201.07759v1>

This figure "preview-web.jpg" is available in "jpg" format from:

<http://arxiv.org/ps/2201.07759v1>

This figure "preview.jpg" is available in "jpg" format from:

<http://arxiv.org/ps/2201.07759v1>